OPTIMAL CALIBRATION AND TRANSIENT CONTROL OF HIGH DEGREE OF FREEDOM INTERNAL COMBUSTION ENGINES

by

Tae-Kyung Lee

A dissertation submitted in partial fulfillment
of the requirements for the degree of
Doctor of Philosophy
(Mechanical Engineering)
in The University of Michigan
2009

Doctoral Committee:

Research Professor Zoran S. Filipi, Chair
Professor Dionissios N. Assanis
Professor Panos Y. Papalambros
Professor Jing Sun
Denise M. Kramer, US ARMY TACOM

© Tae - Kyung Lee 2009
All Rights Reserved

To my parents,
to my wife, Young-Sun, and
to my daughters, Jin and Seo-Yoon

ACKNOWLEDGEMENTS

The series of this research can be successfully achieved due to the help of many people. Professor Zoran S. Filipi, my academic advisor, promoted my passion to the research, and provided the motivation of the leading-edge research topics. His advice and guidance enabled to improve my sense of engineering and even more the sense of human life. Professor Dennis Assanis, the director of W.E. Lay Automotive laboratory, provides the excellent research environment. Thanks to such research environment, my research can be successfully achieved. All committee members are appreciated with their precious instruction, comments, and suggestions.

The author appreciates the financial and technical support from Chrysler LLC. Chrysler LLC proposed actual research topics in developing advanced engines. The proposed project initiated the research direction for developing essential methodologies provided in this dissertation. Denise Kramer and Gregory Ohl contributed in shaping the project. As my laboratory colleague, Robert Prucka supported this research by providing all experimental results, which are used for developing virtual sensing methodologies.

The author also appreciates the financial support from Korea Science and Engineering Foundation. This work was supported by the Korea Science and Engineering Foundation Grant (No. D00003). The financial support from Korea government secured the research environment stable.

Precious classes provided by University of Michigan enabled my research to be successfully achieved. The provided classes cover various disciplines of research area from basic theories to most recent applications. The author also gives thanks to the educational environment of the University of Michigan. The author acknowledged friends, and colleagues for sharing happy experiences in the University of Michigan.

Finally, the author gives a very special thanks to my parents, my wife and daughters.

TABLE OF CONTENTS

LIST OF TABLES

LIST OF FIGURES

NOMENCLATURE

a_i	the network output for the *i*th training sample
A_e	effective flow area
A_f	the flame front area
B	cylinder bore diameter
BMEP	brake mean effective pressure
bsfc	break specific fuel consumption
$bsfc^s$	reference *bsfc*
C_β	adjustable constant of the quasi-D combustion model
C_M	adjustable constant of the quasi-D combustion model
c_p	constant pressure specific heat
c_v	constant volume specific heat
COM	control oriented model
COV_{IMEP}	coefficient of variance in indicated mean effective pressure
di-VVT	dual-independent variable valve timing
H_0	null hypothesis
I_{eff}	effective inertia including the engine and vehicle
K	mean flow kinetic energy
k	turbulent kinetic energy
L	macroscale (the minimum vessel dimension)
L_{CMV}	CMV position
l_I	integral scale
l_M	microscale
LQ	linear quadratic
m	mass within the manifold at any time

m_b	the mass of burned products
$\dot{m}_e$	mass flow rates out of the cylinder
m_e	the mass entrained
$\dot{m}_f$	mass fuel flow rate
$\dot{m}_i$	mass flow rates into the cylinder
MAP	manifold absolute pressure
MBT	minimum spark advance for best torque
mse	mean squared error
N	the total number of training samples
N_{eng}	engine speed
n_{cyl}	the number of cylinders of the engine
NMPC	nonlinear model predictive control
P	production rate of turbulent kinetic energy
P_{amb}	ambient pressure
P_m	intake manifold pressure
Q	heat flow into the manifold
R	specific gas constant
$\mathbf{s}_k$	search direction
S_L	laminar flame speed
SQP	sequential quadratic programming
t	time
t_i	the target output value of the *i*th training sample
$\mathrm{T_C}$	control horizon
$\mathrm{T_P}$	prediction horizon
T_{eng}	engine torque expressed as BMEP
T_{eng}^S	reference engine torque
T_{ext}	external loads on the crankshaft
T_m	manifold temperature
u'	turbulent intensity

V	the instantaneous volume of the combustion chamber
V_d	the displaced or swept volume
V_m	manifold volume
v_i	gas flow velocity into the cylinder
$\hat{\boldsymbol{u}}$	future control inputs
$\boldsymbol{u}_s$	control input set-points
w_i	the network weight of the jth neuron
WOT	wide open throttle
$\hat{\boldsymbol{x}}$	predicted engine states
x_{res}	residual gas fraction
x_{res}^{S}	reference residual gas fraction
$\boldsymbol{x}_s$	engine state set-points
$(dP/d\theta)_{\max}$	the maximum rate of pressure rise
α_k	step length
δ	sampling time
$\Delta\theta_b$	rapid-burning angle (10-90% burn duration)
$\Delta\theta_d$	flame-development angle (0-10% burn duration)
$\Delta\theta_o$	overall burning angle
ΔP_{amb}	ambient pressure difference
ε	dissipation rate of turbulent kinetic energy per unit mass
ϕ_{cyl}	mass flow rate into the cylinders
ϕ_{thrt}	mass flow rate through a throttle body
γ	performance ratio
η	Kolmogorov microscale
η_v	volumetric efficiency
κ	specific heat ratio
σ_{IMEP}	standard deviation of IMEP
$\sigma_{spark,u}$	spark timing control input
σ_{spark}	spark timing

σ_{spark}^{S}	reference spark timing
τ_{act}	a time constant of actuator dynamics
τ_{cycl}	cycle time
τ_{MAP}	a time constant of manifold dynamics
τ_{seg}	the sampling time in seconds
θ_{ETC}^{S}	reference ETC position
θ_{ETC}	ETC control input
ρ_a	air density
ρ_u	density of unburned charge
λ	Taylor microscale
ζ_{actual}	actual actuator response
$\zeta_{commanded}$	actuator command
$\zeta_{CMV,u}$	CMV control input
ζ_{EX}	exhaust cam timing
ζ_{EX}^{S}	reference exhaust valve timing
$\zeta_{EX,u}$	exhaust valve timing control input
ζ_{IN}	intake cam timing
ζ_{IN}^{S}	reference intake valve timing
$\zeta_{IN,u}$	intake valve timing control input

ABSTRACT

OPTIMAL CALIBRATION AND TRANSIENT CONTROL OF HIGH DEGREE OF FREEDOM INTERNAL COMBUSTION ENGINES

by

Tae-Kyung Lee

Increasing engine system complexity for achieving better engine performance and fuel economy induces intricate engine calibration and transient engine control problems. The classical experiment based procedure cannot deal with the exponential increase in size of the calibration problem for the high degree-of-freedom (DOF) engine. The increased number of independent variables leads to complex inter-relationships, and characterizing them by means of traditional experimental sweeps of individual variables is simply not possible. In addition, increased number of actuators creates a new challenge under rapid engine transients. Various devices might have different response times, thus leading to significant excursions of operating parameters during dynamic changes of load and speed. The higher the DOF in the system, the more probability that the engine may deviate from optimum during a transient. Since transients are very frequent during normal driving, the sub-optimum engine behavior during these events can

cause significant performance and emission penalties. Thus, developing transient control methodologies is an indispensable complement to optimal steady-state calibration if we aim to realize the full potential of the modern engine with variable devices and sub-systems.

This dissertation covers the entire procedures for achieving the optimal feed-forward steady-state control strategy and transient control of a high degree-of-freedom engine based on performance, combustion stability and emissions goals. Contributions critical for achieving the overall objective are:

(1) Improved high-fidelity simulation tools as alternative to experiments;

(2) Virtual sensing methodologies using artificial neural networks (ANNs);

(3) Characterization of the combustion stability for the real time estimation;

(4) Simulation based optimization framework for determining optimal actuator set-points in a high DOF engine considering a multi-objective cost function;

(5) Nonlinear model predictive control (NMPC) of engine transients. The NMPC development is enabled by using a proposed control oriented model (COM) and applying a receding horizon concept.

CHAPTER 1

INTRODUCTION

1.1 Background and Motivation

Internal combustion (IC) engines are still a dominant power source for propulsion of vehicles. Since the advent of IC engines, the development of engine technology led to dramatic improvement of fuel efficiency, generated output power, and emission reduction. Due to high energy density, relatively low production costs, well equipped infrastructure, and continuous improvement and validation over long period, the IC engine still maintains its attractiveness compared to the alternative powertrains. Nevertheless, the IC engine needs to be continuously improved to meet both customer needs, which are generally better fuel economy and ultimate engine output, and government regulations. The government regulations have been related to the reduction of toxic emissions, such as carbon monoxide (CO), hydro carbon (HC) and nitrogen oxides (NO_x), and particular matter (PM). In addition, the government regulations started to include greenhouse gas (GHG) emissions, such as carbon dioxide (CO_2), to resolve global warming problems.

Internal combustion engines are one of the most significant sources of the CO_2 emission [1,2]. During the past hundred years, the mean temperature of the earth has

continually increased. To prevent the global warming as well as the air pollution, government regulations for emissions have become stricter. The regulations limit the amount of hydro carbon (HC) and nitrogen oxides (NO_x) as well as the CO_2 emission. To meet the emission regulations, new powertrain technologies need to be introduced, thus, alternative powertrain technologies have been researched intensively to reduce emissions as well as improve fuel economy [3]. The alternative powertrain technologies include fuel cell vehicles [4,5], hydrogen internal combustion (IC) engines [6], and hybrid propulsion systems [7-9] including plug-in hybrids [10,11]. While hydrogen and fuel cells have been candidates in the long term solutions, advanced IC engines will be near-to-mid term solutions while using hydrocarbon fuel to produce mechanical work.

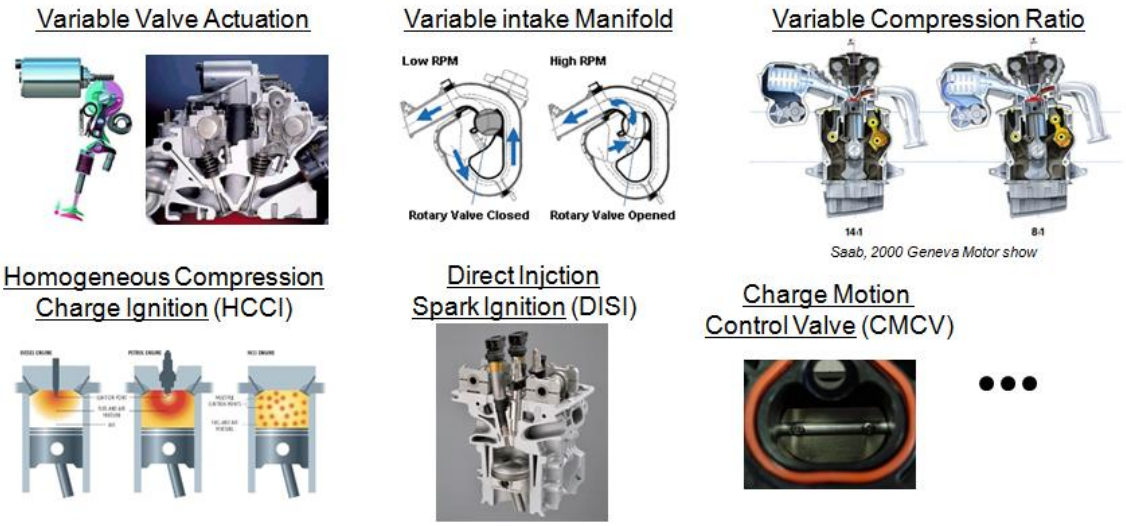

Figure 1-1 Various new technologies to improve engine performance

To improve the engine performance, various new technologies have been introduced for satisfying these requirements. These new technologies include variable valve actuation (VVA), variable intake manifold, variable compression ratio (VCR),

homogeneous charge compression ignition (HCCI), direct injection spark ignition (DISI), and charge motion valves (CMV) to enhance combustion as illustrated in Figure 1-1. Although the new technologies increase hardware potential to achieve better fuel economy, higher torque output, lower noise and vibration, and less emission, they also increase the complexity of engine systems.

The increased complexity introduces two problems, which are optimal engine calibration and transient control to use the full hardware potential. For a conventional engine, engine calibration can be realized using experiment based methodology. Engine transient control is generally executed by the map based feed forward (FF) control, which uses steady-state actuator set-point maps and correction maps of transient engine operation. In contrast, for high DOF engines, faster and more efficient engine calibration methodology is required, because the increase of the DOF of the engine system expands the number of experiments dramatically. To support simulation based engine calibration and transient control, virtual sensing methods to sense engine states and responses have been researched [14], yet, restricted to the simple replacement of physical sensors.

To calibrate high DOF engines, simulation based methodologies have been used for variable valve timing engines [12, 13]. The previous researches usually considered fuel economy and toxic emissions at part load condition as well as output power at full load condition. In addition to the performance and fuel economy, combustion stability becomes other important calibration objective to improve vehicle drivability and driving feel, so it must be predicted in real time. However, real time prediction methodologies of combustion stability have rarely been proposed. In this study, simulation based engine optimal calibration is extended to a multi-objective calibration problem with the

consideration of fuel economy and combustion stability with the support of several virtual sensing methodologies.

Transient control of high DOF engines is another important research area to achieve the full hardware potential. Transient control of engines has been improved long time by many researchers. To design transient control of engines, modeling of engine for the control purpose is the first step. Hence, control oriented models (COM) of engines were proposed and validated by many researchers [15-18]. Although many COMs have been developed for the purpose of the transient control of different types of engines, few engine models cover the whole engine operating ranges considering detailed combustion processes. Thus, a sophisticated COM, which is able to address accurate engine combustion processes, is necessary for the purpose of transient control design.

To manage engine transients, various control methods have been introduced. When a small number of actuators are used to control engines, classical proportional-integral-derivative (PID) control is widely used to improve the engine transient performance [19]. To deal with MIMO system, linear quadratic gaussian (LQG) control was introduced [20]. While applying state feedback control without the linearization procedure, a nonlinear turbo engine model was directly used to manage transience [21]. As another approach to handle system nonlinearity directly, lyapunov function based nonlinear control was applied for transience control of engines [22, 23]. Although many control methodologies have been used to manage engine transients, few methodologies can satisfy sufficient performance specification while achieving system stability at the same time. Thus, in this study, nonlinear model predictive control (NMPC) is proposed to resolve the difficulties in achieving required engine performance under fast transient operating conditions.

1.2 Prerequisites

A realistic way to calibrate conventional engines is generally restricted to steady-state engine operations due to the difficulties in address all possible transience. Although the engine calibration considering transient engine operations is one possible method to improve the transient response of engines, a large number of DOF make it exceptionally difficult due to the excessively large number of all possible combinations of engine transient operating trajectories. The resulting calibration maps require extremely large amount of memory space to store the information of all possible engine transient operations. In most of conventional engines, transient engine control is realized by using the FF control based on the optimally calibrated steady-state actuator set-point maps.

To deal with these optimal calibration problems and transient control problems, adequate simulation tools and virtual sensing methodologies are developed as the prerequisites. The steady-state engine calibration of a high DOF engine is still difficult due to the system complexity. Developing systematic optimal calibration procedures is indispensable to find the optimum actuator set-point maps of a high DOF engine. Then, transient control problems improve transient responses of the target engine.

1.2.1 Simulation Tools as the Substitutes of Experiments

In experiment based engine calibration procedures, exploring all possible engine operating conditions is difficult because of the possible system instability and failure at extreme engine operating conditions. The experiment based engine calibration procedure

is widely used to find the optimal actuators set-point maps with low system complexity. When the number of actuators increases, the number of possible actuator operating combinations is so large that the required time and cost of experiments may exceed the limited resource for engine development. In addition, the high interactions of each actuator on system responses require a systematic way to achieve synergy of actuators.

Simulation based calibration methodology provides a possibility to resolve the problems arising from experiment based engine calibration. Recently, the rapid expansion of computing power and evolving computer aided engineering (CAE) tools enables to predict engine responses with sufficient accuracy accompanying shorter computation time and lower computation cost. Moreover, predictive engine simulation models enable to estimate immeasurable engine responses, which can be used as possible engine calibration objectives.

Therefore, high-fidelity simulation tools are introduced as one of the most powerful tools that are able to treat the increasing system complexity [12,13]. The high-fidelity simulation tools are composed by one-dimensional (1-D) gas dynamics simulation models and quasi-dimensional (quasi-D) combustion models. Although the accuracy of high-fidelity simulation is sufficiently enough to emulate a real engine, the computation time is too long to apply the simulation to the optimal calibration procedure. To overcome the long computation time, artificial neural network (ANN) models are used in this study as fast surrogate models with their capability of learning underlying highly non-linear input-to-output relationships.

1.2.2 Virtual Sensing Methodology of Engine States and Responses

Fast and accurate measurements of engine states and responses is essential for both engine calibration and transient control problems, since more information of engine states and responses enables delicate engine calibration and accurate engine control. However, several engine responses are rarely measured in real engines because of the sensing difficulties and sensor costs. These responses include the mass air flow rate into a cylinder of a complex flexible intake system, the combustion stability, the specific emissions, and the residual gas fraction.

In this study, two virtual sensing methodologies are investigated for estimating the mass air flow rate and the combustion stability respectively. The virtual sensing of the mass air flow rate is realized by introducing ANN models accounting for ambient pressure compensation. The virtual sensing of combustion stability is achieved by using statistical regression analysis considering combustion characteristics. The developed virtual sensing methodologies can be applied to other immeasurable engine states and responses for the purpose of solving various calibration and control problems.

1.3 Research Objectives

The maximum potential performance of a high-degree-of-freedom engine with multiple variable devices critically depends on optimal engine calibration and transient engine control. The optimal engine calibration is a procedure that determines the actuator set-points to achieve the best engine performance over the whole engine operating

conditions. As the DOF of an engine system increases, engine calibration procedures become more complex. The size of the typical mapping problem increases exponentially to the unmanageable point beyond the experimental capability in the test cell. The optimal calibration can be achieved only with a systematic procedure that relies on optimization algorithms. Although experimental approach using a design-of-experiments is capable of calibrating engines, the true optimization is expected to be greatly facilitated with the availability of predictive models and a "*virtual engine system*". As long as the sensitivity of the engine simulation to independent variables corresponds to the sensitivity of the physical system, the search for the optimum is expected to be reliable. In addition, some engine states cannot be directly measured, and model-based estimation (or virtual sensing) becomes necessary for realizing the full benefits for the optimization framework for high DOF system.

The transient control of a high DOF engine is another important issue for improving the engine performance under engine transient operating conditions. Since a high DOF engine is an extremely non-linear system, developing an adequate transient control method has been a challenging problem. Because of the high non-linearity of engine systems, few clear methodologies for transient control have been proposed for covering the entire engine operating conditions.

To use advanced modern control methodologies to a transient control of a high DOF engine, creating an accurate and fast control oriented model (COM) is proposed in this study. The COM must be capable of accurately estimating necessary engine states and responses. However, few studies have introduced unified engine models that simultaneously capture intake, combustion, and exhaust process with sufficient accuracy.

With the difficulties in estimating engine responses, transient control of engines has been commonly achieved using FF control based on the steady-state actuator set-point maps and compensation maps. However, generating adequate compensation maps for transient operations requires excessive time and effort even in the case of a conventional low DOF engine, and the strategies applicable to truly high DOF systems have not been demonstrated.

In this study, the optimal calibration and transient control of high DOF engines are investigated to achieve the ultimate performance of a high DOF engine over entire engine operating ranges. The proposed methodologies can be applied to other complex systems without loss of generality. The expected key contributions include multi-objective optimal calibration technique capable of considering cycle-to-cycle variability, techniques for generating virtual sensor sand inverse models necessary for setting up the optimization frameworks, and design of the nonlinear model predictive control (NMPC) for managing high DOF engine's transients.

1.3.1 Optimal Calibration of a High DOF Engine

To find set-point maps efficiently, systematic procedures for the optimal calibration of a high DOF engine are proposed by using fast and accurate engine models accompanying virtual sensors. As reference inputs for engine transient control, optimally calibrated actuator set-point maps play important roles in improving engine performance. In general, the objective of engine calibration at part load operating conditions is minimization of fuel consumption. In addition to the fuel economy, combustion stability

becomes another critical issue to improve the noise, vibration, and harshness (NVH) of a vehicle. Although the combustion stability determines the smoothness of engine operations, the combustion stability cannot be directly measured in a commercial engine in real time. The combustion stability is measured using the gathered cylinder pressure data over several tens of experiments. Thus, the indirect estimation method of combustion stability needs to be developed to incorporate the combustion stability into engine calibration problems. The development of the virtual sensing methodology for various engine states and responses makes it possible to consider combustion stability as an objective of optimal engine calibration problems.

To deal with a large number of actuators, a systematic engine calibration procedure is proposed by creating an optimal calibration framework. The engine systematic calibration determines the optimal actuator set points over the whole engine operating ranges. For the optimal engine calibration, the multi-objective function is composed using the trained ANN model of the target engine and a virtual sensing of the combustion stability.

1.3.2 Transient Control of a High DOF Engine

Adequate transient control designs are necessary to improve engine responses under transient operating conditions. Although the optimal calibration of a high DOF engine is achieved by considering multi-objectives in steady state engine operating conditions, engine control based on map based FF control cannot guarantee the best engine performances under transient operating conditions. In this study, the nonlinear model

predictive control (NMPC) is used as a preferred control methodology for achieving ultimate engine performance and rejecting undesirable engine responses such as emission peaks and instant combustion instability.

1.4 Outline

Chapter 2 introduces the high-fidelity simulation tools for a high DOF engine, which are composed of 1-D gas dynamic simulation and a quasi-D phenomenological combustion model. The high-fidelity simulation tools have modeling flexibilities to realize new devices that modify gas passages and predict combustion variations with changes of air-to-fuel ratio, residual fraction, and turbulence in the cylinder. The accurate estimation of combustion processes, regardless of engine operating conditions, is achieved by tuning parameters of quasi-D combustion models and calculating the precise flame front area maps.

Next, virtual sensing methodologies are proposed in Chapter 3 and Chapter 4. Since the accurate estimation of the mass air flow rate is critical for the calibration and control of a high DOF engine, the virtual sensing methodology of the mass air flow rate is proposed in Chapter 3. The virtual sensing of the mass air flow rate is realized using trained ANN models with high-fidelity simulation results. As another virtual sensing variable, combustion stability is selected, because the combustion stability cannot be determined in real time and it is necessary to improve engine smoothness, quietness, and driving feel. The measure of combustion stability is coefficient of variation in indicated mean effective pressure (COV_{IMEP}), hence, processing of pressure traces from many

consecutive cycles is necessary for quantitative analysis. Statistical analysis of experimental data with the consideration of the physics of the combustion process is used to correlate the COV_{IMEP} to combustion parameters. The estimation of combustion stability and the selection of key independent variables are realized using a statistical regression analysis of the experimental results. The created virtual sensors are used for the optimal calibration and transient control of engines.

Chapter 5 addresses the optimal calibration of a high DOF engine considering both fuel economy and combustion stability objectives. First, the optimization framework is designed to calibrate engines efficiently over the whole engine operating ranges. Then, the objective function of the optimal calibration is formulated with the consideration of fuel economy and combustion stability. Since the fuel economy and the combustion stability have trade-off relations, an optimization problem with multi objectives is formulated by an introducing weight for each objective. The weights are determined to achieve the best fuel economy while maintaining combustion stability at part load operations. To improve the efficiency of the optimization process, inverse ANN models are introduced as one part of the objective function. At the same time, regular ANN models are also used to estimate immeasurable engine states. With this objective function and constraints, an optimization procedure is proposed to find global optima. The global optimization procedure is composed of two steps, which are to find an adequate initial point and to find a local optimum using SQP as a gradient based algorithm.

Based on the achieved optimal calibration results and the developed virtual sensing methodologies, transient control for a high DOF engine is investigated in Chapter 6 and Chapter 7. First, the COM is created by consisting of a manifold dynamics model, a

rotating dynamics model, and an accurate combustion model. Then, NMPC is designed to improve transient engine responses by compensating for excursions of operating penalty due to a finite response time of actuators and unavoidable physical delays. While applying the NMPC to the transient control of a high DOF engine, a finite control period and prediction period are determined to achieve dead-beat control and smooth engine responses. Finally, the resulting engine responses by the NMPC are evaluated by comparing conventional FF control results. The results indicate faster engine responses with the NMPC without undesirable excursions of engine responses and associated spikes of emissions.

REFERENCES

1. M. E. Pitstick, D. J. Santini, and H. Chauhan, “Reduction in Global Warming due to Fuel Economy Improvements and Emissions Control of Criteria Pollutants: New US. Liaht-Duty Vehicles (19684991)”, SAE Technical Paper No. 929188.
2. S. P. Ho, and T. A. Renner, “Global Warming Impact of Gasoline Vs. Alternate Transportation Fuels”, SAE Technical Paper No. 901489.
3. R.L. Evans, “Reducing Global Warming with Innovative Transportation Technology”, SAE Technical Paper No. 2005-24-028.
4. J. M. Ogden, T. G. Kreutz, and M. Steinbugler, “Fuels for Fuel Cell Vehicles: Vehicle Design and Infrastructure Issues”, SAE Technical Paper No. 982500.
5. M. Brekken, and E. Durbin, “An analysis of the true efficiency of alternative vehicle powerplants and alternative fuels”, SAE Technical Paper No. 981399.
6. C. A. Kukkonen, and M. Shelef, “Hydrogen as an Alternative Automotive Fuel: 1993 Update”, SAE Technical Paper No. 940766.
7. D. F. Polletta, T. Louckes, and A. J. Severinsky, “Fuel Economy and Performance Impact of Hybrid Drive Systems in Light Trucks, Vans & SUV's”, SAE Technical Paper No. 2001-01-2826.
8. K. Jaura, W. Buschhaus, and M. A. Tamor, “Systems Approach in Achieving Higher Fuel Economy in Hybrid Vehicles”, SAE Technical Paper No. 2000-01-1585.
9. D. J. Santini, A. D. Vyas, and J. L. Anderson, “Fuel Economy Improvement via Hybridization vs. Vehicle Performance Level”, SAE Technical Paper No. 2002-01-1901.
10. G. J. Suppes, “Plug-In HEV Roadmap to Hydrogen Economy”, SAE Technical Paper No. 2005-01-3830.
11. E. D. Tate, Michael O. Harpster, and Peter J. Savagian, “The Electrification of the Automobile: From Conventional Hybrid, to Plug-in Hybrids, to Extended-Range Electric Vehicles”, SAE Technical Paper No. 2008-01-0458.
12. B. Wu, R. G. Prucka, Z. S. Filipi, D. M. Kramer, and G. L. Ohl, “Cam-Phasing Optimization Using Artificial Neural Networks as Surrogate Models – Maximizing Torque Output”, SAE Technical Paper No. 2005-01-3757, 2005.
13. B. Wu, R. G. Prucka, Z. S. Filipi, D. M. Kramer, G. L. Ohl, “Cam-phasing Optimization Using Artificial Neural Networks as Surrogate Models – Fuel Consumption and NOx Emissions”, SAE Technical Paper No. 2006-01-1512, 2006.
14. B. Wu, Z. S. Filipi, D. N. Assanis, D. M. Kramer, G. L. Ohl, M. J. Prucka, and E. DiValetin, “Using Neural Networks for Representing the Air Flow Rate through a 2.4 Liter VVT Engine”, SAE Technical Paper No. 2004-01-3054.
15. E. Hendricks, and S. C. Sorenson, “Mean value modeling of spark ignition engines”, SAE Technical Paper No. 900616, 1990.

16. A. G. Stefanopoulou, J. A. Cook, J. S.Freudenberg, and J. W. Grizzle, "Control-Oriented Model of a Dual Equal Variable Cam Timing Spark Ignition Engine", , *ASME Journal of Dynamic Systems, Measurement, and Control*, vol. 120, pp. 257-266, 1998.

17. M. Livshiz, M. Kao, and A. Will, "Validation and Calibration Process of Powertrain Model for Engine Torque Control Development", SAE Technical Paper No. 2004-01-0902, 2004.

18. A. G. Stefanopoulou, J. S. Freudenberg, and J. W. Grizzle, "Variable Camshaft Timing Engine Control", *IEEE Transaction on Control Systems Technology*, Vol 8, No. 1, pp 23-34. January 2000.

19. D. Blomqvist, S. Byttner, U. Holmberg, and T. S. Rognvaldsson, "Different Strategies for Transient Control of the Air-Fuel Ratio in a SI Engine", SAE Technical Paper No. 2000-01-2835, 2000.

20. S. C. Hsieh, J. S. Freudenberg, and A. G. Stefanopoulou, "Multivariable Controller Structure in a Variable Cam Timing Engine with Electronic Throttle and Torque Feedback", *Proc 1999, Conf. on Control Applications*, pp. 465-470, 1999.

21. A. Ekdahl, "Transient Control of Variable Geometry Turbine on Heavy Duty Diesel Engines", *Proceedings of the 2005 IEEE Conference on Control Applications*, pp. 1228-1233, 2005.

22. M. Jankovic, and I. Kolmanovsky, "Constructive Lyapunov Control Design for Turbocharged Diesel Engines", *IEEE Transactions on Control Systems Technology*, Volume 8, Issue 2, Page(s):288 - 299 , 2000.

23. J. Chauvin, G. Corde, and N. Petit, "Transient control of a Diesel engine airpath", *Proceedings of the 2007 American Control Conference*, pp. 4394-4400, 2007.

CHAPTER 2

A CALIBRATION METHODOLOGY OF A QUASI-DIMENSIONAL COMBUSTION MODEL FOR THE ANALYSIS OF ADVANCED SPARK IGNITION ENGINES

2.1 Introduction

The gasoline spark ignition (SI) engine possesses a main place in the automotive industry, with its relative simplicity, high power density, smoothness, and relatively low emissions. To compete with other propulsion systems, such as common rail direct injection diesel engines and hybrid-electric powertrains, gasoline engines need to be more fuel efficient and more powerful to maintain attractiveness. At the same time, combustion stability at low engine speed and load, especially at the idle condition, is another important emerging issue to achieve better NVH performance. Combustion stability is often realized by applying dual spark plugs [1], increasing charge motion with adequate intake port design and additional turbulence generating devices [2-4]. To assess the feasibility of the effectiveness of new technologies, accurate prediction of engine responses is important in overall engine development procedure.

To predict the engine responses along with these newly introduced technologies, computer simulations have been widely used as alternatives of experiment. The computer

simulations enable to emulate engine performances. The simulation models can be ranging from highly detailed three dimensional computational fluid dynamics (CFD) models [5,6] to simplified mean value engine models [7,8]. In general, engine calibration problems require a large number of simulations to cover all possible engine operating conditions with sufficiently high accuracy. Thus, a large number of simulations limit system modeling complexity because of the limitations of computation power and time. To satisfy the computational limitations, a one-dimensional (1-D) gas dynamic simulation accompanying with a quasi-dimensional (quasi-D) phenomenological combustion model [9-11] is selected as a preferred engine simulation tool (called a high-fidelity simulation tool), because of its fast computation time and relatively high simulation accuracy. Moreover, the selected high-fidelity simulation tool is capable of modeling flexible hardware configurations by considering various gas passages and tweaking combustion model parameters.

The high-fidelity simulation is created using a co-simulation approach. The 1-D gas dynamics model is created using the Ricardo WAVE [12, 13] and it is capable of predicting the mass air flow rate into the cylinder with respect to variable valve timings and lifts. The quasi-D combustion model enables to predict combustion process with a sufficiently accuracy and short calculation time. The quasi-D model includes combustion chamber geometry for calculating turbulent flame propagation and heat transfer in engine cylinders to improve simulation accuracy. The quasi-D model was programmed with the name of the spark-ignition simulation (SIS) that is written in FORTRAN language. The SIS has a capability of capturing various combustions at different hardware configurations by tuning combustion model parameters. Due to the predictiveness of the

combustion model, the simulation code has been used in 2- and 4-valve SI engine turbocharger matching studies [9], in valve event optimization studies [10], and in optimizing stroke-to-bore ratio for SI engine design studies [11].

Overall the previous researches using the quasi-D combustion model have restricted to the investigation of combustion characteristics related to parameters of the combustion chamber and in-cylinder combustion processes. However, newly introduced flexible intake system configurations significantly impact on the in-cylinder combustion characteristics, thus, the changes of the combustion characteristics must be considered in the quasi-D combustion simulation. For example, turbulent intensity into the cylinder is significantly increased by an installed device upstream of the combustion chamber. Thus, the increased turbulent intensity changes combustion characteristics significantly, although all parameters related to the combustion chamber hardware remain exactly same. To take into account the flexible intake system configurations, the quasi-D combustion model must be calibrated in systematic ways to capture the effect of the changed upstream flow characteristics on the combustion characteristics due to the newly introduced devices upstream of the combustion chamber.

In this study, a dual-independent variable valve timing (di-VVT) engine accompanying charge motion valves (CMVs) is selected as a preferred engine system to simultaneously improve engine performance, combustion quality, and fuel economy considering cost-effectiveness. The CMV is an air flow restriction device that generates turbulence into a combustion chamber for fast burning rate and is located upstream of the intake valves. The CMV has two operating positions, which are unblocked and blocked positions. At the unblocked position, the CMV valve is aligned parallel to a gas passage.

At blocked position, the CMV valve is aligned perpendicular to a gas passage, thus, increasing turbulence intensity. In this study, the quasi-D combustion model for the di-VVT engine with the CMV is calibrated based on the proposed systematic calibration procedure of the quasi-D combustion model.

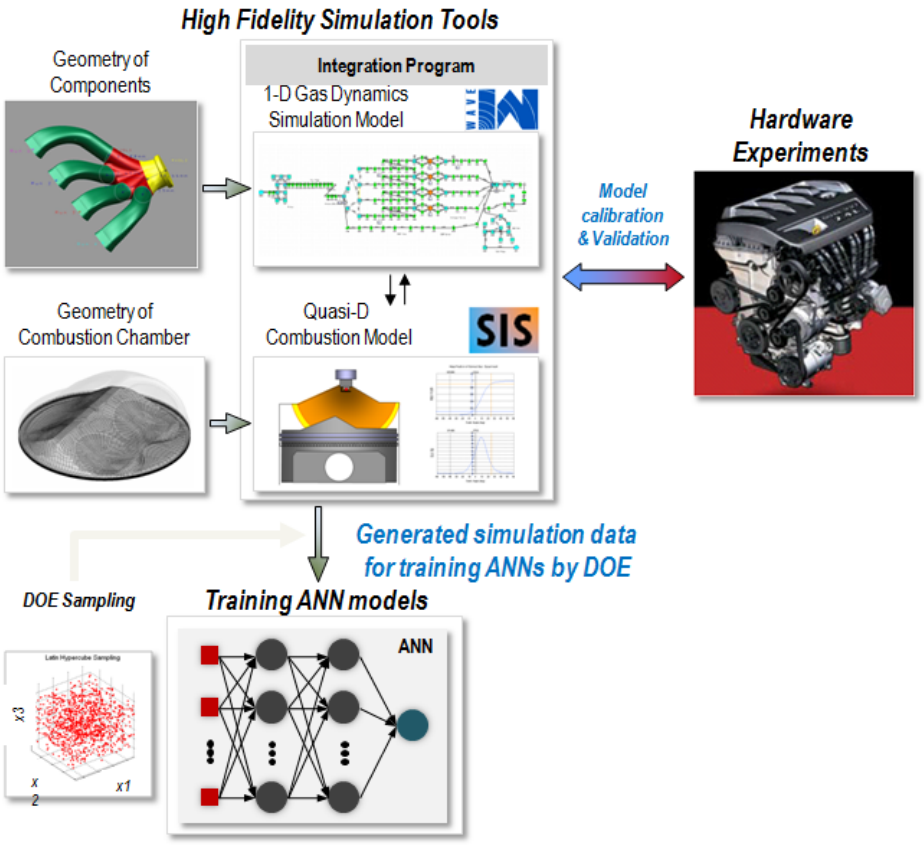

Figure 2-1 Illustration of the procedure to build a fast and accurate non-linear engine model

The ultimate objective of developing the systematic calibration methodology of a quasi-D combustion model is to create fast and accurate engine simulation models for the purpose of optimal engine calibration. Figure 2-1 illustrates one approach of creating a fast and accurate non-linear steady state engine model based on the high-fidelity

simulation. Since the optimal calibration and control design procedure require sufficiently a fast and accurate engine model, artificial neural networks (ANNs) are used as one of the promising methodologies for capturing engine system behavior predicted by a high-fidelity simulation.

This chapter presents a systematic calibration procedure of a quasi-D combustion model for advanced spark ignition engines. First, the high-fidelity simulation tools structure are introduced for a di-VVT engine accompanying the CMV. Then, three parameters, which are flame front area maps, C_{β}, and C_{M}, are selected as tuning parameters for capturing various combustion conditions. The influence of each parameter on the combustion simulation results is analyzed using sensitivity analysis. Finally, the calibrated simulation model is validated by comparing with the experimental data.

2.2 Target Engine

The selected target engine is the Chrysler dual overhead camshaft (DOHC) 2.4 liter inline four (I4) cylinder spark ignition (SI) engine with the di-VVT device and the CMV. Two intake valves and two exhaust valves are used per cylinder and actuated by the dual overhead camshaft. A cast iron cylinder block and an aluminum head structure with pent-roof combustion chamber are used for the skeleton of this engine. Separate ports are assigned to each valve and merged together. The intake manifold is made by composite material for mass reduction while maintaining structure stiffness, and four runners are merged to a plenum chamber at a single point. The CMV is introduced upstream of the intake manifold ahead the intake valves to generate high turbulence for fast combustion

and improved combustion quality. The exhaust manifold has a one piece cast iron structure with a four-to-one runner design. Cast aluminum pistons with pop-up heads are used for achieving light weight and demanded compression ratio. The target engine is originally designed as a conventional fixed-camshaft engine, and dual independent VVT devices are added recently. The di-VVT devices are actuated by two vane type hydraulic type actuators. The critical parameters of the target engine are summarized in Table 2-1.

Table 2-1 Critical parameters of the target engine

Displacement	2.4 liters
Bore/Stroke	87.5/101.0 mm
Compression Ratio	9.4:1
Max. Intake Valve Lift	8.25 mm
Max. Exhaust Valve Lift	6.52 mm
Default Intake Valve Timing Closes/Opens/ Centerline	51^{o} ABDC/ 1^{o} BTDC/ 115^{o} ATDC
Default Exhaust Valve Timing Closes/Opens/ Centerline	9^{o} ATDC/ 51^{o} BBDC/ 111^{o} BTDC
Default Valve Overlap	9^{o} @ 0.5 mm lift
Allowed Intake Cam-phasing Range	$\pm 15^{o}$ Crank Angle
Allowed Exhaust Cam-phasing Range	$\pm 15^{o}$ Crank Angle

2.3 High-fidelity Simulation Tools

The high-fidelity simulation tools consist of a 1-D gas dynamics simulation model, a quasi-D combustion model, and an integration module. To improve the prediction capability of the combustion process over all possible engine operating conditions, quasi-

D combustion model replaces the combustion model in the 1-D gas dynamics simulation model. Thus, gas exchange process related engine states, such as mass flow rate, gas velocity, temperature and composition through intake and exhaust valves, are predicted by the 1-D simulation. Combustion related engine responses are predicted by the quasi-D combustion simulation.

2.3.1 Integration of the 1-D Gas Dynamics Simulation model and the Quasi-D Combustion Simulation model

The 1-D gas dynamic simulation (The Ricardo WAVE) and the quasi-D combustion simulation (SIS) are integrated by a top-level program written in C++ language. That program was originally developed by Wu et al. [18-20] and modified for this study. The overall configuration of the integration program is illustrated in Figure 2-2. First, the integration program calls the 1-D simulation with an initial guess of the burning rate profile to calculate the gas exchange through intake and exhaust valves. Next, the integration program carries the 1-D simulation results to the quasi-D simulation which calculates the burning rate profile, engine output torque, and emissions. Then, the integration program transfer the burning rate profile back to the 1-D simulation for next interaction until the converge criteria including error tolerances of indicated mean effective pressure (IMEP), residual fraction, and volumetric efficiency are satisfied.

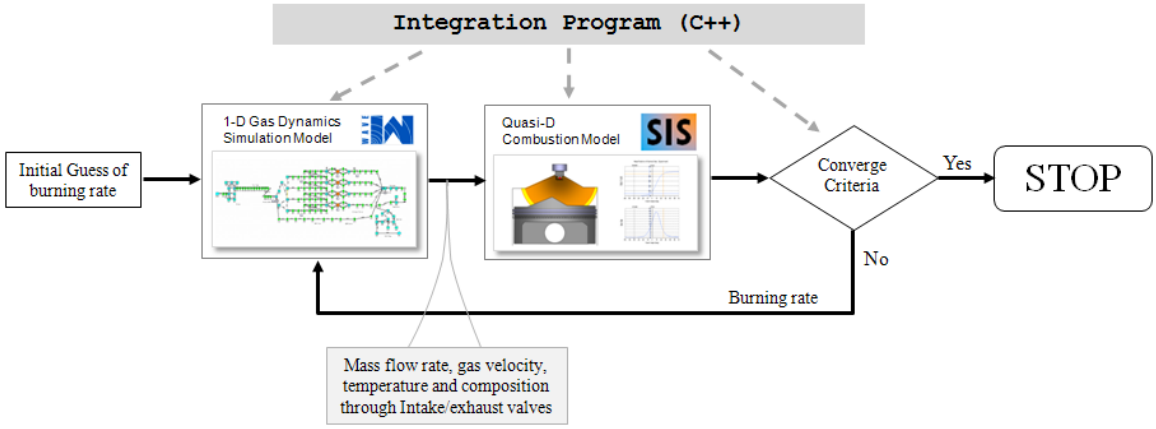

Figure 2-2 Integration of 1-D gas dynamics simulation and Quasi-D combustion simulation

2.3.2 One-Dimensional Gas Dynamics Model

The 1-D gas dynamics model, which is one part of the high-fidelity simulation tools, is created with the commercial software Ricardo WAVE including all air flow paths from the air box to the exhaust tail pipe to predict the accurate gas dynamics. Figure 2-3 shows the gas dynamics simulation model of the entire engine. The piping and manifolds of the intake and exhaust systems are modeled by using duct and junction components. First, the cylinder block is modeled. Each cylinder has two intake and exhaust valves and ports. Air flow paths are connected to the cylinder head to intake and exhaust runners. Air flow coefficients through the valves are found by using experimental data provided by Chrysler LLC, and these values are critical factors to estimate mass air flow rate into the cylinders with high-fidelity. Then, each component of the 1-D gas dynamics model is modeled using exact three-dimensional CAD data, and two-dimensional drawings provided by Chrysler LLC to guarantee the simulation accuracy.

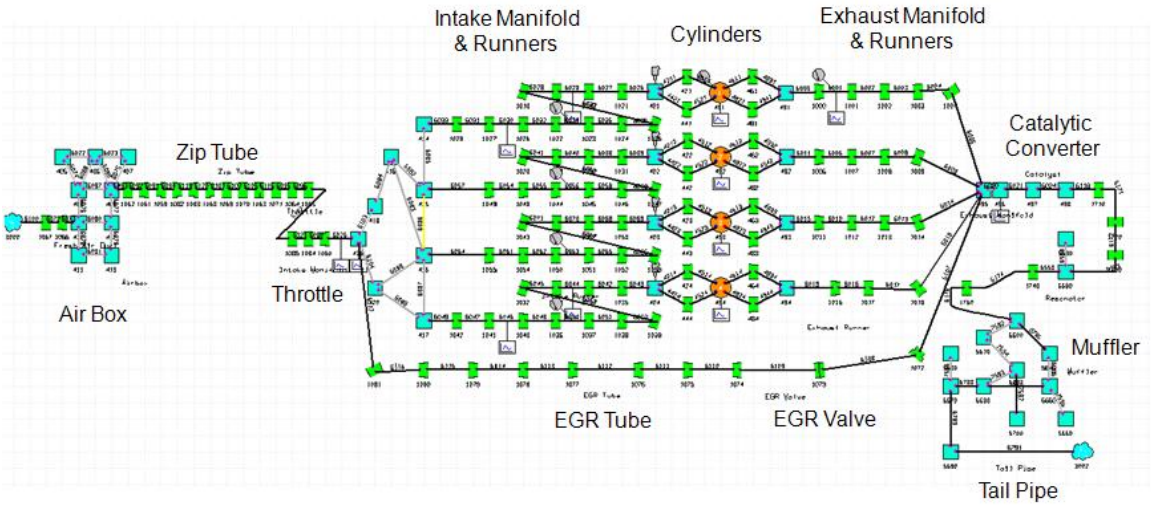

Figure 2-3 One-dimensional gas dynamics simulation model built by the Ricardo WAVE

The throttle valve is emulated by a simple orifice because of the modeling convenience. The maximum orifice diameter is restricted to the maximum intake air path diameter at the throttle body position. The maximum diameter of the orifice is considered as the WOT position. For part load conditions, a throttle opening position is mapped to an equivalent throttle diameter. The equivalent throttle diameters are determined along the different engine operating points by experiments or high-fidelity simulations. Then, the quasi-D combustion model is incorporated as a combustion model for the 1-D gas dynamics simulation to accurately predict combustion characteristics over whole possible engine operation conditions from the idle to the WOT conditions.

2.3.3 Quasi-Dimensional Spark-Ignition Combustion Model

The quasi-D SI engine combustion model (SIS) is based on mass and energy conservation and phenomenological models for turbulence, combustion and heat transfer

in a cylinder. The combustion sub-model is based on the turbulent flame entrainment model concept proposed by Tabaczynski et. al.[15,16], and further refined by Poulos and Heywood [17]. The combustion model is complemented by a single-zone turbulence model, which calculates crank-angle resolved global turbulence throughout the whole cycles. Flame propagation is assumed to move spherically from an ignition point. The governing differential equations are as follows.

The rate of mass entrainment is

$$\frac{dm_e}{dt} = r_u A_f (u' + S_L), \tag{2-1}$$

where m_e is the mass entrained, t is time, ρ_u is density of unburned charge, A_f is the flame front area, u' is turbulent intensity, and S_L is laminar flame speed. Since the magnitude of u' is usually a much larger than the laminar flame speed, the rate of mass entrainment strongly depends on the flame front area and turbulence. Therefore, the exact calculation of flame front area is critical to improve simulation fidelity.

The rate of burning is estimated by the characteristic velocity and length scale. The length scales of turbulence structure are divided into macroscale, L (or integral scale), Taylor microscale, λ, and Kolmogorov microscale, η. The macroscale is the measure of the size of a large energy containing flow structure. The Taylor microscale is useful in characterizing a turbulent flow. It is defined by relating the fluctuating strain rate of turbulent flow field to turbulence intensity. The Kolmogorov scale η defines the smallest structures of flow where small-scale kinetic energy is dissipated via molecular viscosity.

The rate of burning is

$$\frac{dm_b}{dt} = (m_e - m_b)/\tau \tag{2-2}$$

and

$$\tau = \frac{\lambda}{S_L}, \tag{2-3}$$

where m_b is the mass of burned products.

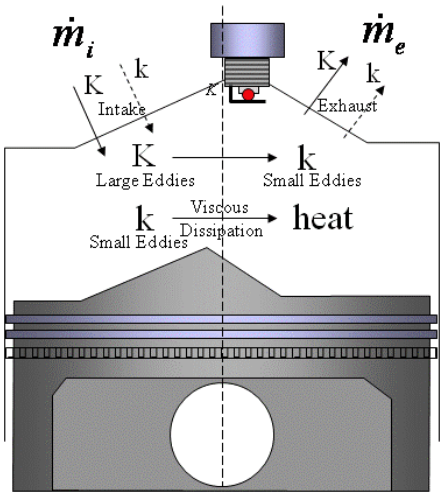

Figure 2-4 Turbulent energy cascade model to estimate turbulent flow

The turbulent model consists of a zero-dimensional energy cascade. Figure 2-4 illustrates the energy cascade model. Mean flow kinetic energy, *K*, is supplied to the cylinder through the valves. Then, the mean kinetic energy, *K*, is converted to turbulent kinetic energy, *k*, through a turbulent dissipation process. The turbulent kinetic energy is converted to heat through viscous dissipation. The mean and turbulent kinetic energy flows into and out of the cylinder through intake valves and exhaust valves. The equations for a zero-dimensional energy cascade are as follows.

$$\frac{dK}{dt} = \frac{1}{2}\dot{m}_i v_i^2 - P - K\frac{\dot{m}_e}{m}\ , \tag{2-4}$$

$$\frac{dk}{dt} = P - m\varepsilon - k\frac{\dot{m}_e}{m}\ , \tag{2-5}$$

where $\dot{m}_i$ and $\dot{m}_e$ are mass flow rates into and out of the cylinder respectively. v_i is the gas flow velocity into the cylinder. ε is the dissipation rate of turbulent kinetic energy per unit mass by assuming turbulence is isotropic. P is the production rate of turbulent kinetic energy and calculated from the equation for turbulence production over flat plates. K is the mean kinetic energy and k is the turbulent kinetic energy defined as

$$K = \frac{1}{2}mU^2\ , \tag{2-6}$$

$$k = \frac{3}{2}mu'^2\ , \tag{2-7}$$

$$\varepsilon = \frac{u'^3}{L} = \frac{\left(2k/3m\right)^{3/2}}{L}\ , \tag{2-8}$$

$$P = 0.3307C_\beta (K/L)(k/m)^{1/2}\ , \tag{2-9}$$

where L is determined by the minimum vessel dimension and is assumed by

$$L = V/(\pi B^2/4) \le B/2\ , \tag{2-10}$$

where V is the instantaneous volume of the combustion chamber, and B is the cylinder bore diameter. C_β is an adjustable constant that tunes the production rate of turbulent kinetic energy with respect to flow patterns in the cylinder during compression and expansion process. When combustion starts, unburned charge is assumed to be

compressed with sufficiently fast rate. Then, non-linear interactions between eddies can be neglected and the angular momentum of each eddy can be assumed to be constant by rapid distortion theory. During combustion process, the conservation of mass and angular momentum of individual eddies leads to the following expressions,

$$L / L_0 = (\rho_{u_0} / \rho_u)^{1/3}, \tag{2-11}$$

$$u' / u'_0 = C_M (\rho_{u_0} / \rho_u)^{1/3}, \tag{2-12}$$

where C_M is a tunable parameter to ensure agreement with experiments. It is typically unity from medium to high load operation conditions. If the mass air flow with intentionally generated turbulence is inducted into the cylinder, this parameter is generally modified to a larger value than unity to capture the increased turbulence intensity.

2.3.4 The Implementation of the CMV into the High-fidelity Simulation

The CMV is a flip valve device that increases the turbulence intensity of air flow into the combustion chamber to improve combustion quality. Figure 2-5 illustrates the operation of the CMV. When the CMV is blocked, turbulence is generated through the restricted air passage, and pressure drops across the CMV. Although the pressure drop can be emulated introducing an orifice at the CMV position in the 1-D gas dynamics model, the increased turbulence intensity cannot be captured in the 1-D simulation model. Calculation of the energy cascade begins with the flow velocity through the intake valve, thus, cannot account for the turbulence enhancing devices mounted upstream of the

intake port. Thus, the parameter C_M in equation (2-12) of the quasi-D combustion model is used as a possible tuning parameter to adjust the turbulence intensity to the real value from experimental results at several operating conditions.

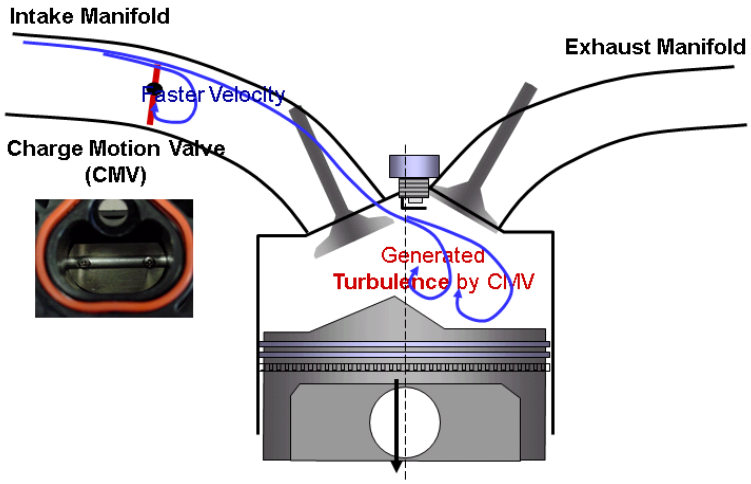

Figure 2-5 Generated turbulence by the CMV to increase combustion rate

2.4 Systematic Calibration Procedure of a Quasi-D Combustion Model

The calibration of the quasi-D combustion model is essential for improving the predictability of an ultimately non-linear engine combustion process. Although many parameters affect combustion process, we wish to choose only a small number of parameters for calibrating the quasi-D model to the all overall possible combustion cases. After intensive investigation of the combustion physics and many quasi-D simulation case studies, three parameters are selected as model tuning parameters. These parameters are: (1) flame front area maps in equation (2-1), (2) C_β in equation (2-9), and (3) C_M in equation (2-12). From the equation (2-1), the flame front area directly affects the mass

entrainment rate, thus shaping the mass fraction burn rate profile with respect to the crank angle. Other two parameters C_β and C_M play a significant role in manipulating zero-dimensional energy cascade. The C_β will be used to achieve accurate predictions of the overall turbulence levels, while the C_M enables an incremental increase of turbulence levels due to the effect of the CMV mounted upstream. The main objective of the quasi-D combustion model calibration is an accurate mass burned fraction profile prediction regardless of the system complexity.

2.4.1 Overall Calibration Procedure

The overall calibration procedure is shown in Figure 2-6. First, flame front area maps are calculated from the 3-D combustion chamber geometry. By using the generated flame front area maps, mass burn rate profile is predicted at the reference engine operation conditions. Then, the mass burn rate profile is reviewed for the compatibility. If turbulent intensity is generated upstream of the combustion chamber, for example, turbulence is generated by the CMV, the increased turbulence must be considered. To consider the turbulent intensity increase, the C_M must be tuned adequately. After determining the C_M value, the turbulent kinetic energy generation and dissipation process in the combustion chamber must be accurately estimated. Thus, the C_β is tuned to emulate the realistic zero-dimensional energy cascade process depending on the combustion chamber shapes and the in-cylinder flow pattern. These procedures are iterated until the desired combustion simulation results are achieved.

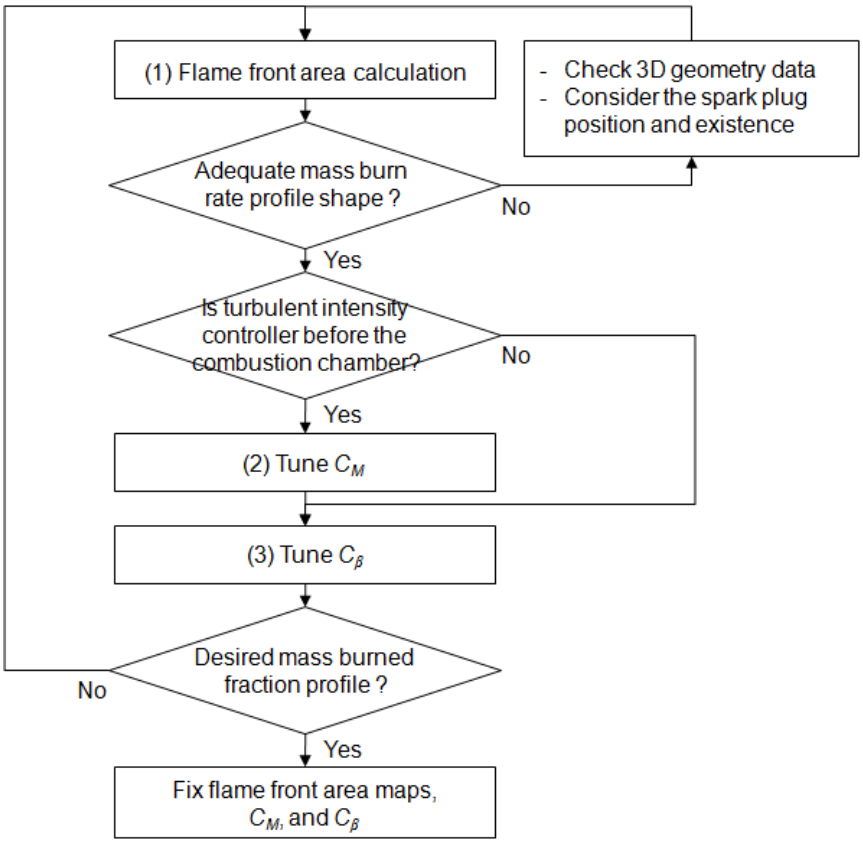

Figure 2-6 Systematic calibration procedure to achieve the highly accurate quasi-D combustion model

2.4.2 Flame Front Area Calculation

Flame front area is a factor critical to determine a mass fraction burned (MFB) profile as combustion characteristics. The MFB profile is a function of crank angle, and has an S-shaped curve as illustrated in Figure 2-7. The MFB profile consists of the flame-development angle ($\Delta\theta_d$), and the rapid-burning angle ($\Delta\theta_b$). The flame-development angle (the 0-10% burn duration), is the crank angle interval between the spark discharge and the time when a small but significant fraction of the cylinder mass has burned or fuel chemical energy has been released.

The rapid-burning angle (the 10-90% burn duration) is the crank angle interval between the end of the flame-development stage and the end of the flame-propagation process. The overall burning angle $\Delta\theta_o$ is the duration of the overall burning process, and it is the sum of $\Delta\theta_d$ and $\Delta\theta_b$. The flame-development stage is primarily influenced by mixture state, composition, and motion in the vicinity of the spark plug. Then, the rapid-burning process is influenced by the interaction between the flame front area and the combustion chamber walls. Thus, the flame front area can be considered as an influential factor common to both stages.

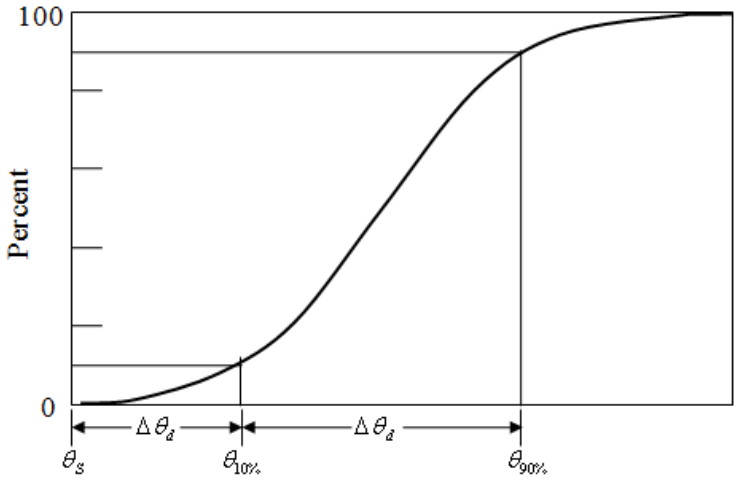

Figure 2-7 Definition of flame-development angle $\Delta\theta_d$, and rapid-burning angle $\Delta\theta_b$ on mass fraction burned versus crank angle curve

The calculation of the flame front area is critical to improve the accuracy of the combustion simulation. In equation (2-1), the interaction between the spherical flame front and the combustion chamber walls defines the flame front area A_f, which is the size of the reaction zone. To guarantee the accuracy of the flame front area calculation, exact

3-D CAD geometries provided by Chrysler LLC are used for the calculation of the flame front area as shown in Figure 2-8.

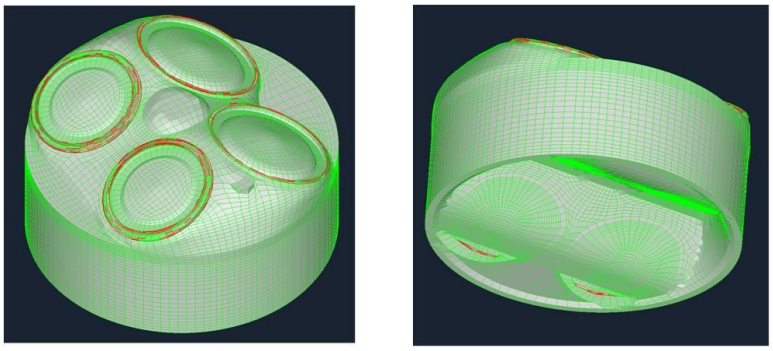

Figure 2-8 3-D CAD geometry of the target engine combustion chamber

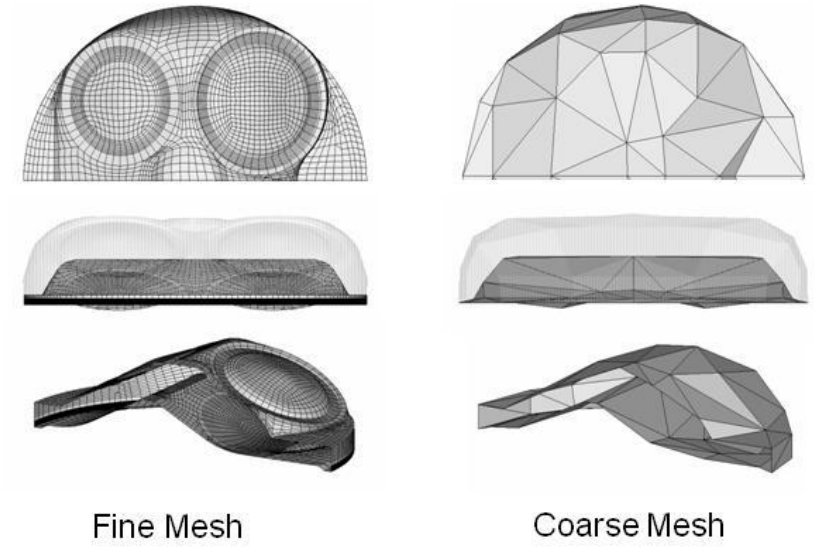

Figure 2-9 Pre-processed and simplified combustion chamber 3-D geometry using finite element pre-processor tools

The complexity of combustion chamber geometry requires accurate flame front area calculation to improve the simulation accuracy. The combustion chamber is a pent-roof shape and the piston top is raised up to maintain compression ratio. The 3-D CAD geometry is converted to adequate 3-D mesh data for calculating the flame front area

maps using a finite element pre-processing tool through a re-meshing procedure as shown in Figure 2-9. The flame front areas at each crank angle are calculated with the coarse mesh data to reduce the calculation time while maintaining the geometry accuracy.

To consider more realistic conditions at the flame front area at the flame development stage, the interference between a spark plug and flame front area is considered by a slight adjustment of the flame front area. In general, mass burn fraction profiles are largely affected by the flame front area. At the very beginning of a combustion process, the flame kernel is formulated near the spark plug. The flame-development angle, $\Delta\theta_d$, is largely affected by the flame front area and air-fuel mixture motion near the spark plug. Therefore, a small change of flame front area near the spark plug largely affects the flame-development period. Figure 2-10 illustrates the flame front area propagation at the beginning of combustion with the existence of the spark plug.

Then, the flame front area, which propagates toward the cylinder walls, cylinder head, and piston top, is calculated considering the intersection area between spherical flame front area and the combustion chamber. At the rapid burning stage, the mass burn fraction profile is accurately predicted by considering exact combustion chamber geometry and the exact spark plug position. Figure 2-11 illustrates the flame front area propagation until the flame front is reached the cylinder wall.

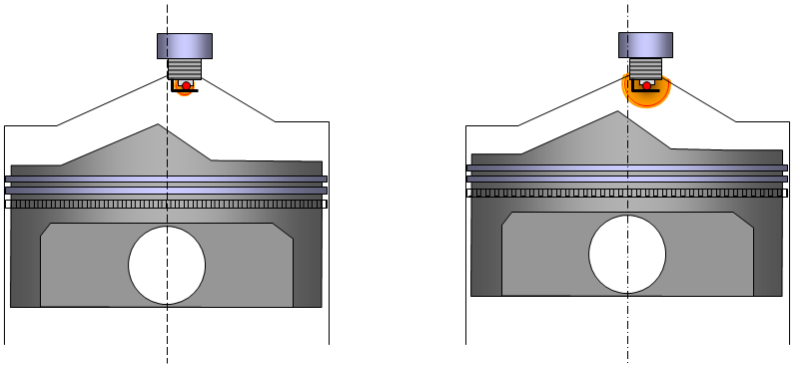

Figure 2-10 Illustration of flame front area propagation at the beginning of combustion and the consideration of spark plug existence

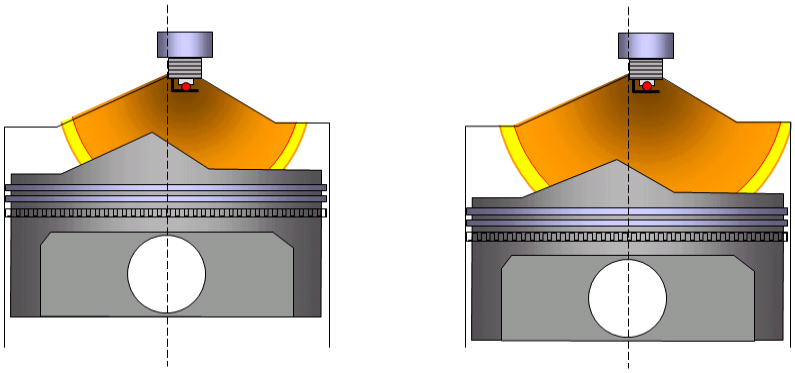

Figure 2-11 Illustration of flame front area propagation beyond the spark plug to the combustion chamber walls

2.4.3 Influence of Flame Front Area Maps

While calculating the flame front area maps over all possible piston positions in the combustion chamber, the exact 3-D geometry, the exact spark plug position, and the spark plug existence are used to attain the precise interaction between flame front and the combustion chamber wall. To show the influence of the change of the flame front area maps on the mass fraction burned profile, two different flame front area maps are

generated as shown in Figure 2-12. The flame front area maps in Figure 2-12 (a) are generated with an inaccurate spark plug position, and the flame front area maps in Figure 2-12 (b) are generated using an exact spark plug position.

During the combustion process, the flame front area increases as its radius extends until the flame reaches the combustion chamber walls. When the flame reaches to the cylinder wall, the flame front area rapidly decreases, and the flame is extinguished. The increase rate of the flame front area at the very beginning of the combustion process largely influences the flame-development angle. The peak shape and the final slope of the flame front area maps influence the mass fraction burned profile shape during the rapid-burning angle.

As shown in Figure 2-12 (a) and (b), the flame front area maps are significantly changed from the difference of the spark plug position. The different flame front area maps results in the different burning rate profiles, which characterize the combustion process. Figure 2-13 shows that burning rate profile and mass fraction burned profile are precisely predicted by using accurate flame front area maps calculation (case 2). When the flame front area map is calculated with inaccurate spark plug position (case 1), the combustion profile tends to be excessively skewed and not matched with the experimental data. Thus, calculating sufficiently accurate flame front area maps is the first step of the quasi-D combustion model calibration procedure.

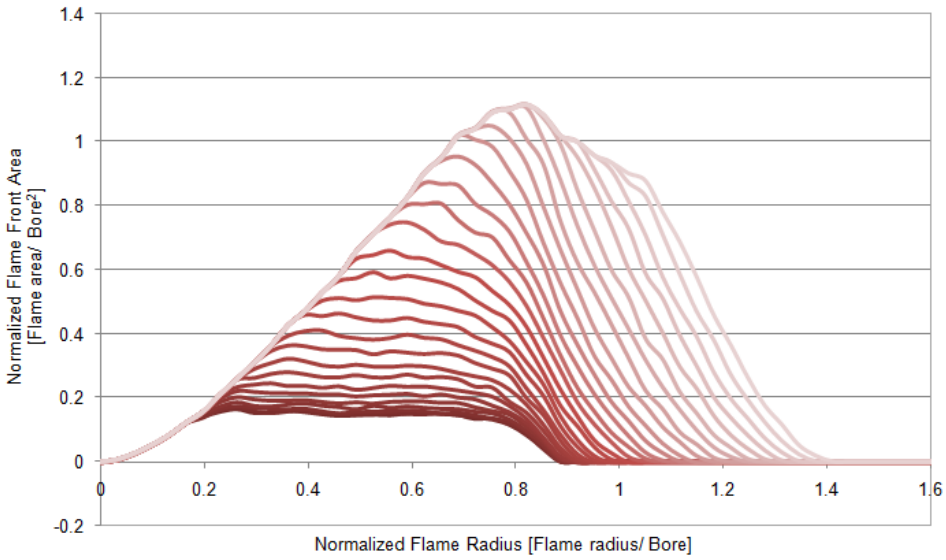

(a)

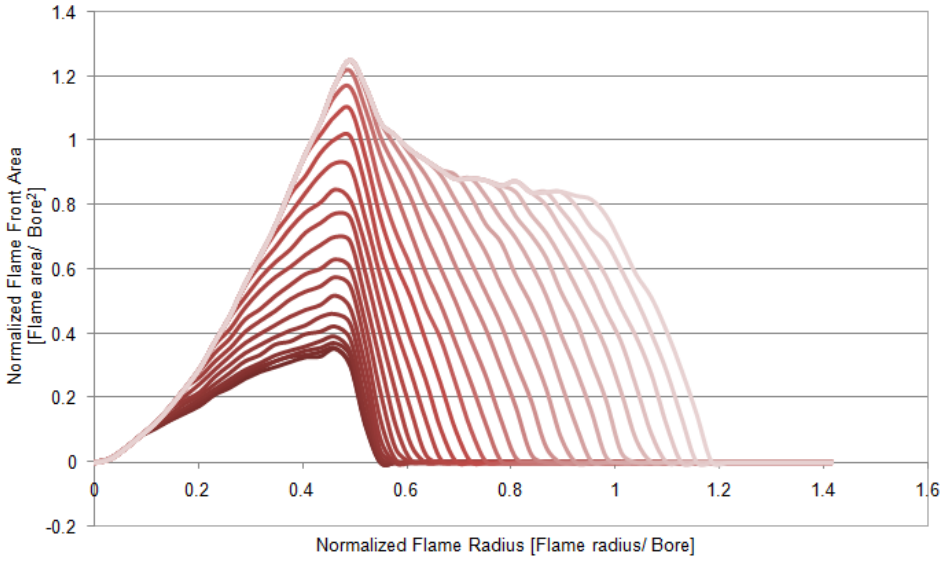

(b)

Figure 2-12 Comparison of flame front area maps: (a) with an inaccurate spark plug position; (b) with the accurate spark plug position

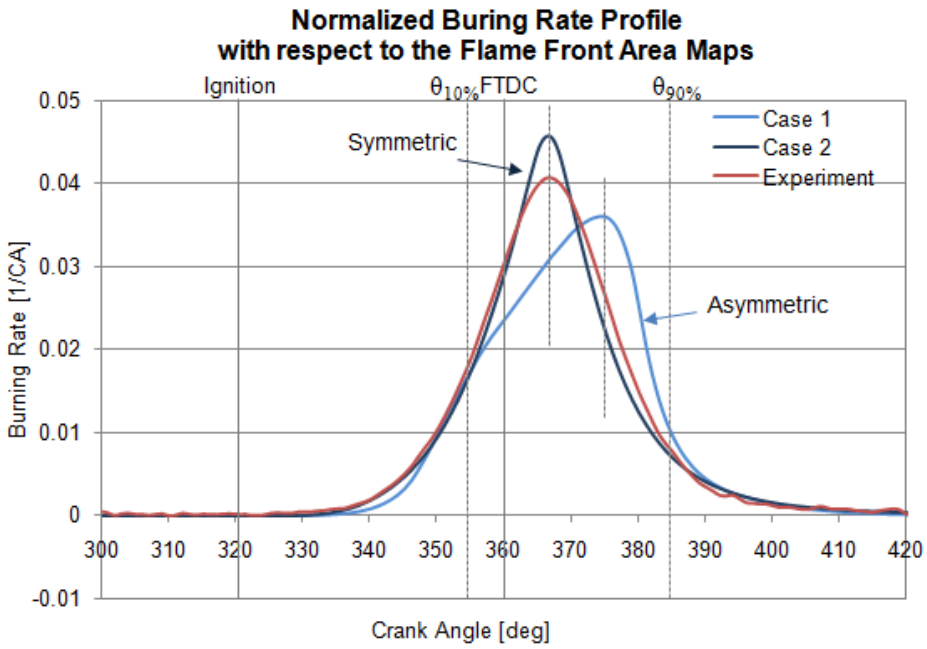

(a)

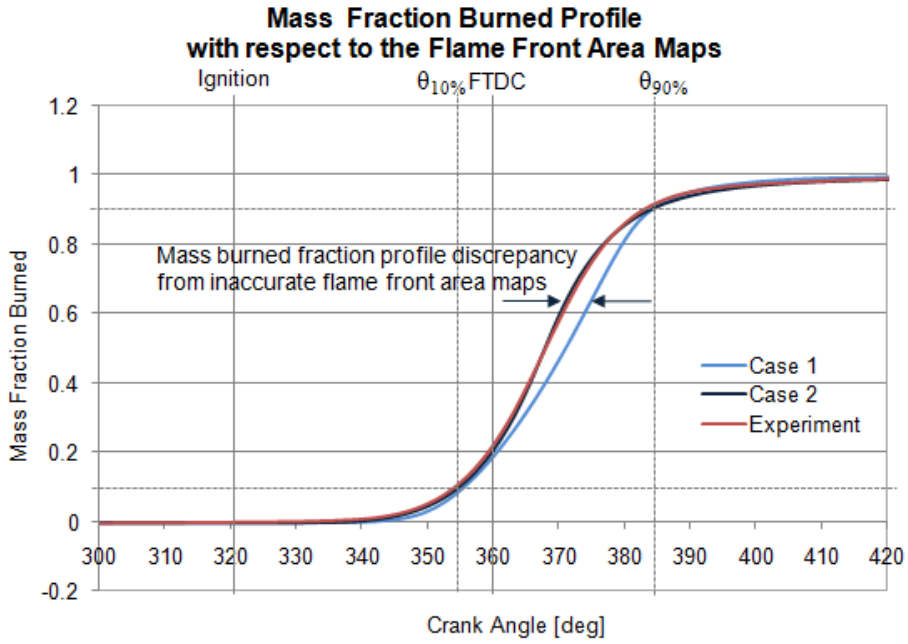

(b)

Figure 2-13 Influence of different flame front area maps: (a) normalized burning rate profiles; (b) mass fraction burned profiles

2.4.4 Influence of C_M

Another tuning parameter is the C_M in equation (2-12), which is introduced as a multiplier for adjusting turbulent the intensity of the inducted air flow into the cylinder. When additional devices are attached upstream of the intake port, thus, resulting in the turbulent intensity increase, the calculated mass air flow rate by 1-D gas dynamics simulation model cannot take into account the turbulent intensity change.

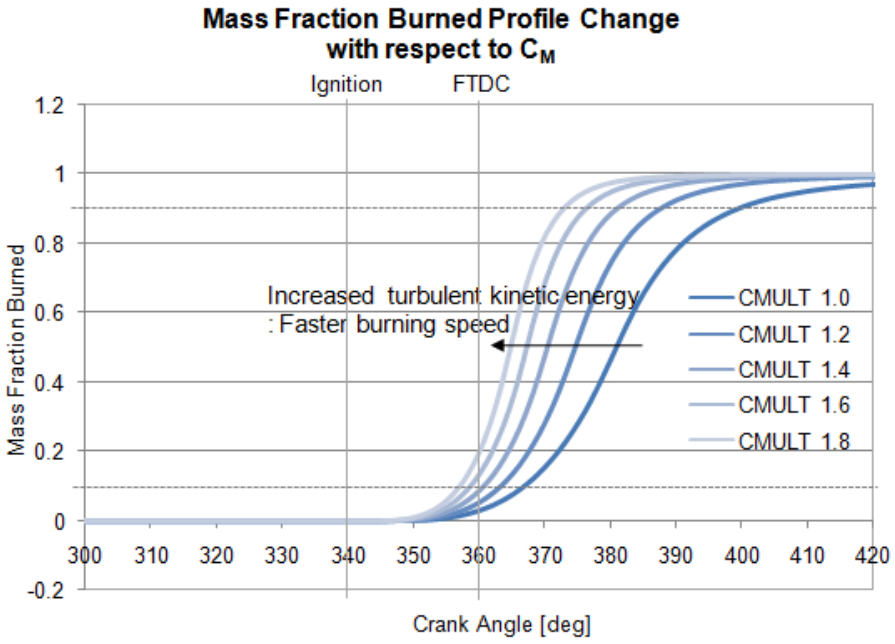

Figure 2-14 Influence of the C_M on the mass fraction burned profiles

Figure 2-14 shows the influence of the C_M on the mass fraction burned profile. Larger than unit value (one) of the C_M implies the increased turbulent intensity of the inducted mixture ahead the combustion chamber. In general, the increased turbulent intensity results in faster combustion and can be realized by special port design or devices.

In this study, the increased combustion speed due to the CMV can be captured by adjusting the C_M value. Thus, the actual combustion process can be predicted from the quasi-D combustion simulation by adequate tuning of the C_M.

2.4.5 Influence of C_β

In addition to the C_M, another tuning parameter is C_β in equation (2-9) can also manage the combustion speed. While the C_M handles the combustion speed by the direct adjustment of the turbulent intensity, the C_β enables to indirectly consider the 3-D in-cylinder flow pattern with respect to the combustion chamber shape. The C_β manages the combustion speed by manipulating the zero dimensional energy cascade process in equations (2-4) through (2-9).

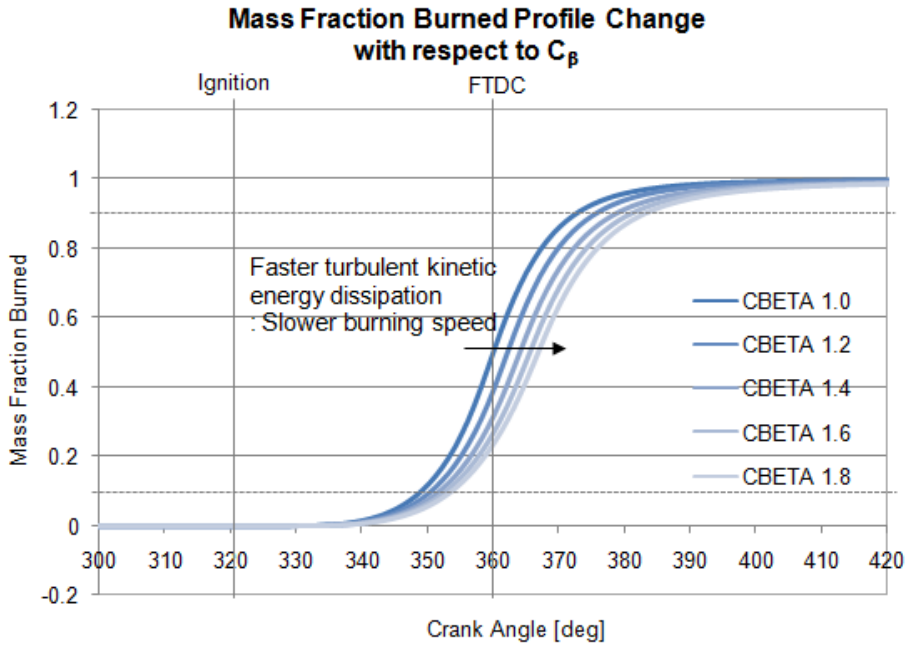

Figure 2-15 Influence of the C_β on the mass fraction burned profiles

Larger C_β implies slower mean kinetic energy conversion to the turbulent kinetic energy and faster turbulent kinetic energy dissipation into heat as shown in Figure 2-15. Thus, the combustion speed becomes slower due to the lower turbulent intensity. The turbulent kinetic energy production and dissipation rate are largely affected by the in-cylinder flow pattern. Thus, the C_β can compensate the relative simplicity of the quasi-D combustion model by indirect consideration of in-cylinder flow pattern.

2.5 Quasi-D Combustion Model Calibration Results

The combustion characteristics are significantly different depending on the generated turbulent intensity upstream of the combustion chamber. When the CMV is unblocked, turbulent intensity remains same to the conventional engine case. In contrast, the blocked CMV position generates additional turbulence. Thus, the resulting combustion characteristics are significantly different at both cases.

First, the flame front area maps are generated to achieve an accurate combustion profile shape. Then, the tuning parameters, C_M and C_β, are determined at both the CMV blocked and unblocked cases by following the proposed systematic calibration procedure shown in Figure 2-6. When the CMV is blocked, the C_M value is swept from a unit value to larger value. Then, when further calibration is required, the C_β value is tuned to reproduce the real combustion profile. When the CMV is unblocked, the C_M value is set to a unit value. Then, the C_β is swept from a unit value to larger value until the real combustion profile is reproduced. The tuned quasi-D combustion model is validated at low to medium engine speeds within the entire engine load conditions.

Figure 2-16 shows the validation of the quasi-D combustion simulation results compared to the experimental data. The same quasi-D simulation model with the different values of the C_M and C_β is used to capture the totally different combustion characteristics. The flame-development angles at each case agree with the experiment data with a high accuracy. The rapid-burning angles at each case correspond with the experiment data with high fidelity. Thus, the proposed systematic quasi-D combustion model calibration procedure shows the capability of capturing the various combustion characteristics regardless of hardware configurations.

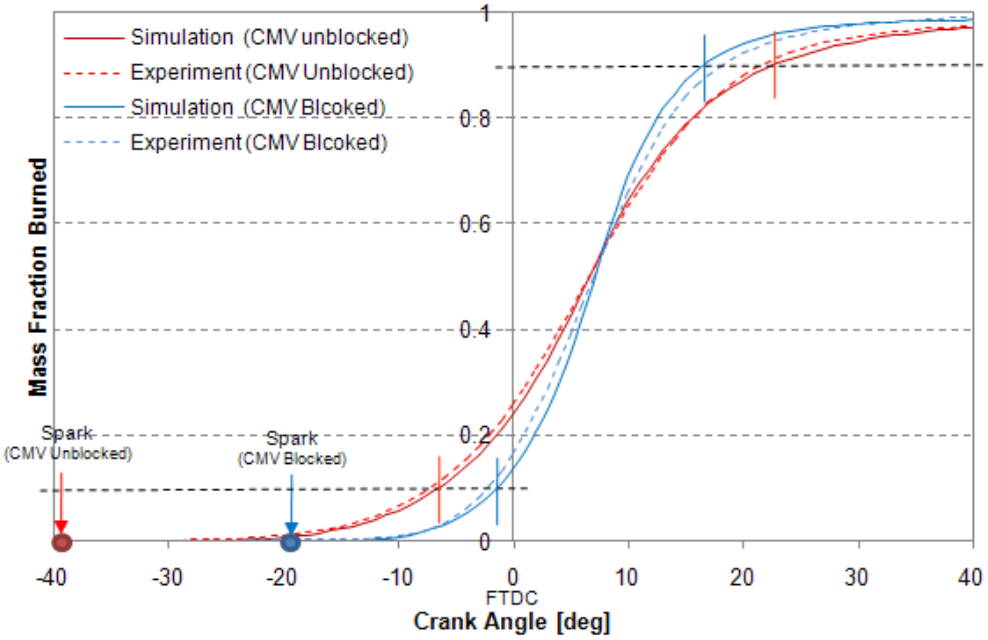

Figure 2-16 Comparison of simulation results with experimental results of the mass fraction burned at the engine speed of 2000 rpm, and the engine load of BMEP 2 bar at the CMV Unblocked and Blocked cases

2.6 Summary

In this study, the high-fidelity simulation tools are presented to predict the high DOF engine responses and to overcome the limitations of engine development time and cost. The high-fidelity simulation tools consists of a 1-D gas dynamic simulation model and a quasi-D phenomenological combustion simulation model to predict engine responses satisfying both relatively fast calculation time and high accuracy.

The most challenging problem of the high-fidelity simulation is the accurate prediction of combustion processes regardless of engine hardware configurations and operating conditions. Thus, a systematic calibration procedure of the quasi-D combustion simulation is proposed in this study to deal with the challenging problem. During the calibration procedure, three tuning parameters are selected based on the analysis of the phenomenological combustion model equations. These parameters are flame front area maps, C_M, and C_β.

The generation of accurate flame front area maps is the key procedure for the improvement of simulation fidelity. The influence of the flame front area maps on the combustion profile is assessed by using different flame front area maps. To create the accurate flame front area maps, the exact 3-D combustion chamber geometry and spark plug position are used while processing the 3-D geometry using a finite element pre-processing methodology. Then, the parameters C_M and C_β are sequentially adjusted depending on the system hardware configurations until the desired combustion profiles are achieved.

The proposed quasi-D combustion simulation calibration procedure is validated at a di-VVT engine with the CMVs. The combustion characteristics of the target engine changes significantly depending on the CMV positions. When the CMV is blocked, the combustion speed suddenly increases up to twice of the CMV unblocked case. After determining the tuning parameters values, the combustion profiles at the different CMV positions are predicted with a sufficient accuracy. Due to the accurate calibration of the quasi-D combustion model, the high-fidelity simulation tools can be used as substitute of experiments for many engine calibration and control problems.

REFERENCES

1. R. E. Lee, P. G. Hartman, G. R. Macfarlane, D. B. Maru, G. Pannone, T. Martinez , J. Cruz, and M. Winship, "The New DaimlerChrysler Corporation 5.7L HEMI® V8 Engine", SAE Technical Paper No. 2002-01-2815.
2. J. B. Heywood, *Internal Combustion Engine Fundamentals*, McGrawHill, 1998.
3. Charles Fayette Taylor, The Internal-combustion engine in Theory and Practice Volume I : Thermodynamics, Fluid Flow, Performance, The M.I.T. Press. 1985.
4. Heinz Heisler, *Advanced Engine technology*, Society of Automotive Engineers, Inc., 1995.
5. D. C. Haworth, "A Review of Turbulent Combustion Modelling for Multidimensional In-Cylinder CFD", SAE Technical Paper 2005-01-0993, 2005.
6. A. D. Gosman, "CFD modelling of flow and combustion for IC engines," *Proceedings of the 2nd European Computational Fluid Dynamics Conference*, Vol. 5, No. 1, September, 1994, Stuttgart, Germany, pp 133-143.
7. J. A. Cook, and B. K. Powell, "Modelling of an Internal Combustion Engine for Control Analysis," *IEEE Control Systems Magazine*, Vol. 8, No. 4, 1988, pp 20-26.
8. E. Hendricks, and S. C. Sorenson, "Mean value modeling of spark ignition engines," SAE Technical Paper No. 900616, 1990.
9. Z. S. Filipi, and D. N. Assanis, "Quasi-dimensional computer simulation of the turbocharged spark-ignition engine and its use for 2- and 4-valve engine matching studies", SAE Technical Paper No. 910075, 1991.
10. Z. S. Filipi, "Investigation of Variable Valve Area Strategies for a Turbocharged SI-Engine." *Proceedings of the IMechE 1994-6, 5th International Conference on Turbocharging and Turbochargers*, London, 1994, pp. 93–102.
11. Z. S. Filipi, and D. N. Assanis, "The Effect of Stroke-to-Bore Ratio on Combustion, Heat Transfer and Performance of a Homogeneous-Charge Spark-Ignited Engine of Given Displacement." *International Journal of Engine Research*, Volume 1, No. 2, JER0500, London, 2000, pp. 191-208.
12. WAVE V8 Basic Reference Manual, Ricardo Software, Ricardo, Inc., 2008.
13. WAVE V8 Engine Reference Manual, Ricardo Software, Ricardo, Inc., 2008.
14. T. Morel, M. Flemming, and L. A. LaPointe, "Characterization of manifold dynamics in the Chrysler 2.2l S.I. engine by measurements and simulation," SAE Technical Paper No. 900679, 1990.
15. R. J. Tabaczynski, C. R. Ferguson, and K. Radhakrishnan, "A turbulent entrainment model for spark-ignition engine combustion", SAE Technical Paper No. 770647, 1977.

16. R. J. Tabaczynski, F. H. Trinker, and B. A. Shannon, “Further refinement and validation of a turbulent flame propagation model for spark-ignition engines”, *Combustion and Flame*, Vol. 39, No. 2, 1980, pp. 111-121.

17. S. G. Poulos, and J. B. Heywood, “The effect of chamber geometry on spark-ignition engine combustion.”, SAE Technical Paper No. 830334, 1983.

18. B. Wu, R. G. Prucka, Z. S. Filipi, D. M. Kramer, and G. L. Ohl, “Cam-Phasing Optimization Using Artificial Neural Networks as Surrogate Models – Maximizing Torque Output”, SAE Technical Paper No. 2005-01-3757, 2005.

19. B. Wu, Z. S. Filipi, D. Assanis, D. M. Kramer, G. L. Ohl, M. J. Prucka, E. DiValetin, “Using Neural Networks for Representing the Air Flow Rate through a 2.4 Liter VVT Engine”, SAE Technical Paper No. 2004-01-3054.

20. B. Wu, R. G. Prucka, Z. S. Filipi, D. M. Kramer, G. L. Ohl, “Cam-phasing Optimization Using Artificial Neural Networks as Surrogate Models – Fuel Consumption and NOx Emissions”, SAE Technical Paper No. 2006-01-1512, 2006.

CHAPTER 3

VIRTUAL SENSING OF MASS AIR FLOW RATE OF DUEL-INDEPENDENT VVT ENGINES WITH CHARGE MOTION CONTROL USING ARTIFICIAL NEURAL NETWORKS

3.1 Introduction

The improvement of engine performance while reducing emission and enhancing fuel economy has been continuous challenges of the automotive industry. Many new technologies have been introduced to meet these demands. Although new technologies improve engine performance, the resultant increased system complexity requires significant efforts to resolve optimal calibration and transient control problems. For any engine calibration and transient control problem, sensing and estimating necessary engine states are indispensable. However, not all engine states are measurable, and some states are very difficult or expensive to be measured.

Thus, virtual sensing methodologies [1-3] have been introduced to estimate the engine states that are required in engine calibration and control. The virtual sensing methodologies have many advantages, such as no sensor delay, no sensor cost, and the capability of predicting difficult to measure system responses. In contrast, the virtual sensing methodology requires additional computational power. As long as the later is

negligible or additional hardware for computation is not required, virtual sensing is a plausible technology for mass produced engines. For virtual sensors to be beneficial, the virtual sensors require high accuracy, fast computation time, and low computational cost.

Among many engine states, the precise estimation of the mass air flow rate into the cylinders has been an important issue for accurate control of the air-to-fuel ratio. Thus, the precise estimation enables to achieve less emission and better engine transient response. In conventional engines, the measurement of the mass air flow rate into the cylinders is realized using either a mass air flow (MAF) sensor or an intake manifold absolute pressure (MAP) sensor.

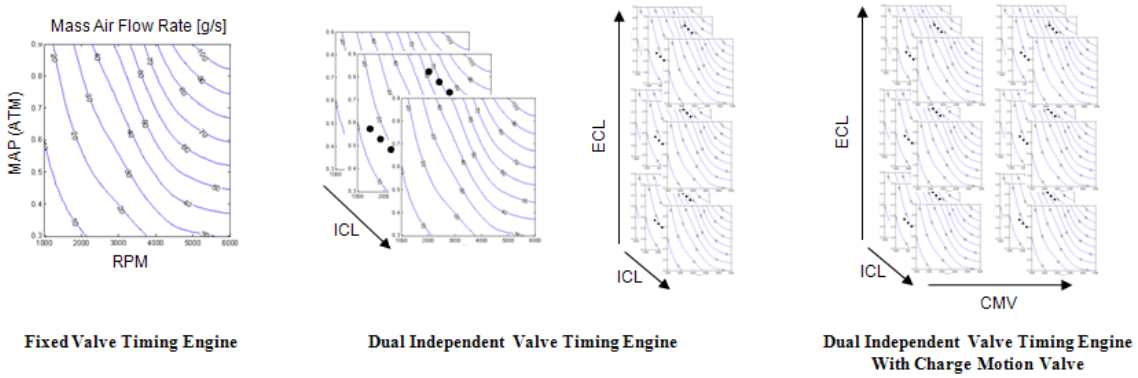

Figure 3-1 Conventional orthogonal grid lookup tables with respect to the increasing number of degree of freedom

In conventional engines using a MAP sensor, look-up tables or empirical equation based estimation have been used as adequate methods for the indirect prediction of the air mass flow rate using measured manifold absolute pressure. However, the extended degree-of-freedom (DOF) in advanced engines increases the number of required maps exponentially as illustrated in Figure 3-1, thus, increases cost and calibration difficulty.

As alternatives of lookup tables, artificial neural networks (ANNs) can be used as one of the best indirect prediction methodologies of system states and responses. The ANNs are capable of learning highly complex and non-linear underlying input-to-output relationships from the well organized and sufficient number of training sets [4-8]. The training data sets are generally created from experiments or simulations. Although experiment data obtained by appropriate measurements guarantee the accuracy of training data, additional system complexity increases the number of possible engine operating conditions exponentially beyond the limited time and cost for experiments. Thus, simulation based methods have been introduced as substitutes of experiments to predict the mass air flow rate in high DOF engines [14].

This chapter presents a virtual sensing methodology for the mass air flow rate of a di-VVT engine with the CMV by using the ANNs. First, the virtual sensing problem and difficulties of the target engine system are presented. Then, the architecture of the virtual sensor of the mass air flow rate is provided. As tools of engine simulations, the high-fidelity engine simulation tools are introduced. Then, as basic components of the virtual sensing methodology, the ANNs and an ANNs training procedure are investigated. The ANNs are trained using the training data set generated by the high-fidelity simulation. Finally, the developed virtual sensing methodology is validated by experimental data.

3.2 Target Engine and Problem Difficulties

We chose a dual independent variable valve timing (di-VVT) system among new technologies, because it is one of the most promising technologies in automotive industry

widely used to improve both fuel economy and engine performance over the entire engine operation ranges. The di-VVT system is a valve actuation system that controls intake and exhaust valve timing independently to adjust gas exchange characteristics over the entire engine operation ranges. The di-VVT system not only increases the amount of inducted air into a cylinder to maximize engine performance, but also manages residual gas fraction to improve fuel economy and to control emissions.

In addition, we chose a charge motion valve (CMV) as the preferred solution for resolving the combustion stability related problems considering both cost-effectiveness and engine performance. Combustion stability is another important issue in maintaining drivability and quietness of vehicles. The CMV is a flip valve device that intensifies the turbulence of intake air into the cylinders to improve combustion quality. The CMV has two operating positions: (1) an unblocked position, when the valve position is parallel to a gas passage, and (2) a blocked position, when the valve position is perpendicular to a gas passage.

The selected target engine is a Chrysler dual overhead camshaft (DOHC) 2.4 liter inline four (I4) cylinder spark ignition (SI) engine with a di-VVT device and the CMV. Two intake valves and two exhaust valves are used per cylinder and actuated by the dual overhead camshaft. The critical parameters of the target engine are summarized in Table 3-1.

Table 3-1 Critical parameters of the target engine

Displacement	2.4 liters
Bore/Stroke	87.5/101.0 mm
Compression Ratio	9.4:1
Max. Intake Valve Lift	8.25 mm
Max. Exhaust Valve Lift	6.52 mm
Default Intake Valve Timing **Closes/Opens/ Centerline**	51^{o} ABDC/ 1^{o} BTDC/ 115^{o} ATDC
Default Exhaust Valve Timing **Closes/Opens/ Centerline**	9^{o} ATDC/ 51^{o} BBDC/ 111^{o} BTDC
Default Valve Overlap	9^{o} @ 0.5 mm lift
Allowed Intake Cam-phasing Range	$\pm 15^{o}$ Crank Angle
Allowed Exhaust Cam-phasing Range	$\pm 15^{o}$ Crank Angle

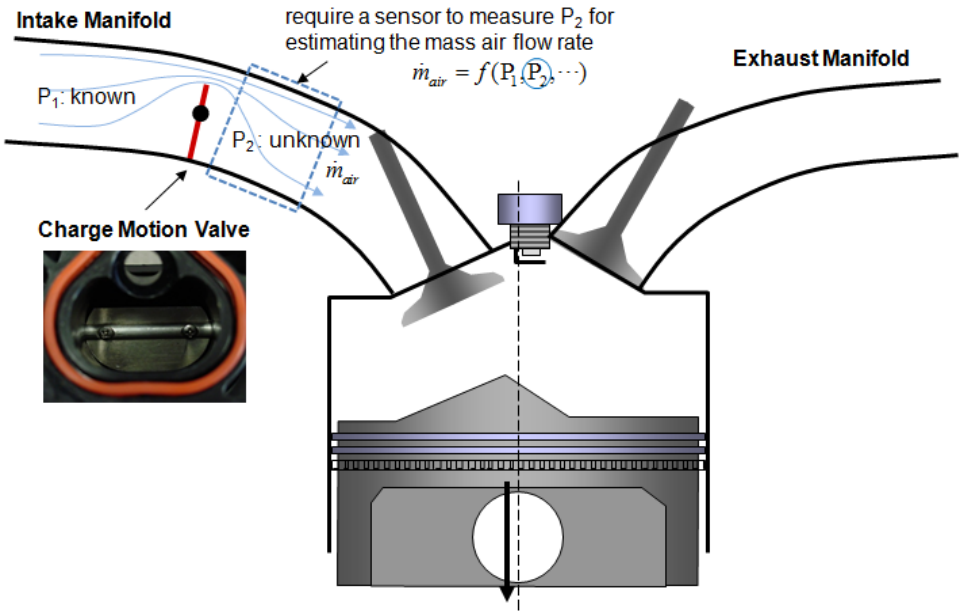

Figure 3-2 Target engine including the di-VVT devices and the CMV

The mass air flow rate into the cylinders is affected by many variables, which include throttle valve positions, engine speed, valve timings, and ambient atmosphere conditions. When an additional device is introduced to the system, the precise air mass flow rate estimation requires an additional number of sensors or a more complicated engine model. Figure 3-2 illustrates the target engine, which has the CMV upstream of the intake runners. When CMVs are installed upstream of the intake runners, the pressure behind the CMVs differs from the manifold absolute pressure. To predict the mass air flow rate into the cylinder accurately, additional pressure sensors need to be installed behind the CMVs.

Since design modification of the head structure for installing additional pressure sensor results in the high costs for engine development and production, developing alternative methods for estimating the mass air flow rate is necessary for this special case. When the gas dynamics of the intake system is accurately modeled, the mass air flow rate can be accurately predicted by the model. Thus, the high-fidelity engine simulation tools can be used to predict engine responses based on accurate modeling of the engine gas dynamics system and combustion system.

3.3 Virtual Sensing of the Mass Air Flow Rate

The overall procedure of developing the virtual sensor of the mass air flow rate is illustrated in Figure 3-3. The accuracy of the virtual sensor of the mass air flow rate depends on the modeling fidelity of the target engine. The high-fidelity simulation is the one of the best tools to achieve the high prediction accuracy. After creating the high-

fidelity simulation model, the model is calibrated and validated by using experimental data.

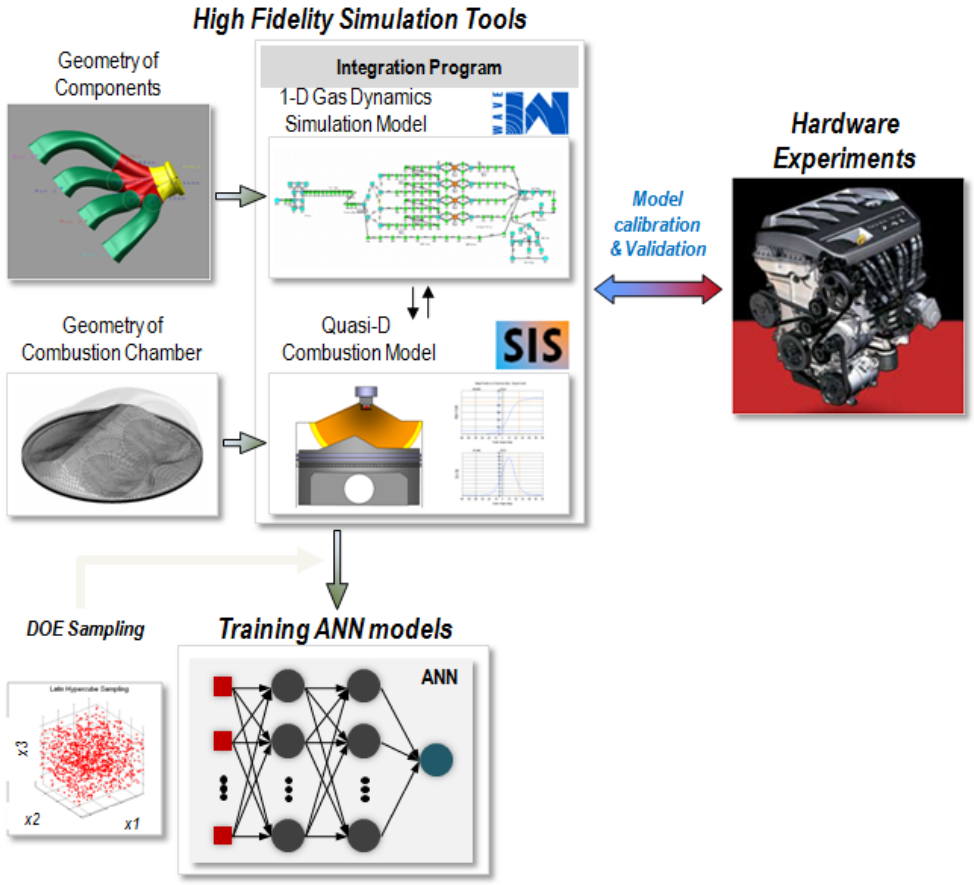

Figure 3-3 Illustration of the overall procedure of achieving desired ANN models: (1) create the high-fidelity simulation tools; (2) validate the simulation tools; (3) generate training data sets; (4) train the ANN models

The validated simulation model can predict engine responses over the whole possible engine operating conditions. The data sets for training ANNs are systemically generated using Latin hypercube sampling (LHS) as a design of experiments (DOE) sampling technique [9-13]. Then, the ANN models for prediction engine responses are trained using systematic ANNs training procedure. The inputs for the virtual sensor of

the mass air flow rate are : (1) engine speed (RPM), (2) intake cam location (ICL), (3) exhaust cam location (ECL), (4) manifold absolute pressure (MAP),(5) charge motion valve position (CMV), and (6) ambient pressure difference (ΔP_{amb}).

3.3.1 High-Fidelity Simulation Tools

The high-fidelity simulation tools consist of a one-dimensional (1-D) gas dynamics simulation model and a quasi-dimensional (quasi-D) in-cylinder combustion model. The 1-D gas dynamics simulation model is created by the commercial software named the Ricardo WAVE and includes the complete air flow paths from the air filter box to the exhaust tail pipe. The quasi-D combustion model is constructed using the in-house software named spark-ignition simulation (SIS), which is written in the FORTRAN language. The SIS has been refined over time and has been used routinely at the University of Michigan for research purposes.

First, the 1-D gas dynamics model estimates the mass air flow rate into the cylinders, the velocity of intake air, and the temperature and composition of mixture through the intake and exhaust valves. Then, mass fraction burned rate is calculated using the quasi-D combustion code with these 1-D simulation results as boundary conditions, and delivered to the 1-D simulation model until the high-fidelity simulation results converge within the desired error bound. The effect of the CMV on the mass air flow can be predicted by using the high-fidelity simulation tools.

3.3.2 Artificial Neural Networks

Artificial neural networks (ANNs) are assembly of simple elements operating in parallel. These elements are inspired by biological nervous systems. The ANNs can be trained to perform a particular function by adjusting the values of the connections (weights) between elements based on the comparison of the output and target until the ANNs output satisfies a convergence criterion as illustrated in Figure 3-4 [8]. Such neural networks have been used in various fields, including pattern recognition, identification, classification, speech, vision, and control systems. Nowadays, the application area of ANNs has expanded to engineering, financial, and other practical applications.

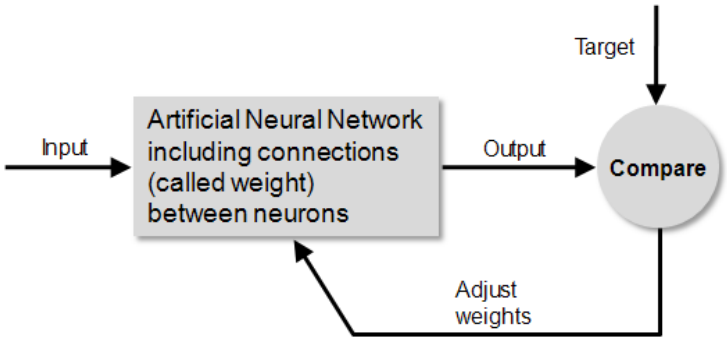

Figure 3-4 Illustration of the training process of ANNs

Feed forward ANNs with biases, at least one sigmoid layer, and a linear output layer are capable of approximating any function with a finite number of discontinuities. Therefore, multi-layer feedforward networks can be regarded as universal function approximators. The feed forward networks created for this research are illustrated in Figure 3-5 [8]. Each neuron receives a sum of wieghted inputs from the previous layer

and then adds bias *b*. Then, a specific transfer function *f* is applied and transferred to the next layer. Each neuron in the previous layer is connected with all neurons in the next layer with a connecting weight *w*. The linear output layer lets the network produce values outside the range −1 to +1.

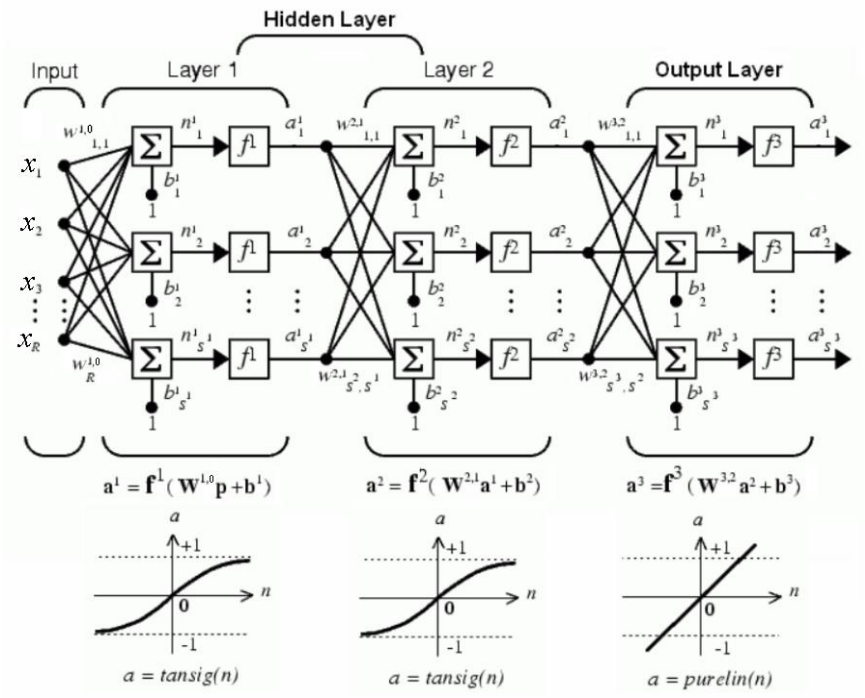

Figure 3-5 Illustration of a multi-layer feed forward neural network consisting of two hidden layers with sigmoid neurons and one output layer with pure linear neurons

With the given numbers of inputs and outputs, an adequate ANN structure are determined as follows. First, the number of neurons in hidden layers is initially assumed to be an adequate number, and the network weights and biases of created ANNs are initialized for training. Then, training data sets from experiments or simulation results are prepared to train the ANNs. During the training process, the weights and biases of the network are iteratively adjusted to minimize the network performance function, which is

generally selected as the mean square error between the network outputs and the target output.

$$mse = \frac{1}{N}\sum_{i=1}^{N}(t_i - a_i)^2 \ , \tag{3-1}$$

where, *mse* is the mean squared error, *N* is the total number of training samples, t_i is the target output value of the *i*th training sample, a_i is the network output for the *i*th training sample.

When the network size becomes larger than the required size, overfitting problems may occur. Overfitting is a special situation in which the fitted model accuracy becomes worse when the number of neurons exceeds the information content of the training data. This effect occurs because the network has memorized the training data too much to generalize to new situations. Thus, a modified performance function is used to improve generalization by adding a term that consists of the mean of the sum of squares of the network weights and biases.

$$msereg = \gamma\, mse + (1-\gamma)\, msw, \tag{3-2}$$

where γ is performance ratio, and

$$msw = \frac{1}{n}\sum_{j=1}^{n} w_j^{\,2}\ , \tag{3-3}$$

where w_i is the network weight of the jth neuron.

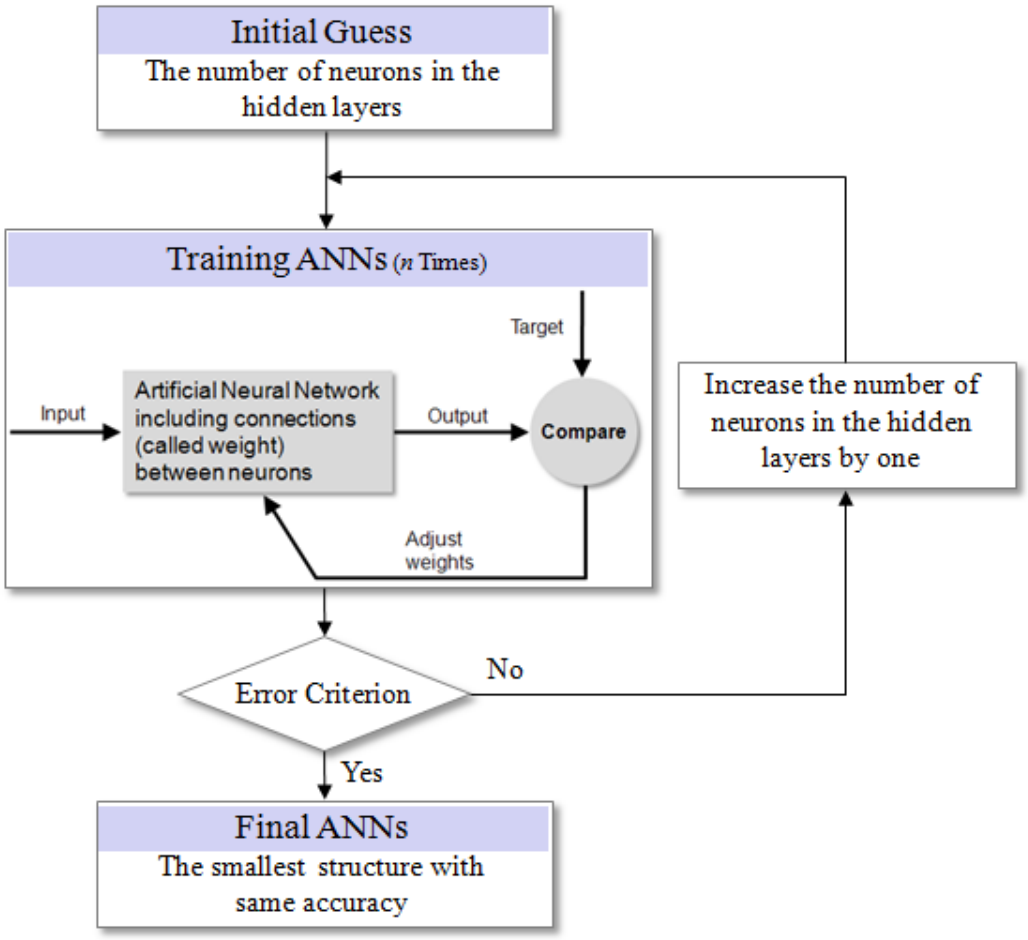

Figure 3-6 Systematic procedure to decide the best ANN structure

To achieve faster calculation speed and better efficiency, the smallest ANN structure maintaining the same fitting accuracy is determined as the best ANN structure. Thus, a systematic procedure by iterating training processes is introduced to find the best ANN structure. Figure 3-6 shows the systematic ANN structure decision procedure. In this study, after reviewing different structures, a two hidden layers structure with sigmoid neurons is selected as a preferred ANNs structure to estimate the mass air flow rate. Then, the data sets for training ANNs are divided into a train data set, which is used to

train the ANNs, and a test data set, which is used to detect overfitting. When the calculated error with the test data set is much larger than that with the train data set, overfitting is considered to occur, and this ANNs structure is neglected. If the calculated error of the ANN structure exceeds the error criterion, the number of neurons in the hidden layers is increased by one until the error criterion is satisfied. When the error criterion is satisfied, the resulting number of neurons is determined as the optimal number for the best ANN structure.

3.4 Architecture of the Virtual Sensor

The estimation of the mass air flow rate into the cylinders should consider the ambient pressure and temperature effects which change the amount of inducted air into the cylinders with variable valve timing. Without considering ambient pressure compensation, the air flow rate is either underestimated or overestimated. The ambient pressure change effects constitute a significant percentage, up to 15~20 percent, of the total air flow rate [14].

The architecture for estimating the mass air flow rate is composed by the two ANN models for ambient pressure compensation and the temperature compensation model proposed by Bin Wu et al. [14] as shown in Figure 3-7. The effect of ambient temperature change on the mass air flow rate is easily calculated using simple thermodynamics equations. However, with complex interactions with the valve timings and the CMV positions, the change of ambient pressure highly influences the mass air flow rate into the cylinders. Thus, we mainly focused on the prediction of the mass air flow rate

considering ambient pressure compensation. The compensated mass air flow rate model structure is created by augmenting an ANN model for the ambient pressure compensation of the mass air flow rate to the ANN model for predicting the mass air flow rate at the reference ambient pressure and temperature.

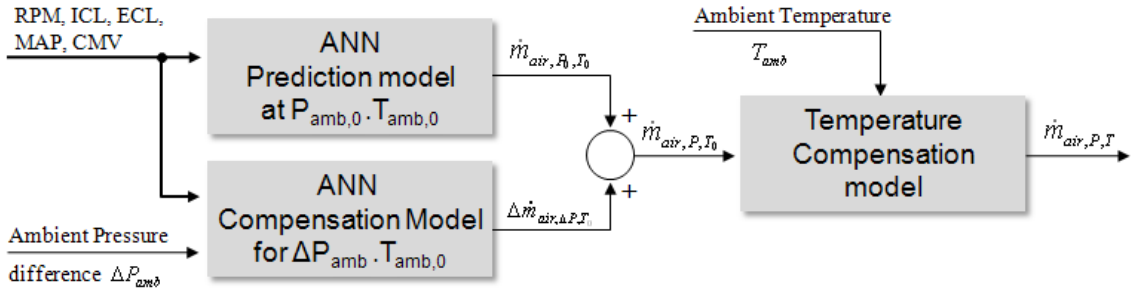

Figure 3-7 Illustration of the architecture for the virtual sensing of the mass air flow rate of dual independent VVT engines with the CMV

Initially, an ANN model to predict the mass air flow rate into the cylinders at the reference ambient pressure and temperature is determined by the systematic training procedure in Figure 3-6 with five input variables: RPM, ICL, ECL, MAP, and CMV. Then, the compensation of the mass air flow rate is calculated from the ANN model for pressure compensation with the six input variables: the same five inputs plus the ambient pressure difference (ΔP_{amb}). The data sets for training ANNs are generated using the Latin hypercube sampling (LHS) method to reduce the total number of simulations.

For the ambient pressure compensation model, two configurations of the ANN structures are considered as illustrated in Figure 3-8. The first configuration in Figure 3-8 (a) is created by using two identically structured ANN models at current pressure and at reference ambient pressure respectively. The other configuration in Figure 3-8 (b) is realized using the ambient pressure difference as an input of the ANN model.

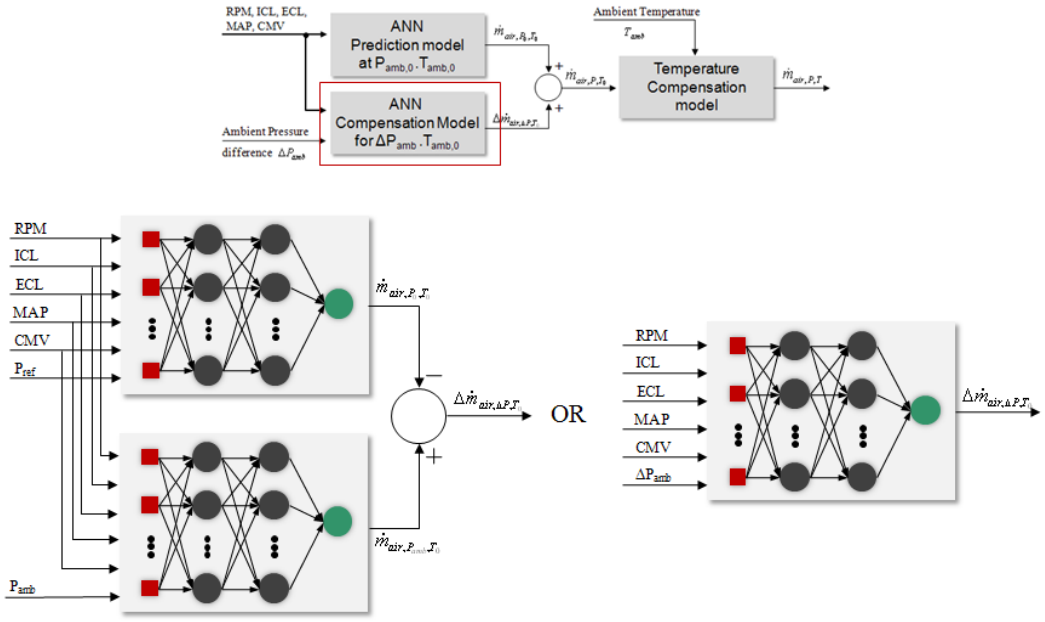

(a) **(b)**

Figure 3-8 Two configurations for the ambient pressure compensation model: (a) configured with the difference of two parallel ANNs; (b) directly modeled with single ANNs using ambient pressure difference

When taking into account a conventional calibrating procedure of the mass air flow rate, the mass air flow rate is initially calibrated at reference ambient atmosphere conditions, then, different ambient conditions are additionally considered by correcting the mass air flow rate difference due to the ambient pressure change. Thus, the configuration in Figure 3-8 (b) is selected as a preferred configuration based on the conventional mass air flow rate calibrating procedure.

3.5 ANN Model Decision

3.5.1 Training Data Sets Generation by High Fidelity Simulations

The ranges of input variables for the high-fidelity simulation are shown in Table 3-2. Since the ANNs cannot guarantee the extrapolation of the range of training data sets, the ranges of input variables must cover the possible whole engine operation ranges with adequate margins. Among these variables, the equivalent throttle diameter inputs cannot be directly determined, because the equivalent throttle diameter is determined from the given BMEP output. Thus, the equivalent throttle diameter inputs are sampled by the LHC method to achieve evenly distributed BMEPs in percentage.

Table 3-2 Input variables and ranges of the high-fidelity simulation for the virtual sensing of the mass air flow rate into a cylinder

Variable	Lower Bound	Upper Bound
Engine Speed (RPM)	600	6500
ICL (CA)	ATDC 95 deg	ATDC 135 deg
ECL (CA)	BTDC 91 deg	BTDC 131 deg
Equivalent Throttle Dia. (cm)	0.3	4.2 (WOT)
P_{amb} (atm)	0.7	1.3
CMV	Unblocked	Blocked

Figure 3-9 shows the generated samples to train the ANNs for the virtual sensing of the mass air flow rate. The resulting mass air flow rate data for both cases are evenly distributed throughout the whole engine operating ranges. For the CMV unblocked case in Figure 3-9 (a), the maximum flow rate increases in linear trends according to the

increasing engine speed. By contrast, in the CMV blocked case in Figure 3-9 (b), the maximum mass air flow rate is restricted from medium to high engine speed ranges. The restriction of the maximum mass air flow rate comes from the choking effect by the CMV, and results in the reduction of engine output power.

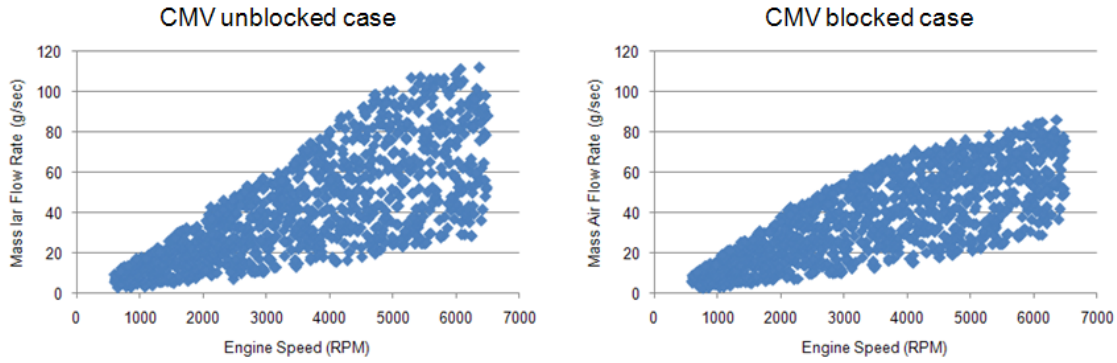

(a) **(b)**

Figure 3-9 Generated data sets for training ANNs for virtual sensing of the mass air flow rate using a LHS method: (a) CMV unblocked case; (b) CMV blocked case

3.5.2 Training Results of ANN models

The preferred ANN structure for estimating the mass air flow rate consists of two hidden layers with sigmoid functions and one output layer with pure linear functions, considering convergence time, network size, and regression accuracy of ANNs. The number of neurons is determined using the proposed systematic training process. In this study, we follow the convention of symbolizing the network structure in the form of *i-h1-h2…-o*. Where, *i* represents the number of inputs; *hj* represents the number of hidden neurons in hidden layer *j* and *o* represents the number of outputs.

The best ANN structure is the smallest structure that satisfies the required accuracy. The initial number of neurons in the hidden layers is assumed to be a small number. Then, the ANNs are trained several times with the same structure within the maximum training epoch, and checked an error criterion. When the ANNs do not satisfy the desired error criterion, the number of neurons is increased by a unit number until the ANNs meet the error criterion. The best ANN structures for the reference ambient pressure condition and for the ambient pressure compensation are determined as the structures of 5-18-18-1 and 6-10-10-1 respectively.

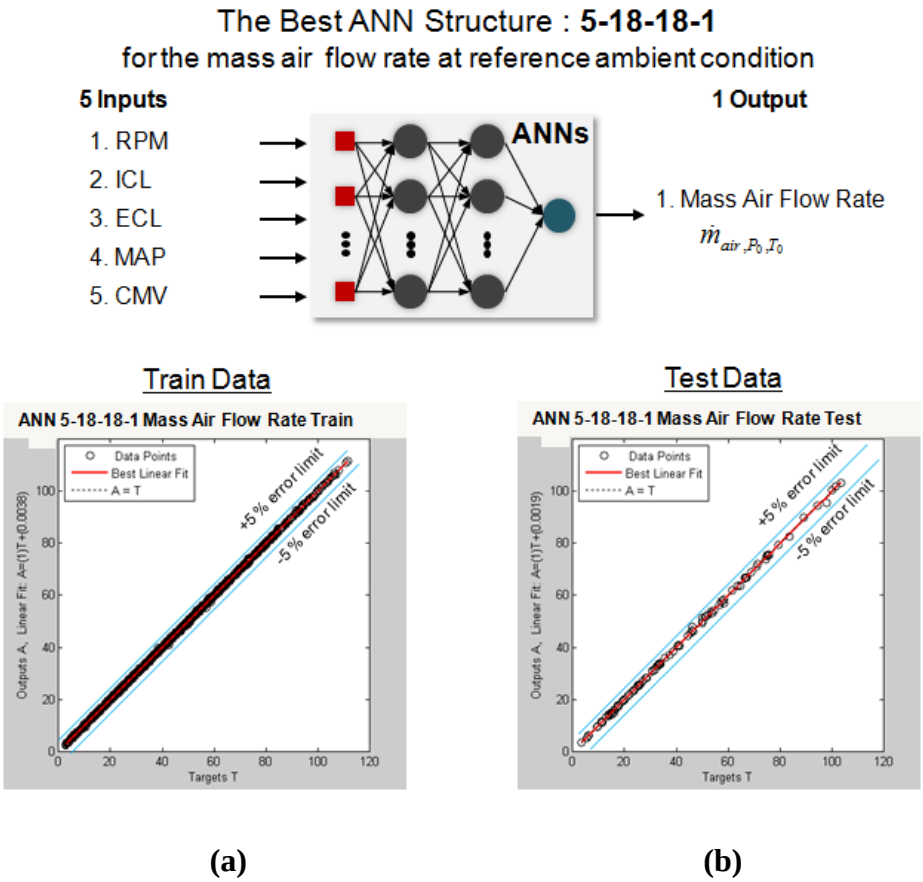

Figure 3-10 Preferred best ANN structure (5-18-18-1) of the mass flow rate at reference ambient pressure and the fitting quality: (a) training data set; (b) test data set

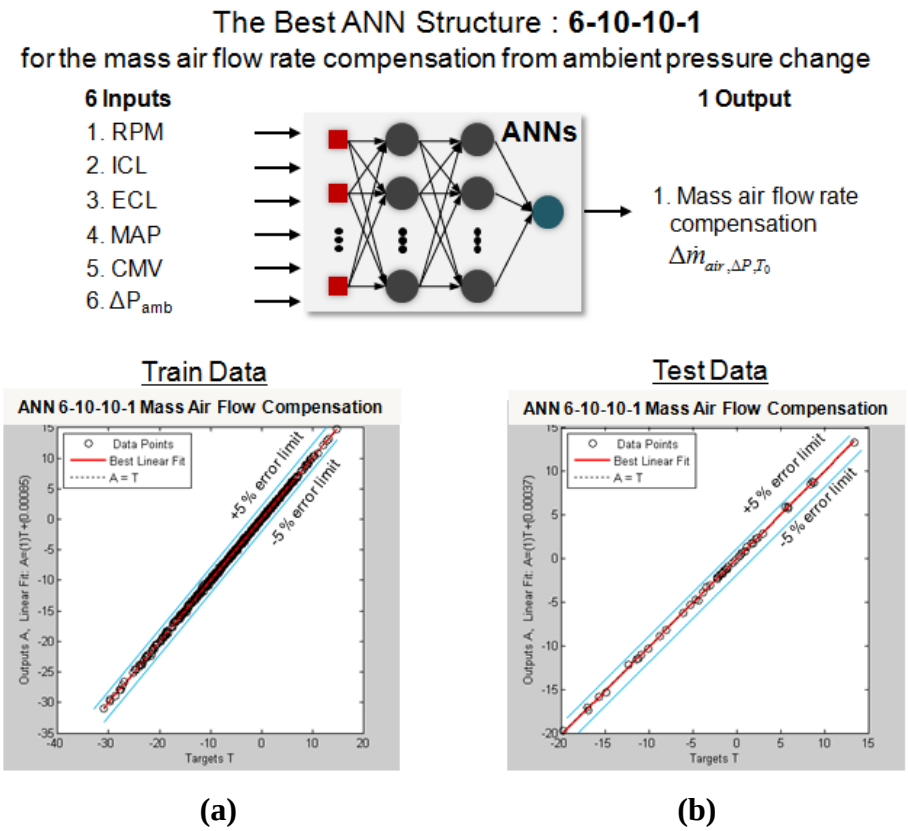

(a) **(b)**

Figure 3-11 Preferred best ANN structure (6-10-10-1) for the mass flow rate compensation from the ambient pressure change and the fitting quality: (a) training data set; (b) test data set

Although the number of inputs of ANNs for the compensation of the ambient pressure change are one more than that of ANNs at reference ambient conditions, the number of neurons in the hidden layer of the ANNs for the compensation of the ambient pressure is smaller. The smaller number of hidden layer of the ANNs implies that the effect of the ambient pressure change on the mass air flow rate is less complex than the effects from other input variables such as ICL and ECL.

Figure 3-10 and Figure 3-11 show the best ANN structures and fitting qualities. The error criterion, which is ± 5 percent, is depicted as solid lines. All data points from train

data set and test data set congregate tightly within error bounds along the 45° diagonal lines that represent perfect fitting. The good fitting quality of test data demonstrates the rare possibility of the existence of overfitting. These ANN structures are finally assembled to the proposed virtual sensor structure for the mass air flow rate in Figure 3-7.

3.6 Virtual Sensing Results and Validation

To assess the developed virtual sensing methodology, virtual sensor outputs are validated by comparing with the experimental data at several engine operating points as shown in Figure 3-12. The virtual sensing results show that the CMV positions highly affect the mass air flow rate. The virtually sensed mass air flow rate also varies non-linearly under variable cam timing. Because the effect of the intake and exhaust valve timing is highly interconnected, this effect of variable valve timing on the mass air flow rate is too complex to be predicted with simple equations.

First, the virtual sensing results in fixed ICL, ECL, and reference ambient conditions are shown to capture the effect of the CMV positions on the mass air flow rate in Figure 3-12. When the engine speed is set in the low speed range, for example, below 3000 RPM, the mass air flow rate is almost not affected by the position of the CMV, because the mass flow rate is too low to be restricted by the CMV. However, increasing engine speed and engine load raise the difference of the mass air flow rate between the different CMV positions, because the CMV acts as an orifice that restricts the air flow, thus, causes the pressure drop across the CMV.

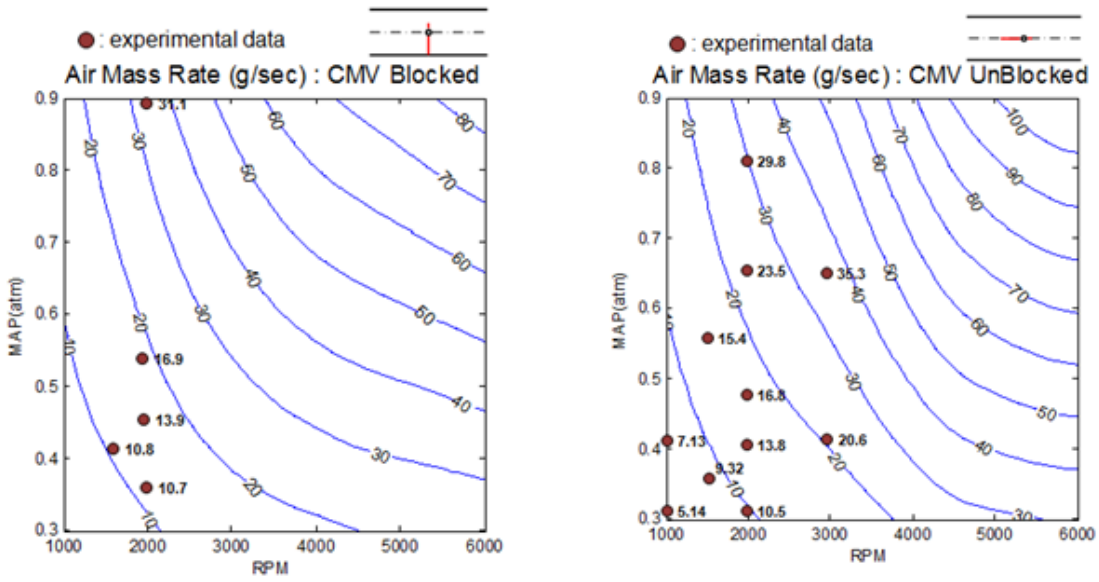

(a) **(b)**

Figure 3-12 Virtual sensing results of mass air flow rate at the fixed ICL of ATDC 115 deg and the fixed ECL of BTDC 111 deg: (a) CMV unblocked case; (b) CMV blocked case

At the engine speed of 6000 RPM and the MAP of 0.9 atm, the mass air flow rate at the CMV blocked case is reduced by up to 23 percent. The virtual sensing results show that the CMV causes the decrease of engine output power at mid to high engine speed ranges. Thus, the CMV operating region needs to be optimized to trade off the improvement of combustion quality and the degradation of engine performance.

Next, the effect of the variable valve timing is investigated to present the trends of the mass air flow rate at different engine operating conditions to estimate the accurate amount of inducted mixture into the cylinders. The information about these trends enables the optimization of the variable valve timing with a specific objective, for example, the maximization of the mass air flow rate. The virtual sensing results in Figure

3-13 and Figure 3-14 show the effect of the VVT on the mass air flow rate at reference ambient conditions.

At low engine speeds, the effect of the CMV positions is insignificant, and almost the same resulting mass air flow rate surfaces are maintained regardless of the CMV positions as shown in Figure 3-13. When the engine speed and engine load becomes higher, the trends of the mass air flow rate at different CMV positions become dissimilar as shown in Figure 3-14. These results imply that, with respect to the CMV position, the optimal ICL and ECL positions are different and need to be optimized separately.

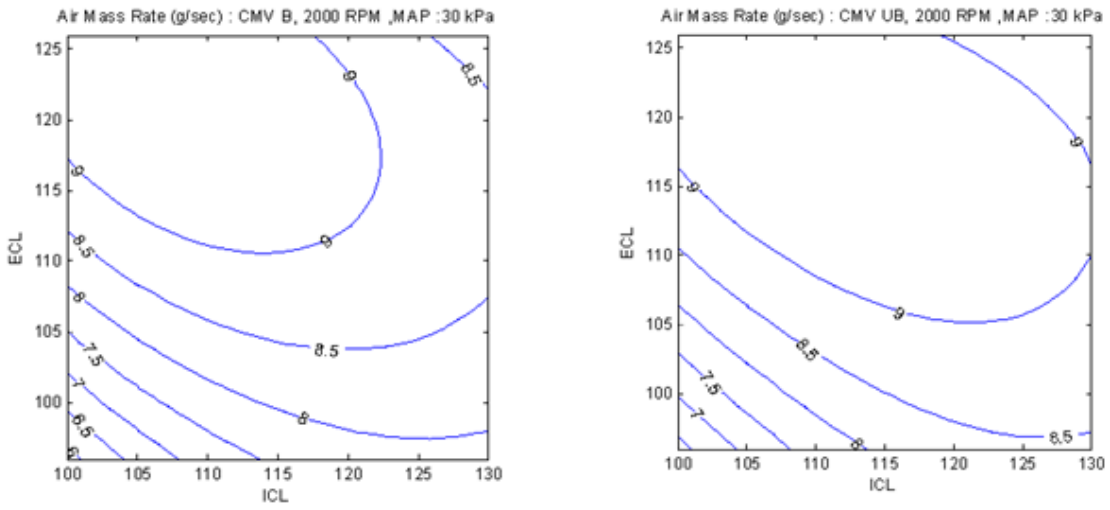

(a) **(b)**

Figure 3-13 Estimated mass air flow rate with respect to ICL and ECL at the reference ambient pressure and temperature with the engine speed of 2000 RPM and the MAP of 30 kPa: (a) CMV unblocked case; (b) CMV blocked case

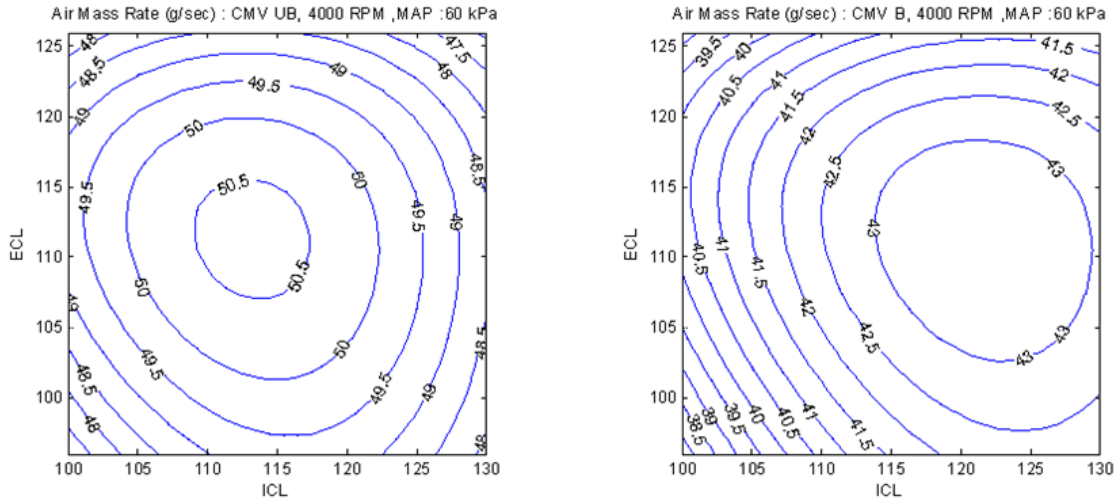

(a) **(b)**

Figure 3-14 Estimated mass air flow rate with respect to ICL and ECL at the reference ambient pressure and temperature with the engine speed of 4000 RPM and the MAP of 60 kPa: (a) CMV unblocked case; (b) CMV blocked case

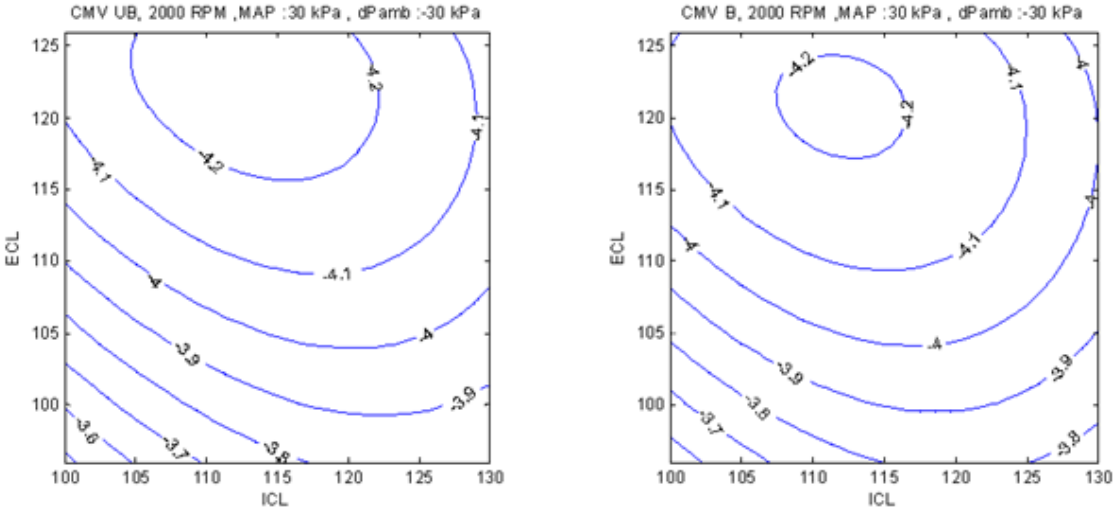

(a) **(b)**

Figure 3-15 Estimated ambient pressure compensation of the mass air flow rate with respect to ICL and ECL at the engine speed of 2000 RPM, the MAP of 30 kPa, and the ambient pressure difference of -30 kPa: (a) CMV unblocked case; (b) CMV blocked case

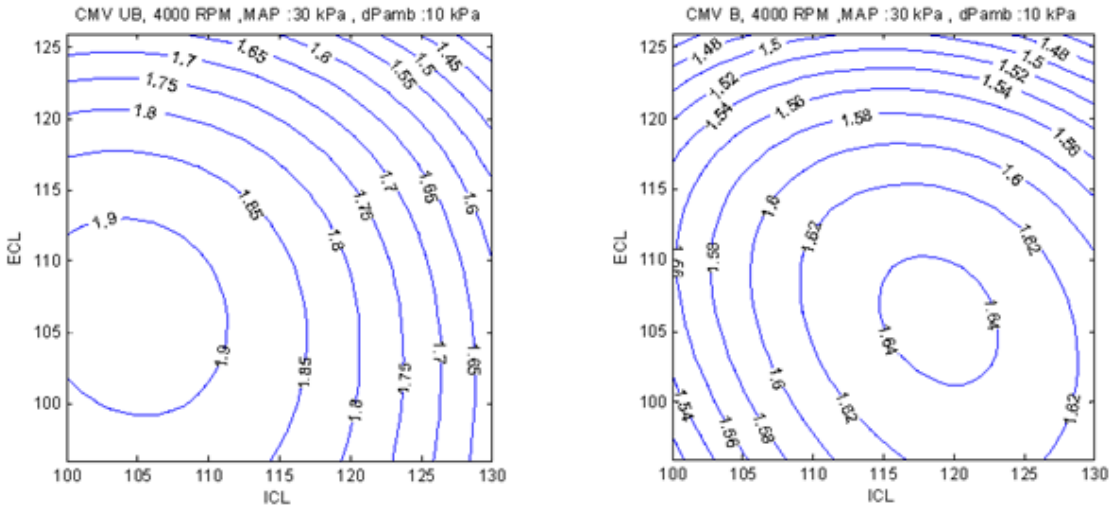

(a) **(b)**

Figure 3-16 Estimated ambient pressure compensation of the mass air flow rate with respect to ICL and ECL at the engine speed of 4000 RPM, the MAP of 30 kPa, and the ambient pressure difference of +10 kPa: (a) CMV unblocked case; (b) CMV blocked case

Finally, the effect of the ambient pressure change is investigated to show the significance of ambient pressure compensations during the estimation of the mass air flow rate. Figure 3-15 and Figure 3-16 show the predicted compensation results at the different engine speeds and ambient pressures. The compensated mass air flow rate changes significantly with respect to the variable valve timings. At low engine speeds, the trends of the ambient pressure compensation are very similar at the different CMV positions as shown in the Figure 3-15. In contrast, the trends of the ambient pressure compensation do not coincide at the both CMV positions at high engine speeds and engine loads as shown in the Figure 3-16. These results inform that the mass air flow rate should be determined accounting for the ambient pressure compensation.

3.7 Summary

The accurate estimation of the mass air flow rate is a critical issue for the calibration and control of high DOF engines. The high complexity of incorporating new technologies into a modern engine induces difficulties in estimating engine states. With a high cost and technical difficulties of implementing sensors for the direct detecting the mass air flow rate into the cylinders, a virtual sensing method is introduced as an alternative of a real sensor in a di-VVT engine with a CMV in the intake port.

To develop a virtual sensor of the mass air flow rate, a specific virtual sensor structure configuration is investigated using two ANNs for the reference ambient conditions and the ambient pressure compensation respectively. Each sensing part is realized using the ANNs, which consist of one input layer, two hidden layers with sigmoid function, and one output layer with pure linear function to represent highly non linear-relations with sufficient accuracy. The ANN structures are determined by a systematic procedure and trained using the generated training data sets from high-fidelity simulation results. The training data sets are generated applying the LHS method as a DOE sampling to reduce the total number of simulations. The high-fidelity simulation can capture the states and responses of our target engine with a sufficient accuracy. The high-fidelity simulation tools are verified with experiment data.

The best ANN structures for the virtual sensing at the reference ambient conditions and for the ambient pressure compensation are determined to be 5-18-18-1 and 6-10-10-1 respectively. The virtual sensing results of the air mass flow rate are assessed at both the CMV unblocked and blocked cases. At low engine speed and engine load conditions

with fixed engine speed and valve timing, virtual sensing of the mass air flow rate at the different CMV positions showed no significant difference in results. In contrast, at the high engine speed and engine load conditions, the mass air flow rate is significantly influenced by the CMV positions, resulting in a reduction of the mass air flow rate of up to 23 percent in the CMV blocked case.

The virtual sensing results show that valve timings have significant effects on the mass air flow rate over the whole engine operating ranges. The results also show that ambient pressure change should be compensated accounting for the variable valve timing and the CMV positions. Based on the virtual sensing results, the optimal VVT position must be determined with regards to the real ambient pressure and the CMV positions. The developed virtual sensing methodology in this study can be applied to the sensing of other engine states and responses, which are difficult to be directly measured.

REFERENCES

1. I. Arise, M. M. Marotta, C. Pianese, and M. Sorrentino, “Experimental validation of a Neural Network Based A/F Virtual Sensor for SI Engine Control”, SAE Technical Paper No. 2006-01-1351, 2006.
2. C. M. Atkinson, T. W. Long, and E. L. Hanzevack, “Virtual Sensing: A Neural Network-based Intelligent Performance and Emissions Prediction System for On-Board Diagnostics and Engine Control”, SAE Technical Paper No. 980516.
3. M. R. Grimes, J. R. Verdejo, and D. M. Bogden, “Development and Usage of a Virtual Mass Air Flow Sensor”, SAE Technical Paper No. 2005-01-0074, 2005.
4. K. Mehrotra, C. K. Mohan, and S. Ranka, *Elements of Artificial Neural Networks*, the MIT Press, Cambridge, Massachusetts, 1997.
5. D. R. Hush, and B. G. Horn, "Progress in Supervised Neural Networks", *IEEE Signal Processing Magazine*, Vol. 10, No. 1, pp. 8-39, New York, 1993.
6. K. Hornik, M. Stinchcombe, and W. Halbert, “Multilayer feedforward networks are universal approximators”, *Neural Networks*, Vol. 2, No. 5, pp359~366, 1989.
7. K. Hornik, “Approximation capabilities of multilayer feedforward networks”, *Neural Networks*, Vol. 4, No. 2, pp251~257, 1991.
8. H. Demuth, M. Beale, and M. Hagan, *Neural Network Toolbox User’s Guide (Version 4.0.6)*, Mathworks Inc., 2005.
9. D. C. Montgomery, *Design and Analysis of Experiments*, John Wiley, 2005.
10. G. E. P. Box, W. G. Hunter, and J. S. Hunter, *Statistics for Experimenters*, John Wiley, 2005.
11. C. F. J. Wu, and M. Hamada, *Experiments Planning, Analysis, and Parameter Design Optimization*, Wiley Interscience, 2000.
12. H. M. Wadsworth, *Handbook of Statistical Methods for Engineers and Scientists*, McGrawHill, 1990.
13. R. V. Hogg, and J. Ledolter, *Applied Statistics for Engineers and Physical Scientists*, Macmillan, 1992.
14. B. Wu, Z. S. Filipi, D. N. Assanis, D. M. Kramer, G. L. Ohl, M. J. Prucka, and E. DiValetin, “Using Neural Networks for Representing the Air Flow Rate through a 2.4 Liter VVT Engine”, SAE Technical Paper No. 2004-01-3054.

CHAPTER 4

CHARACTERIZATION OF COEFFICIENT OF VARIANCE IN INDICATED MEAN EFFECTIVE PRESSURE BY SUBSTITUTIVE MEASUREMENTS

4.1 Introduction

Combustion stability emerges as an important problem in the development of engines, accompanying the better fuel economy and higher engine performance. Combustion stability is directly related to the passenger comfort, because engine smoothness as well as noise, vibration, and harshness (NVH) is highly affected by the combustion stability. To achieve high engine output power, many technologies have been introduced [1-2]. The introduced technologies have been mainly focused on the improvement of output power and fuel economy, and the combustion stability has not been the first objective in developing engines. However, the combustion stability has become a more critical issue to satisfy the customer driving feel and to improve engine NVH.

The combustion stability is directly related to the turbulence intensity in the combustion chamber. The combustion quality at near idle conditions depends strongly on burn rates. Slow burning due to low turbulence and increased residual fraction extends

the combustion process until late in the expansion stroke. At the late expansion stroke, piston is moving rapidly away from the cylinder head, and the increase of the cylinder volume magnifies the effects of combustion variability. Hence, faster burning reduces the combustion variability, and one way of achieving that is increasing turbulence. Thus, the improvement of the combustion stability is achieved by technologies that enable to generate additional turbulence ahead the combustion chamber.

The technologies to improve turbulence include special inlet port designs for generating turbulence [1], dual spark plug systems [1], and variable valve lift (VVL) systems [3-10]. Although special inlet port designs generate turbulence, they also increase pressure drop throughout the port, thus, result in the decrease of the maximum engine output power. Dual spark plug systems provide alternative methods by increasing the size of the flame front. However, this comes with the increased wall area covered by the burned gases and much higher heat losses compared to the state-of-the-are combustion chamber design with the spark plug in the center. VVL systems effectively provide the flexibility in managing turbulence. However, VVL systems require expensive hardware and increase control complexity. In this study, a charge motion valve (CMV) device is introduced to achieve high turbulence by simply mounting it upstream of the intake port.

Although many hardware configurations to increase turbulence have been proposed, quantitative prediction methods to predict combustion stability in real time were not proposed in previous research. In this study, a method for characterizing the combustion stability in real time is proposed using statistical regression analysis by substitute measurements. First, the combustion stability is analyzed by investigating the combustion

process to characterize the combustion stability. In spark ignition (SI) engines, combustion is initiated by the spark discharge, and the flame evolution is governed by the turbulent flame propagation process, which is affected by turbulent flame speed and burning rate specified from a turbulent model. The cycle-by-cycle variations are influenced by the flame propagation phase and represented by the flame development angle change. The flame development angle, $\Delta\theta_d$, is expressed as

$$\Delta\theta_d = C\left(\frac{l_I}{u'}\right)^{1/3}\left(\frac{l_M}{S_L}\right)^{2/3}, \tag{4-1}$$

where l_I, u', and l_M are the integral scale, turbulence intensity, and microscale respectively [1]. From equation (4-1), the increase of the turbulence intensity reduces the flame development angle, thus, reducing the variation of cycle-by-cycle combustion variability.

Then, the coefficient of variation in the indicated mean effective pressure (COV_{IMEP}) is selected as a quantitative measure of the combustion stability. The COV_{IMEP} related parameters are selected from the engine states or responses that can be evaluated by simulations. The selections are based on the investigation of the combustion related parameters. To find the best relations between the COV_{IMEP} and selected parameters, statistical regression analysis procedures are devised. Thus, the combustion stability can predicted using the regression equations of measured substitutive responses.

This chapter is organized as follows. First, the COV_{IMEP} is introduced as a measure of the combustion stability. Then, several parameters that affect on the COV_{IMEP} are determined accounting for the combustion related parameters. To achieve the indirect estimation of the combustion stability from substitute measurements, a statistical

regression analysis procedure is proposed. This analysis procedure includes a trend analysis, a general regression analysis, and assessment steps. Finally, the resulting regression equations for estimating the combustion stability are determined as the functions of the 10-90% burn duration and manifold absolute pressure (MAP).

4.2 Target Engine and Problems in Measuring Combustion Stability

In this study, a charge motion valve (CMV) is introduced as a device for increasing turbulence intensity to achieve combustion stability accounting for cost effectiveness. Although changing port design [1] and variable valve lift (VVL) system [3-10] enable to improve combustion stability, the difficulty in head design change and increasing system complexities become other problems to be resolved.

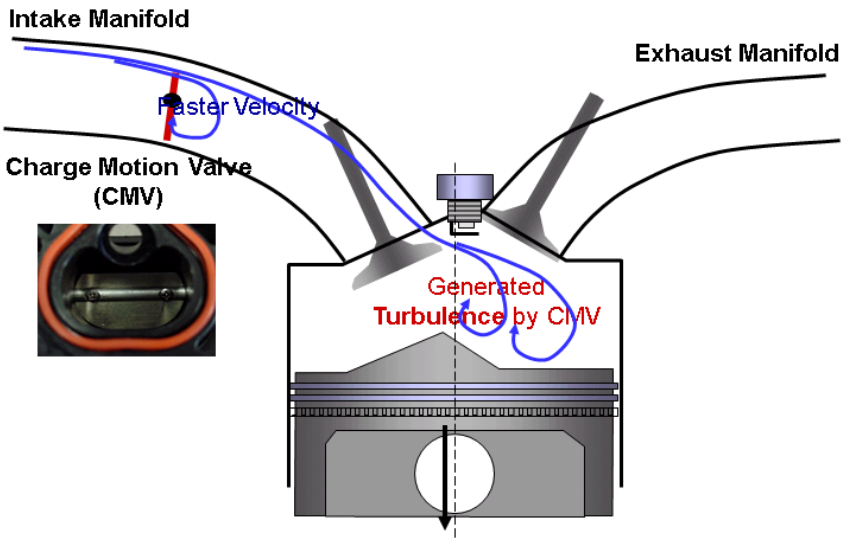

Figure 4-1 Illustration of the CMV and the generated turbulence at the blocked CMV position to increase combustion rate

The CMV is a special device that increases turbulence intensity in a combustion chamber to make the combustion burning rate faster. The CMV has two different operating positions, which are an unblocked position, aligned parallel to a gas passage, and a blocked position, aligned vertical to a gas passage as illustrated in Figure 4-1. The blocked CMV position induces turbulence, thus, resulting in improving the combustion stability.

The cycle-by-cycle variations of combustion are usually investigated by experiments, and the measure of cyclic variability is represented by the COV_{IMEP}. The COV_{IMEP} is calculated from the several tens of IMEP data obtained from experimental results. Thus, a calculation procedure of the COV_{IMEP} cannot be accomplished in real time. In addition, a tremendous number of experiments must be executed to evaluate the COV_{IMEP} over the whole possible engine operating conditions to use the combustion stability as an objective of engine calibration. Thus, the indirect estimation method of the COV_{IMEP} is investigated to realize the real time prediction of the combustion stability for optimal calibration and transient control of high DOF engines.

4.3 Definition of COV_{IMEP} and Parameters related to COV_{IMEP}

The COV_{IMEP} is a parameter that represents cyclic variability calculated from measured pressure data during several tens cycles of experiments and is defined as the standard deviation in IMEP divided by the mean IMEP in Equation (4-2).

$$COV_{IMEP} = \frac{\sigma_{IMEP}}{IMEP} \times 100, \tag{4-2}$$

where σ_{IMEP} is the standard deviation of IMEP.

The COV_{IMEP} is directly related to the combustion stability. Its magnitude becomes higher at low engine speed and load conditions, particularly at the idle operation, under relatively slow mixture motion, larger residual gas fraction, and small turbulence intensity. At a higher engine speed and load, the combustion process becomes more repeatable with short combustion duration and smaller residual gas fraction.

Table 4-1 shows the parameters that are related to the COV_{IMEP}. The COV_{IMEP} related parameters shown in Table 4-1 can be measured by experiments or estimated by simulations. The analysis of the relation between cycle-by-cycle combustion variability and these parameters enables us to indirectly predict the COV_{IMEP}. The parameters that affect on the cycle-by-cycle combustion variability are categorized into pressure-related parameters, burn-rate-related parameters, and flame front position parameters as shown in Table 4-1.

To address the COV_{IMEP} for an engine calibration or an engine control, the related parameters of the COV_{IMEP} must be easily measured or calculated instantaneously. In addition, to achieve higher accuracy in estimating the COV_{IMEP}, using more parameters for finding regressions is beneficial because of the provided additional tuning capability. In contrast, more number of parameters makes the implementation of COV_{IMEP} more complex, and the resulting regression functions using more number of parameters than necessary may cause overestimations. In other words, the number of parameters exceeds the number of the necessary basis for the resulting regression functions.

Table 4-1 COV_{IMEP} related parameters and considered parameters of COV_{IMEP} from high-fidelity simulation results for indirect sensing COV_{IMEP}

Parameters that affect on COV_{IMEP}	**Selected parameters of COV_{IMEP} from high fidelity simulation results**
<u>Pressure-related parameters</u> - Maximum cylinder pressure : p_{max} - Location of peak pressure : θ_{max} - Maximum rate of pressure rise : $(dp/d\theta)_{max}$ - Crank angle at $(dp/d\theta)_{max}$ <u>Burn-rate related parameters</u> - Maximum heat-release rate : $(dQ/d\theta)_{max}$ - Maximum mass burning rate : $(dm_b/dt)_{max}$ - Flame development angle : $\Delta\theta_d$ - Rapid burning angle : $\Delta\theta_b$ <u>Flame front position parameters</u> - Flame radius - Flame front area, enflamed or burned volume - Flame arrival time at given location	(1) 10-90% Burn duration ($\Delta\theta_b$) or $(dP/d\theta)_{max}$ (2) Engine Speed (RPM) (3) Valve Overlap Period (4) Manifold Absolute Pressure (MAP) (5) Spark Timing

The following five parameters are initially selected as the candidates of the representative parameters for estimating the COV_{IMEP} ;

(1) 10-90% burn duration $\Delta\theta_b$ (or, the maximum rate of pressure rise $(dP/d\theta)_{max}$), which represents the pressure-related characteristics.

(2) Engine speed, which represents engine operating conditions.

(3) Valve overlap period, which indirectly represents in-cylinder mixture states such as residual gas fraction.

(4) Manifold absolute pressure (MAP), which represents engine output torque.

(5) Spark timing, which affects the mass burn rate.

Except for 10-90% burn duration, all variables can be easily measured or estimated under engine operations. The 10-90% burn duration can be estimated using an artificial neural network (ANN) based virtual sensing methodology as illustrated in Figure 4-2.

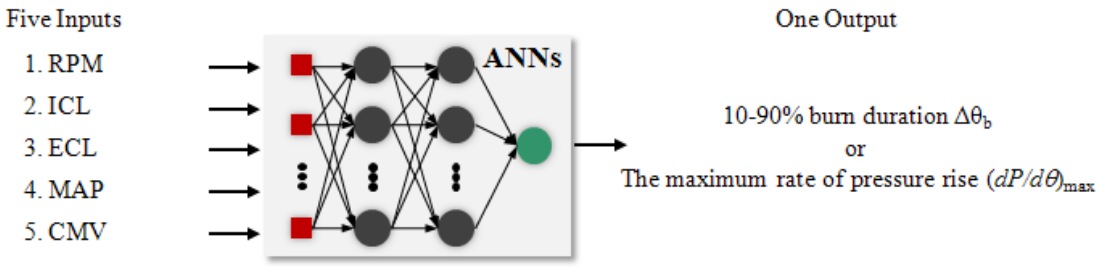

Figure 4-2 Virtual sensor structure for estimating the 10-90% burn duration or the maximum rate of pressure rise using ANNs

4.4 Trend Analysis

First, the trends of the COV_{IMEP} with respect to the selected parameters are investigated to recognize the sensitivity of each parameter and the tendency of the COV_{IMEP} response to each parameter. Since the combustion stability has a tendency to be worse at low engine speed and load operating conditions, the experiments are executed within the engine speed of 3000 RPM and the engine brake mean effective pressure (BMEP) of 400 kPa. While executing the experiments, spark timing is maintained close to the minimum spark advance for best torque (MBT), and air-to-fuel ratio is maintained as stoichiometric. Valve timing and spark timing are scheduled to the optimal set-points for minimum fuel consumption. Two different CMV positions are investigated to assess the effectiveness of the CMV on the combustion stability. Then, the cylinder pressure

profiles are directly measured several tens number of times (in this study, 84 times) at every candidate engine speed and BMEP for calculating the COV_{IMEP}.

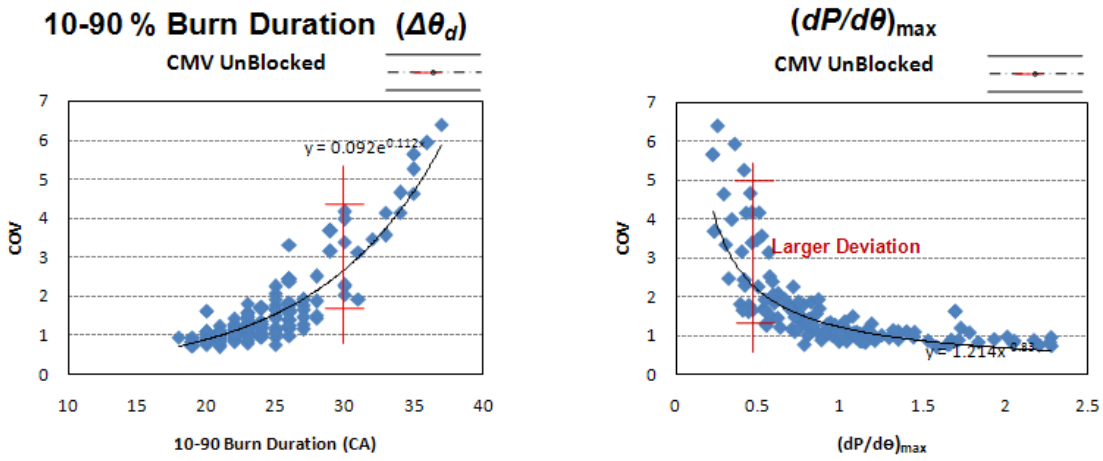

(a) **(b)**

Figure 4-3 Scatter plots of experimental data at the CMV unblocked case: (a) between COV_{IMEP} and 10-90 % burn duration; (b) between COV_{IMEP} and $(dP/d\theta)_{max}$

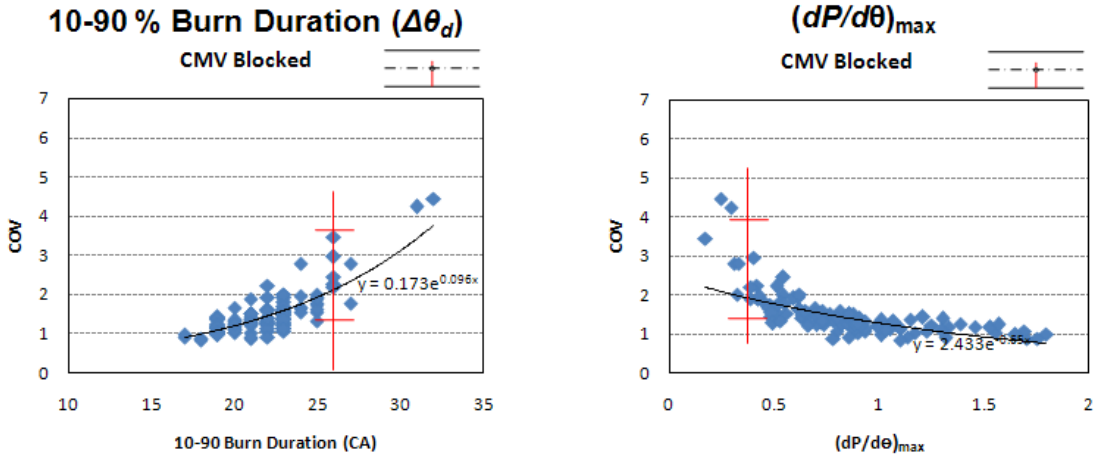

(a) **(b)**

Figure 4-4 Scatter plots of experimental data at CMV blocked case: (a) between COV_{IMEP} and 10-90 % burn duration; (b) between COV_{IMEP} and $(dP/d\theta)_{max}$

The selected five parameters are analyzed to qualify the correlation between the COV_{IMEP} and each parameter. The trend analysis results indicate that the 10-90% burn duration $\Delta\theta_b$ and the maximum rate of pressure rise $(dP/d\theta)_{max}$ show strong trends as shown in Figure 4-3 and Figure 4-4. Since both $\Delta\theta_b$ and $(dP/d\theta)_{max}$ are pressure related parameters, the $\Delta\theta_b$, which has smaller deviation, is selected as a COV related parameter to avoid redundancy. The other parameters show unclear trends or weak trends. Since the combustion characteristics are highly influenced by the CMV positions, the COV_{IMEP} trends are analyzed separately at different CMV positions.

4.5 Regression Analysis

To find the simplest regression equations while maintaining the same level of the regression accuracy, a systematic regression analysis procedure is proposed using statistical analysis methods. Since the structure complexity of the COV_{IMEP} regression function is unknown, more than necessary number of parameters is initially used for determining regression equations. Then, the least significant parameter is removed until the simplest regression equations with the same accuracy are obtained.

To find the best relations between variables, the experimental or simulation data are gathered about the explanatory variables of interest, and regression analysis is applied to estimate the response of the explanatory variables (independent variables) upon a target variable (dependent variable or response variable). The selection of explanatory variables is determined by assessing statistical significance.

4.5.1 General Regression Model and Regression Analysis Methods

The first step of regression analysis is the selection of an adequate regression model. A regression model can be composed with several explanatory variables x_i, a response variable y, and statistical relationships. The statistical relationships can be simple linear functions, quadratic functions, or general functions. The regression model has the coefficient of each regression function β_0, β_1, … , β_i, and the variance σ^2, which accounts for random scatter around the regression line. These parameters are unknown and must be estimated from sample data.

Except for very particular cases, experimental data can often be modeled by the general linear model that is also called the multiple regression models. Suppose that the response y is related to p explanatory variables x_1, x_2, …, x_p as follows:

$$y = \beta_0 + \beta_1 x_1 + \ldots + \beta_p x_p + \varepsilon, \tag{4-3}$$

where ε is the random part of the model, which is assumed to be normally distributed with mean 0 and variance σ^2. i.e. $\varepsilon \sim N(0, \sigma^2)$. The explanatory variables can be selected as a function of other variables.

The estimator of y, $E(y)$ is

$$\begin{aligned} E(y) &= \beta_0 + \beta_1 x_1 + \ldots + \beta_p x_p + E(\varepsilon) \\ &= \beta_0 + \beta_1 x_1 + \ldots + \beta_p x_p. \end{aligned} \tag{4-4}$$

If N observations are collected in an experiment, equation (4-3) is available to each observation, and the form is

$$y_i = \beta_0 + \beta_1 x_{i1} + \ldots + \beta_p x_{ip} + \varepsilon_i, \quad i = 1, \ldots, N, \tag{4-4}$$

where y_i is the ith value of the response and $x_{i1}, x_{i2}, \ldots, x_{ip}$ are the corresponding values of the p explanatory variables.

Equation (4-4) can be expressed in matrix form as

$$\boldsymbol{Y} = \boldsymbol{X\beta} + \boldsymbol{\varepsilon}, \tag{4-5}$$

where $\boldsymbol{y} = (y_1, \ldots, y_N)^T$ is the $N \times 1$ vector of responses, $\beta = (\beta_0, \beta_1, \ldots, \beta_p)^T$ is the $(p+1)\times 1$ vector of regression coefficients, $\boldsymbol{\varepsilon} = (\varepsilon_1, \ldots, \varepsilon_N)^T$ is the $N \times 1$ vector of errors, and $\boldsymbol{X}$, the $N \times (p+1)$ model matrix, is given as

$$\boldsymbol{X} = \begin{pmatrix} 1 & x_{11} & \cdots & x_{1P} \\ \vdots & \vdots & \ddots & \vdots \\ 1 & x_{N1} & \cdots & x_{Np} \end{pmatrix}. \tag{4-6}$$

The regression analysis is a sequential procedure used to find the unknown coefficient vector $\boldsymbol{\beta}$. If the least square criterion is used, the least square estimator $\hat{\boldsymbol{\beta}}$ is calculated by minimizing the sum of squared residuals.

$$\sum_{i=1}^{N} \left(y_i - \left(\beta_0 + \beta_1 x_{i1} + \cdots + \beta_p x_{ip} \right) \right)^2. \tag{4-7}$$

The matrix notation of the equation (4-7) is

$$\boldsymbol{r}^T \boldsymbol{r} = \left(\boldsymbol{y} - \boldsymbol{X\beta} \right)^T \left(\boldsymbol{y} - \boldsymbol{X\beta} \right), \tag{4-8}$$

where the vector $\boldsymbol{r}$ is residual of response $\boldsymbol{y}$.

When equation (4-8) is the minimum value, its partial derivative with respect to $\boldsymbol{\beta}$ should be zero.

$$\frac{\partial \boldsymbol{r}^T \boldsymbol{r}}{\partial \boldsymbol{\beta}} = -2\boldsymbol{X}^T(\boldsymbol{y} - \boldsymbol{X}\boldsymbol{\beta}) = 0. \tag{4-9}$$

The solution to this equation is the least squares estimate which is

$$\hat{\boldsymbol{\beta}} = (\boldsymbol{X}^T\boldsymbol{X})^{-1}\boldsymbol{X}^T\boldsymbol{y}. \tag{4-10}$$

After determining the regression model and finding the least square estimates, the significance of the least square estimates is assessed. The explanatory variables whose regression coefficients are not significant may be removed from the previous regression model. A more compact model with fewer variables is preferred as long as it can express the original data tightly.

The way to assess the significance of individual explanatory variables is to investigate if the following null hypothesis

$$H_0 : \beta_j = 0 \tag{4-11}$$

holds. If the null hypothesis (4-11) holds, the following *t* statistic is used

$$t_j = \frac{\hat{\beta}_j}{\sqrt{\hat{\sigma}^2 \left(\boldsymbol{X}^T\boldsymbol{X}\right)^{-1}_{jj}}}, \tag{4-12}$$

where $\hat{\sigma}^2$ is the mean-square error (MSE), which is

$$\hat{\sigma}^2 = \left(\boldsymbol{y} - \boldsymbol{X}\hat{\boldsymbol{\beta}}\right)^T \left(\boldsymbol{y} - \boldsymbol{X}\hat{\boldsymbol{\beta}}\right) / \left(N - p - 1\right), \tag{4-13}$$

where $N-p-1$ is the degree of freedom of $\boldsymbol{y}-\boldsymbol{X}\hat{\boldsymbol{\beta}}$. By the *t*-test, the j^{th} least square estimate is declared to be significantly different at level α, if

$$\left|t_j\right| > t_{N-p-1,\alpha/2} \ . \tag{4-14}$$

In addition to the *t* test, using a graphical method to judge effect significance is often preferred.

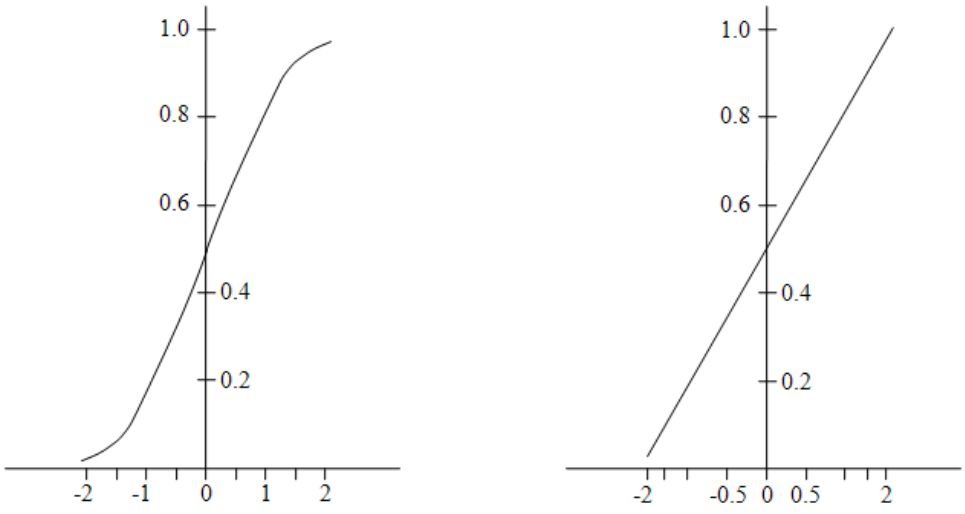

(a) **(b)**

Figure 4-5 Normal probability plots of normal cumulative distribution function: (a) without transformed scale; (b) with transformed scale

In this study, normal probability plots of residuals are used to assess the regression model and associated regression equations. The normal probability plots are calculated by the following procedures. The normality assumption of the errors can be assessed by the following method called a normal probability plot of residuals. Let $r_{(1)} \leq \ldots \leq r_{(N)}$ denote the ordered residuals. If the errors were normally distributed, the plot of the cumulative

probabilities $p_i = (i-0.5)/N$ versus the ordered residuals $r_{(i)}$ should ideally be S-shaped, which is the shape of the normal cumulative distribution function as illustrated in Figure 4-5 (a). By modifying the horizontal axis with adequate transformation, the ideal curve becomes a straight line on the transformed scale as shown in Figure 4-5 (b).

Suppose that the residuals $r_{(i)}$ are normally distributed with the same variance. Then, $\Phi(r_{(i)})$ has a uniform distribution over [0,1]. The uniform distribution of $\Phi(r_{(i)})$ implies that the expected values of $\Phi(r_{(i)})$, $i = 1, \ldots, N$, are spaced uniformly over [0,1]. Thus, the N points $(p_i, \Phi(r_{(i)}))$, $p_i = (i-0.5)/N$, should fall on a straight line. By applying the Φ^{-1} transformation to the horizontal and vertical scales, the N points

$$\left(\Phi^{-1}(p_i), r_{(i)}\right), \quad i = 1, \ldots, N \tag{4-15}$$

must roughly appear as a straight line. If the response data deviates from a straight line calculated from the regression equations, the normality of the constant variance assumption for the errors is violated. In this case, some variables should be introduced or removed to obtain better regression equations.

4.5.2 Regression Models Decision

Decision of adequate regression models is indispensable to find accurate regression equations. When considering the physics of the combustion process, a longer period of 10-90% burn duration has a tendency to cause a higher combustion cyclic variation, and the combustion cyclic variation is always nonnegative. By assessing the trends of the response variable (COV_{IMEP}) with respect to the explanatory variables, an adequate type

of function for regression models is determined as an exponential function. Figure 4-3 and Figure 4-4 also show that the COV_{IMEP} trends with respect to $\Delta\theta_d$ correspond well to an exponential function.

To introduce exponential functions as general regression models, the log transformation of a response variable is applied as

$$\ln y = \beta_0 + \beta_1 x_1 + \cdots + \beta_p x_p \quad . \tag{4-16}$$

This log transformation is a special case of power transformations

$$z = f(y) = \begin{cases} \dfrac{y^{\lambda} - 1}{\lambda}, & \lambda \neq 0 \\ \ln y, & \lambda = 0 \end{cases} . \tag{4-17}$$

First, the appropriateness of this transformation needs to be assessed to maintain the generality of the regression analysis. If the transformation does not change the error trend over all data, then its application to the raw data is adequate. The assessment of this transformation is accomplished by exploring the standard deviation of the transformed variable.

The standard deviation of z can be derived from that of y as follows. Suppose a variable $z = f(y)$ is a random variable defined as a smooth function of another random variable y, and $y = \mu + \varepsilon$. The standard deviation of y is proportional to some power of α the mean μ of y, i.e. $\sigma_y \propto \mu^{\alpha}$. Where μ and σ_y^2 are the mean and variance of y respectively. Using a Taylor series expansion of $f(y)$ around μ,

$$z = f(y) \approx f(\mu) + f'(\mu)(y - \mu) . \tag{4-18}$$

Then,

$$\sigma_z^2 = Var(z) \approx (f'(\mu))^2 Var(y) = (f'(\mu))^2 \sigma_y^2 \ . \qquad (4\text{-}19)$$

For the power transformation in equation (4-17), $f'(\mu) = \mu^{\lambda-1}$ and equation (4-19) becomes

$$\sigma_z \approx |f'(\mu)| \sigma_y = \mu^{\lambda-1} \sigma_y \propto \mu^{\lambda-1} \mu^{\alpha} = \mu^{\lambda+\alpha-1} \ . \qquad (4\text{-}20)$$

By setting the exponent of an equation (4-20) to be zero, σ_z can be made constant regardless of the mean of *y*.

When $\lambda = 0$ and $\alpha = 1$, the power transformation becomes a *log* transformation, and the variance of the transformed variable remains as a constant value. Therefore, the *log* transformation can be applied without loss of generality since it does not affect the accuracy of the regression model.

4.5.3 Regression Analysis Procedure and Results

The objective of regression analysis in this study is to find the simplest regression equations for the COV_{IMEP} with a sufficient accuracy. The least significant variable is removed while the regression equations can capture the trend of original data with the same level of accuracy. Since the CMV makes a huge impact on the combustion characteristics, regression analyses are separately executed at the unblocked and blocked CMV positions respectively.

The procedure to find the simplest regression equations is shown in Figure 4-6. The initially selected explanatory variables are (1) 10-90 % burn duration, $\Delta\theta_d$, (2) spark timing, (3) MAP, (4) engine speed, N, and (5) valve overlap period. Then, the response variable, the COV_{IMEP}, is transformed using log transformation in equation (4-16) to formulate an adequate form of regression equations.

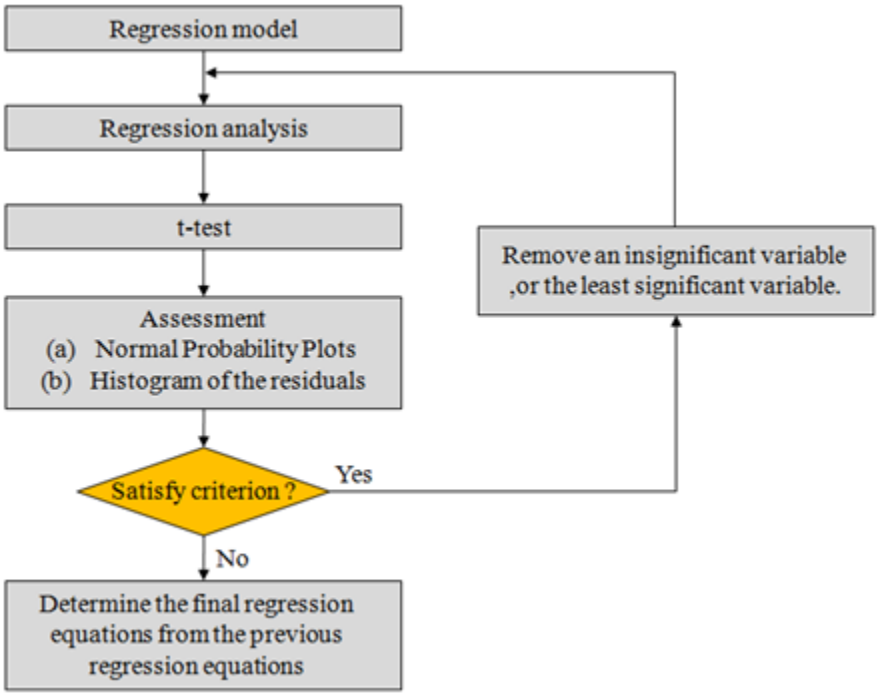

Figure 4-6 Statistical regression analysis procedure to find the best regression equations for the COV_{IMEP}

First, regression equations are determined with all five nominated explanatory variables. The significance of each variable is assessed using the *t*-test. Then, the regression equations are assessed using the normal probability plots of the residuals and the histogram of the residuals. When the residuals of the response variable data are tightly fitted on the straight line at the normal probability plots, and the histogram of the

residuals converges to the normal distribution or *t*-distribution, the determined regression equations are good enough to represent the response variable. Next, the least significant explanatory variable is removed to make the regression equations simpler. Then, the same regression analysis procedures with the remaining variables are performed again. When the resulting regression equations are inadequate to represent the original response variable with sufficient accuracy, the previous regression equations are considered as the best ones.

Table 4-2 Regression analysis results of COV_{IMEP} with two explanatory variables at the CMV unblocked case

Predictor	Coefficient (β_j)	t- value	p-value
Constant	–1.9594	–12.67	0.000
10-90 % burn duration $\Delta\theta_d$ (CA)	0.105891	22.55	0.000
MAP (kPa)	–0.005167	–3.80	0.000

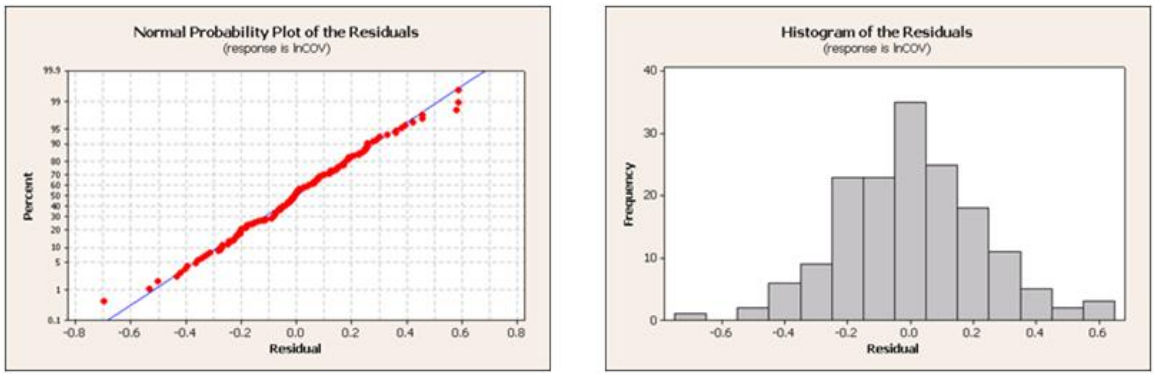

(a) **(b)**

Figure 4-7 (a) Normal probability plot of the residuals; (b) histogram of the residuals with two explanatory parameters: CMV unblocked case

Table 4-3 Regression analysis results of COV_{IMEP} with two explanatory variables at CMV blocked case

Predictor	Coefficient (β_j)	t- value	p-value
Constant	–1.0789	–5.47	0.000
10-90 % burn duration $\Delta\theta_d$ (CA)	0.080034	11.28	0.000
MAP (kPa)	–0.006981	–4.75	0.000

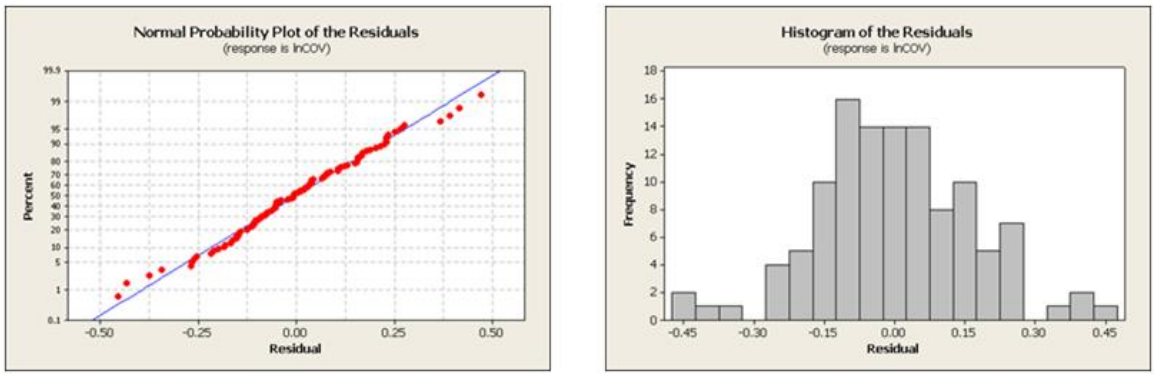

(a) **(b)**

Figure 4-8 (a) Normal probability plot of the residuals; (b) histogram of the residuals with two explanatory parameters: CMV blocked case

Using this procedure, the final regression equations are determined with two explanatory variables, which are the 10-90% burn duration and MAP, regardless of the CMV positions. The resulting regression equations are expressed as

$$COV_{IMEP} = \exp(-1.96 + 0.106 \times \Delta\theta_d - 0.00517 \times MAP) \quad (4\text{-}21)$$

$$COV_{IMEP} = \exp(-1.08 + 0.08 \times \Delta\theta_d - 0.00698 \times MAP) \quad (4\text{-}22)$$

at the CMV unblocked case and CMV blocked case respectively.

Tables 4-2 and 4-3 show the final regression analysis results with two explanatory variables. The p-values of the two variables are close to zero, which means that these variables are significant, and the tightness of the regression equations to the experimental

data of the COV_{IMEP} is verified using the normal probability plots and histogram of the residuals as seen in Figures 4-7 and 4-8. Therefore, the resulting regression equations with the two explanatory variables of 10-90 % burn duration $\Delta\theta_d$ and MAP are considered as the simplest regression equations for the COV_{IMEP}.

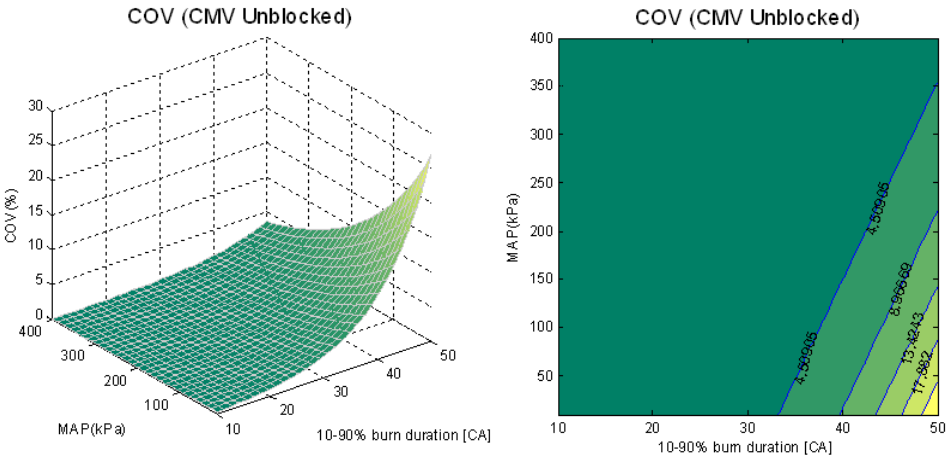

Figure 4-9 COV_{IMEP} response surface predicted from the regression equation with two variables of 10-90 % burn duration and MAP at the CMV unblocked case

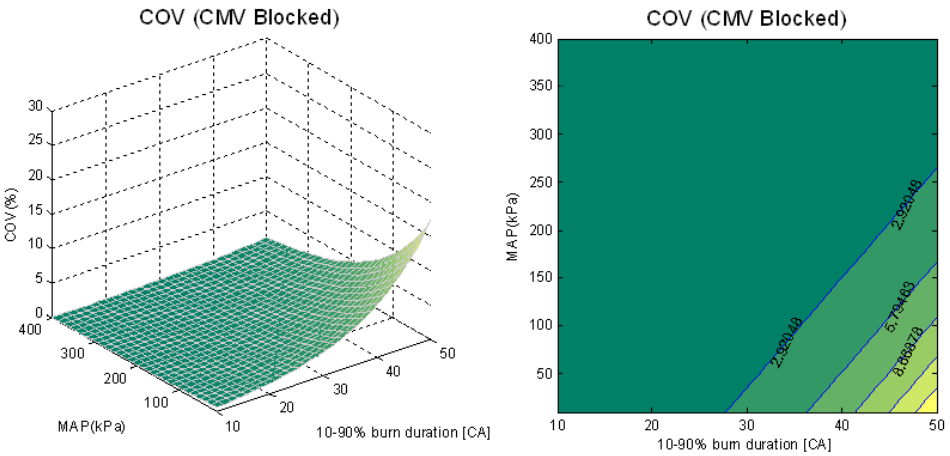

Figure 4-10 COV_{IMEP} response surface predicted from the regression equation with two variables of 10-90 % burn duration and MAP at the CMV blocked case

To investigate the trends of the COV_{IMEP} at each CMV position, the estimated COV_{IMEP} response surfaces, which are generated by the determined regression equations, are illustrated in Figure 4-9 and Figure 4-10. The longer burn duration and higher MAP, the higher COV_{IMEP} at both CMV unblocked and blocked case. The resulting trends correspond well with the expectation accounting for the physics of combustion. When the CMV is blocked to increase combustion speed, the intensified turbulence into the cylinders induces the faster combustion speed, and stabilizes the combustion variability. The resulting regression equations enable to predict the COV_{IMEP} in real time using substitute measurement of the MAP and the virtual sensing of the 10-90 % burn duration.

4.6 Summary

The methodology to predict the combustion stability in real time from substitute measurements is created by introducing statistical regression analysis procedures. Since the combustion stability is directly related to the engine smoothness and NVH, improving the combustion stability becomes very important to satisfy customer needs. To address the combustion stability in engine calibration procedures and transient control, a real time prediction of the COV_{IMEP} is indispensable. The combustion stability is generally assessed in terms of combustion cyclic variability. The cycle-by-cycle variability of combustion can be quantified by $COV_{IMEP,}$ which is defined as the standard deviation in IMEP divided by the mean IMEP. In general, the COV_{IMEP} is calculated from several tens of cycles of measured cylinder pressure data, which is directly measured at the same operating conditions.

To develop a real time estimation methodology of the COV_{IMEP}, a statistical regression analysis procedure is proposed by using substitute measurements and virtual sensing of combustion stability related parameters. After investigating combustion physics and related parameters, five explanatory variables are selected to find regression equations of the COV_{IMEP}. Then, by exploring the trends of the COV_{IMEP} with respect to each parameter, regression equation models are determined as exponential forms through the *log* transformation to the response variable.

The objective of the proposed statistical regression analysis procedure is to find the simplest regression equations without degrading regression accuracy. To achieve the objectives, the least significant parameters are removed using the *t*-test and statistical assessment methods while the resulting equation accuracy is maintained. The determined final regression equations have two variables, $\Delta\theta_d$ and MAP. Finally, the regression equations for the COV_{IMEP} provide an indirect estimation method of the combustion cycle-by-cycle variability in real time for the optimal engine calibration and transient control objectives.

REFERENCES

1. J. B. Heywood, *Internal Combustion Engine Fundamentals*, McGrawHill, 1998.
2. C. F. Taylor, The Internal-combustion engine in Theory and Practice Volume I : Thermodynamics, Fluid Flow, Performance, The M.I.T. Press. 1985.
3. P. Kreuter, P. Heuser, J. Reinicke-Murmann, R. Erz, and U. Peter, "The Meta VVH System – The Advantages of Continuously Mechanical Variable Valve Timing", SAE Technical Paper No. 1999-01-0329, 1999.
4. R. Flierl, and M. Klüting, "The Third Generation of Valvetrains – New Fully Variable Valvetrains for Throttle-Free Load Control", SAE Technical Paper No. 2000-01-1227, 2000.
5. M. Nakamura, S. Hara, Y. Yamada, K. Takeda, N. Okamoto, T. Hibi, S. Takemura, and S. Aoyama, "A Continuous Variable Valve Event and Lift Control Device (VEL) for Automotive Engines", SAE Technical Paper No. 2001-01-0244, 2001.
6. C. Brüstle and D. Schwarzenthal, "VarioCam Plus – A Highlight of the Porsche 911 Turbo Engine", SAE Technical Paper No. 2001-01-0245, 2001.
7. P. Kreuter, P. Heuser, J. Reinicke-Murmann, R. Erz, U. Peter, and O. Böcker, "Variable Valve Actuation – Switchable and Continuously Variable Valve Lifts", SAE Technical Paper No. 2003-01-0026, 2003.
8. M. Sellnau, and E. Rask, "Two-Step Variable Valve Actuation for Fuel Economy, Emissions, and Performance", SAE Technical Paper No. 2003-01-0029, 2003.
9. W. Hannibal, R. Flierl, L. Stiegler, and R. Meyer, "Overview of Current Continuously Variable Valve Lift Systems for Four-Stroke Spark-Ignition Engines and the Criteria for their Design Ratings", SAE Technical Paper No. 2004-01-1263, 2004.
10. R. Flierl, D. Gollasch, A. Knecht, and W. Hannibal, "Improvements to a Four Cylinder Gasoline Engine Through the Fully Variable Valve Lift and Timing System UniValve®", SAE Technical Paper No. 2006-01-0223, 2006.
11. D. C. Montgomery, *Design and Analysis of Experiments*, John Wiley, 2005.
12. G. E. P. Box, W. G. Hunter, and J. S. Hunter, *Statistics for Experimenters*, John Wiley, 2005.
13. C. F. J. Wu, and M. Hamada, *Experiments Planning, Analysis, and Parameter Design Optimization*, Wiley Interscience, 2000.
14. H. M. Wadsworth, *Handbook of Statistical Methods for Engineers and Scientists*, McGrawHill, 1990.
15. R. V. Hogg, and J. Ledolter, *Applied Statistics for Engineers and Physical Scientists*, Macmillan, 1992.

CHAPTER 5

OPTIMAL CALIBRATION OF DUAL-INDEPENDENT VVT ENGINES WITH CHARGE MOTION CONTROL CONSIDERING FUEL ECONOMY AND COMBUSTION STABILITY: PART LOAD OPERATING CONDITIONS

5.1 Introduction

The improvement of engine performance and fuel economy while decreasing emissions are main research concerns of the automotive industry. The recent increase of the petroleum price pressures customers to buy cars that have better fuel economy, yet customers refuse to sacrifice performance in the name of fuel efficiency. As one vehicle system level solution of these intractable problems, hybrid electric vehicles (HEV) was introduced by combining electrical motor and traditional internal combustion engine. At the same time, the internal combustion (IC) engine itself remains as the main stream in the automotive industry through continuous improvement by introducing new technologies. Among modern engine technologies, variable valve timing (VVT) system is widely used in a modern IC engine as one of the most promising technologies to improve overall engine performance through managing gas exchange process over the whole engine operating ranges without adding excessive system complexity.

In addition to the performance and fuel economy, engine quietness and smoothness have become other important problems to be improved for satisfying customer needs. The engine smoothness can be achieved by improving combustion stability. To improve the combustion stability, special inlet port designs for generating turbulence [10], dual spark plug systems [10], and variable valve lift (VVL) systems have been introduced [1-8]. However, these technologies require significant cylinder head design change, or expensive actuators cost.

In this study, a dual-independent VVT (di-VVT) engine with charge motion valves (CMVs) are selected as the target engine to achieve ultimate output power and better fuel economy as well as high combustion stability, after the intensive consideration of the cost effectiveness, product development time, and engine performance requirements. The di-VVT system is composed of intake VVT devices and exhaust VVT devices that modify intake and exhaust valve timing independently. The di-VVT can adjust gas exchange characteristics over the whole engine operating ranges. The CMV is a flip valve device, which is located upstream of the intake runner before the intake valves. The CMV increases turbulence intensity of the intake air to enhance combustion speed. However, the additional system complexity by introducing new technologies increases the degree of freedom (DOF) of engines, thus, results in the difficulties in the experiment based engine calibration.

To resolve the difficulties in the experiment based calibration of high DOF engines, simulation based calibration methodologies have been used to achieve optimal engine calibration [14,16]. Optimal calibration of conventional engines has been achieved by experiment based procedures. In the experiment based calibration, the optimal actuator

set-points are obtained by searching the best engine operating conditions throughout all possible engine operating conditions. When addressing optimal calibration problems of high DOF engines, the number of possible engine operating conditions increases exponentially to the unmanageable point beyond the experimental capability in the test cell.

To develop a simulation based engine calibration methodology, fast and accurate engine simulation tools are indispensable, because they reduce the engine calibration time and costs. Thus, high-fidelity simulation is presented by combining one-dimensional gas dynamics simulation and quasi-dimensional simulation to achieve moderately fast and sufficiently accurate simulation results. Although the high-fidelity simulation estimates engine responses accurately, it is inadequate for an optimal calibration procedure due to its relatively long calculation time. In addition, simulation based optimal calibration of a high DOF engine requires numerous calculations of objective functions to find the optimum at given engine operating condition.

Thus, as an alternative of the high fidelity simulation, artificial neural networks (ANNs) are selected due to the fast computation time and the capability of capturing highly nonlinear input-to-output relationships. The ANN models are introduced as surrogate engine models, and trained by training procedures using sufficient simulation data generated by the high-fidelity simulation tools. By using the fast surrogate engine models, optimal calibration of high DOF engines can be achieved without excessively long computation time.

In this study, engine calibrations with multi objectives at part load conditions are proposed accounting for both fuel economy and combustion stability. In conventional

engine calibration problems, the best fuel economy at part load operating conditions is generally used as calibration objectives. Compared to the engine calibration problem at the WOT, the engine calibration at part load conditions is challenging due to the difficulty in predicting combustion characteristics accounting for various in-cylinder states. Moreover, the consideration of the combustion stability during engine calibration process requires sensing methodologies capable of estimating the combustion stability with fast computation and sufficient accuracy.

The combustion stability is quantified using coefficient of variance in indicated mean effective pressure (COV_{IMEP}). Since COV_{IMEP} is calculated by measuring several tens cycle of in-cylinder combustion pressure profiles, COV_{IMEP} cannot be measured in real time. To resolve the real time measurement problem, a virtual sensing of COV_{IMEP}, which is developed from the statistical regression analysis, is incorporated to the objective function of the optimal calibration problem. By using engine ANN models and a virtual sensing of the combustion, a multi-objective engine optimal calibration framework is created to find the best actuator set-points. The optimal engine calibrations are achieved by optimizing the multi-objective cost function of the engine calibration problem accounting for the engine operating constraints.

This chapter is organized as follows. First, an optimization frame work is introduced. Then, the objective function of the optimal calibration problem is formulated using inverse and regular ANN models, and statistical regression models. After the experimental design for generating high-fidelity simulation results are proposed, the ANN model training procedures and results are shown. Finally, optimal engine calibration results at part load conditions are provided and evaluated.

5.2 Optimization Framework

The optimization framework, which was originally proposed by Bin Wu [16], is used to build a systematic procedure for the calibration of a di-VVT engine with the CMV over the whole engine operating conditions as illustrated in Figure 5-1. Over the whole engine operating ranges, optimal actuator set points are determined at every fixed engine operating condition, which is expressed by means of an engine speed and a break mean effective pressure (BMEP). As the control variables at an engine operating condition, an intake cam lobe location (ICL), an exhaust cam lobe location (ECL), spark timing, and a charge motion valve (CMV) position are selected. These control variables at each engine operating condition determine engine responses.

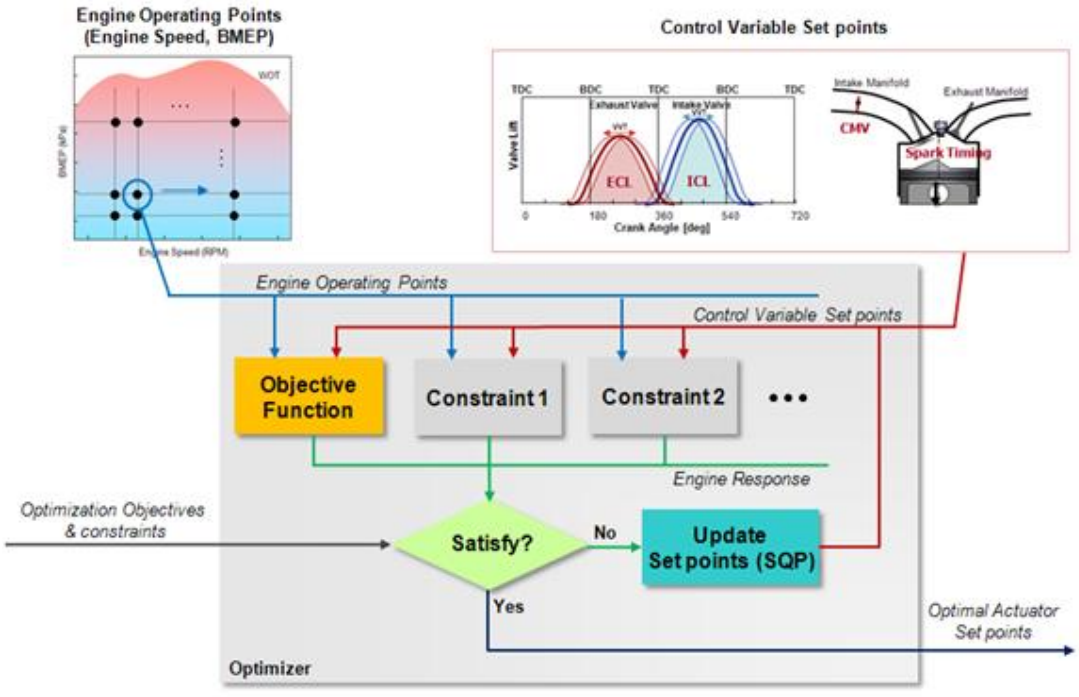

Figure 5-1 Optimization framework for calibrating independent control variables in high DOF engines

The optimal actuator set points are determined using an optimization algorithm based on nonlinear programming at every engine operating points. The optimization for finding the optimal actuator set-points is repeated until the whole engine operating points are fully covered. The complete sets of the optimal actuator set-points are used to build optimal actuator set-point maps for each actuator.

The objective function of the optimal engine calibration problem in this study includes both a fuel economy objective and a combustion stability objective. The objective function must have short computation time while guaranteeing sufficient accuracy, because the entire engine operating points is large and the optimization algorithm requires a large number of evaluations of the objective function. Thus, a fast and accurate engine model must be used to create the objective function.

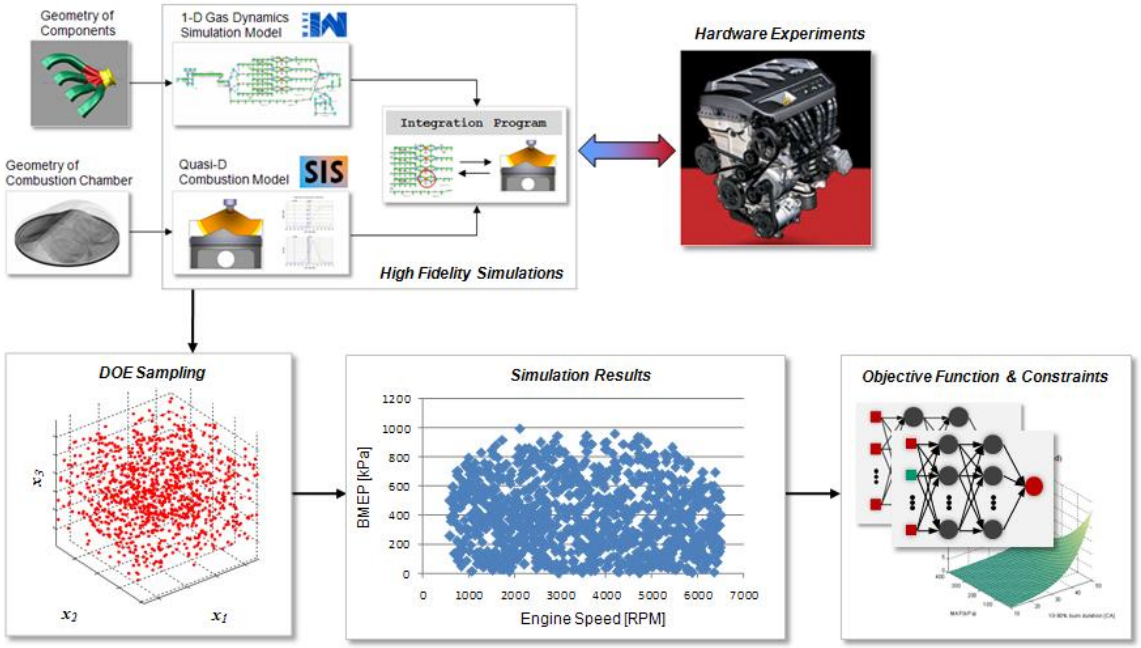

Figure 5-2 Illustration of the procedure to build an objective function and constraints

Figure 5-2 illustrates the procedure to create the fast and accurate objective functions and applied constraints using the ANN models. The objective functions are created by the following steps:

(1) To guarantee the simulation accuracy, a high-fidelity simulation model is created by combining a 1-D gas dynamics simulation model and a quasi-D combustion model.

(2) The high-simulation is validated at several important engine operating points by using experimental data.

(3) The necessary simulation cases are determined using the Latin hypercube sampling (LHS) method to reduce the total number of experiments. The simulation cases must cover all possible combinations of actuator inputs and engine operating points.

(4) Simulation results are generated at selected simulation cases.

(5) ANN models, which are fast and accurate surrogate engine models, are trained to capture the highly nonlinear engine input-to-output relations.

(6) Concurrently, other virtual sensing method may be used to estimate engine responses not easily measurable by experiments.

(7) The final objective functions are formulated by combining the ANN models and virtual sensors.

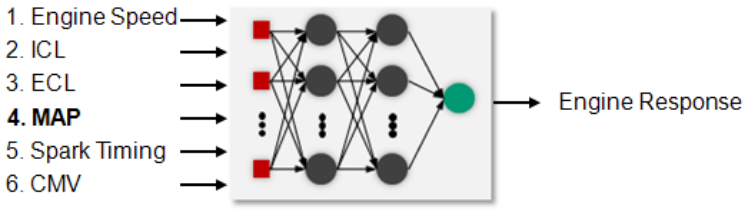

(a)

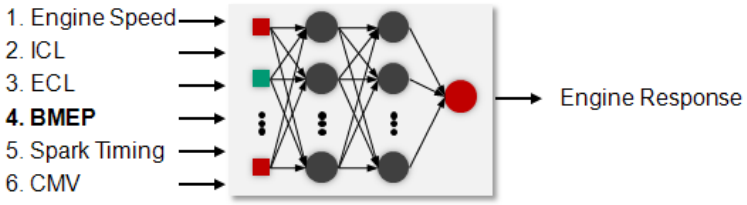

(b)

Figure 5-3 Two types of ANNs to estimate engine responses: (a) regular transfer function; (b) inverse transfer function

The ANN models used for creating the objective function are categorized into the regular ANN model and the inverse ANN model as shown in Figure 5-3. The regular ANN model relates engine control inputs and engine measured states to engine responses. In contrast, the inverse ANN model uses at least one engine response as the input to the ANN model to create a transfer function for other engine responses. The regular ANN model is used as a virtual sensor to formulate the objective function, and the inverse ANN model is used to improve the computational efficiency during the optimization procedure.

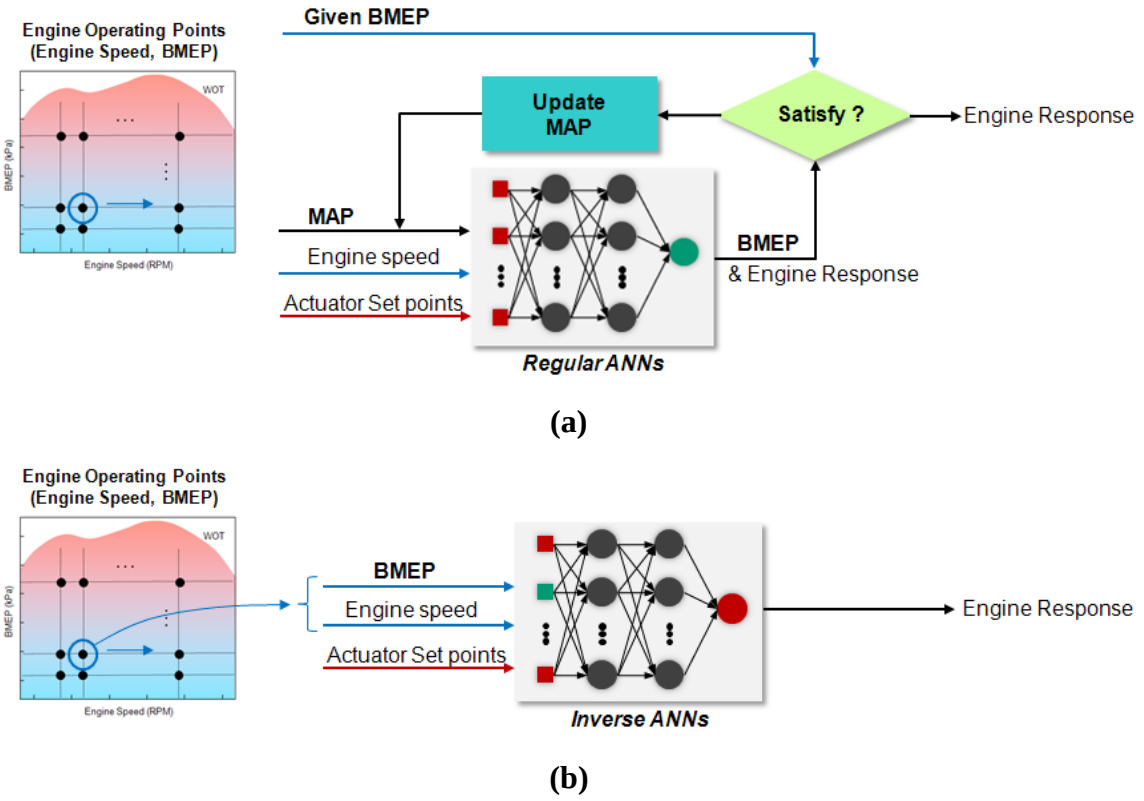

Figure 5-4 Illustrations of the procedure to find engine response at given engine speed and BMEP by using: (a) Regular ANNs; (b) Inverse ANNs

To reduce the computation time for determining adequate actuator inputs and to achieve a desired BMEP, the inverse ANN model is used a shown in Figure 5-4 (b). In general, actuator set-points are defined at every engine operating point, which is determined by a given engine speed as a horizontal axis and a given break mean effective pressure (BMEP) as a vertical axis. When the regular ANN model is used, iteration is required to find adequate actuator control inputs to attain the given BMEP output as illustrated in Figure 5-4 (a). In contrast, the inverse ANN model enables to assign arbitrary actuator inputs for evaluating engine responses at a given BMEP without any iteration.

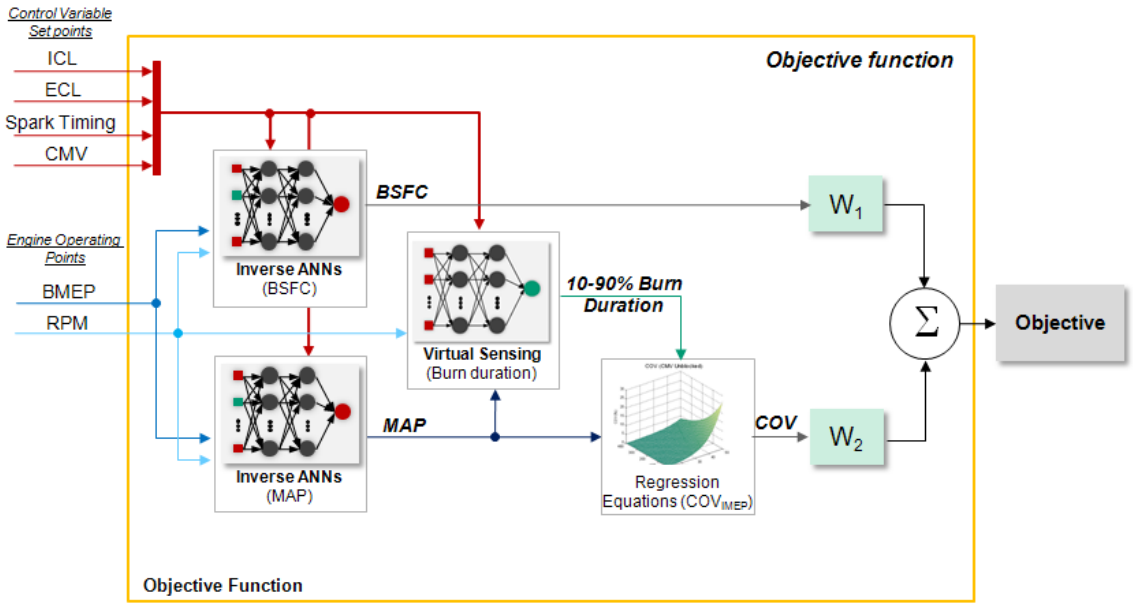

Figure 5-5 Structure of the objective function for the optimal calibration of actuators with the consideration of the COV_{IMEP}

The structure of the objective function including both fuel economy and combustion stability objectives is illustrated in Figure 5-5. While combustion stability is improved by activating the CMV, fuel economy tends to be deteriorated over wide ranges of the engine operating conditions, and vice versa. Thus, an optimization problem with multi objectives is introduced to find the best trade-off operations. The multi objective function is formulated by combining *bsfc* and the COV_{IMEP} and by multiplying adequate weighting factors to each objective. The *bsfc* is evaluated using the inverse ANN model, and the COV_{IMEP} is estimated by the regression equations with the 10-90% burn duration and the MAP inputs. The 10-90% burn duration and the MAP are estimated by an inverse ANN model and a regular ANN model respectively.

5.3 Training and Validation of the ANNs for Representing Engine Responses

The ANN models to represent engine models are trained using high fidelity simulation results. The training data are generated to cover the whole possible engine operating conditions by using the LHS method to reduce the total number of simulations. The total number of simulations is elected to capture the complexity of the target engine responses with sufficient accuracy. After reviewing the engine responses, the total number of simulations is finally determined to two thousand, and the total number of simulations is enough to capture all possible engine responses within the concerning engine operation ranges.

Then, the ANN models are determined by a systematic ANN model training procedure. The ANN model structure is determined as the combination of one input layer, two hidden layers with sigmoid functions, and one output layers with linear functions. The systematic ANN model training procedures are as follows:

(1) Decide the ANN structure considering the convergence efficiency and complexity of the ANNs.

(2) Divide the data set generated by the high-fidelity simulation into a train data set, which is used to train the ANNs, and a test data set, which is used to validate the trained ANNs.

(3) Check the error criterion. When the calculated error exceeds the error criterion, increase the number of neurons in the hidden layers by one until the error criterion is satisfied.

By following the ANN model training procedures, the preferred best inverse ANN structures for the *bsfc* and the MAP are determined as a 6-12-12-1 and a 6-24-24-1 structure respectively. The training results of the inverse ANNs are shown in Figure 5-6 and Figure 5-7. The blue lines, depicted on the graphs, indicate ±5 % error bounds, and small circles on the graph indicate the training data points. Overall data of the train and test sets are located within the error bound. The preferred best inverse ANN models capture the input-to-output relations with the same accuracy of the high-fidelity simulation results. Therefore, the determined inverse ANN models can be used as good fast surrogate models for estimating engine responses.

To verify the ANN models, estimated *bsfc* maps by the ANN models are compared to the achieved *bsfc* maps by the high-fidelity simulation under part load conditions at both the CMV blocked and unblocked cases. The *bsfc* is calculated by

$$bsfc(\text{g/kW•h}) = \frac{\dot{m}_f(\text{g/h}) \times 2 \times 10^3 \times 60}{\text{BMEP(kPa)} \times V_d(\text{dm}^3) \times N_{eng}(\text{RPM})} \ , \tag{5-1}$$

where $\dot{m}_f$ is the mass fuel flow rate in g/h, V_d is the displaced or swept volume in dm^3, and N_{eng} is engine speed in RPM. In this study, the *bsfc* is calculated from the mass fuel flow rate to avoid high nonlinearity close to the 0 kPa of the BMEP.

Figure 5-8 shows *bsfc* maps achieved from both inverse ANN models and the high-fidelity simulation results at both the CMV blocked and unblocked cases. Throughout the reviewed engine operating ranges, both *bsfc* contours coincide well both at CMV blocked and unblocked cases. Thus, the trained ANN models are capable of substituting the high-fidelity simulation models without the loss of simulation accuracy.

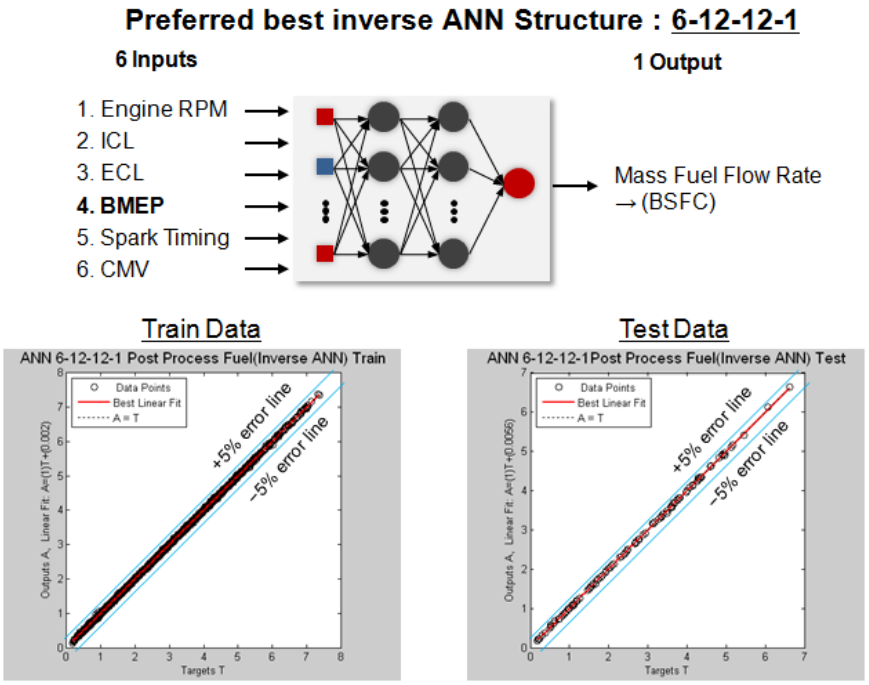

Figure 5-6 Preferred best inverse ANN structure of the fuel mass flow rate, the training results with the train data set, and the test data set

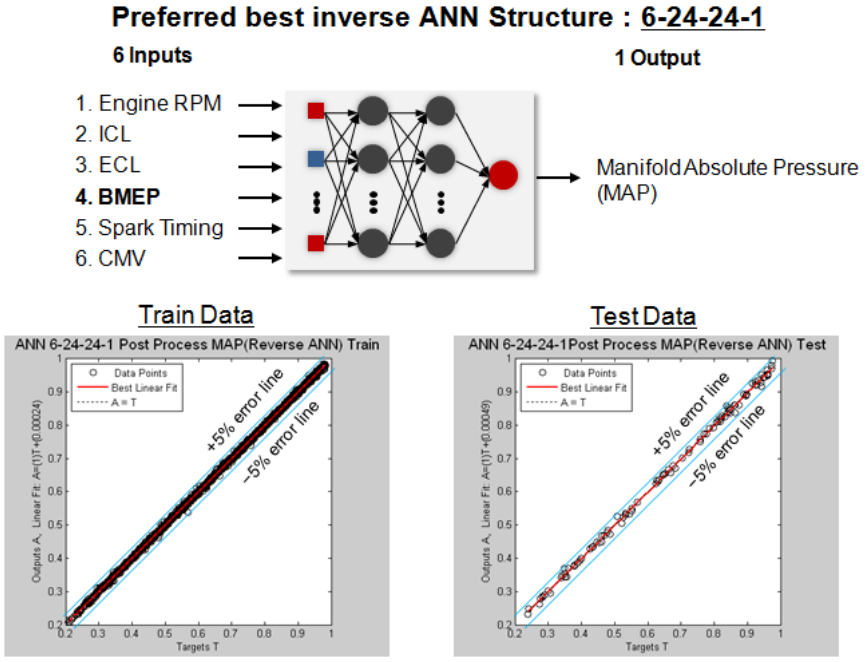

Figure 5-7 Preferred best inverse ANN structure of the MAP, the training results with the train data set, and the test data set

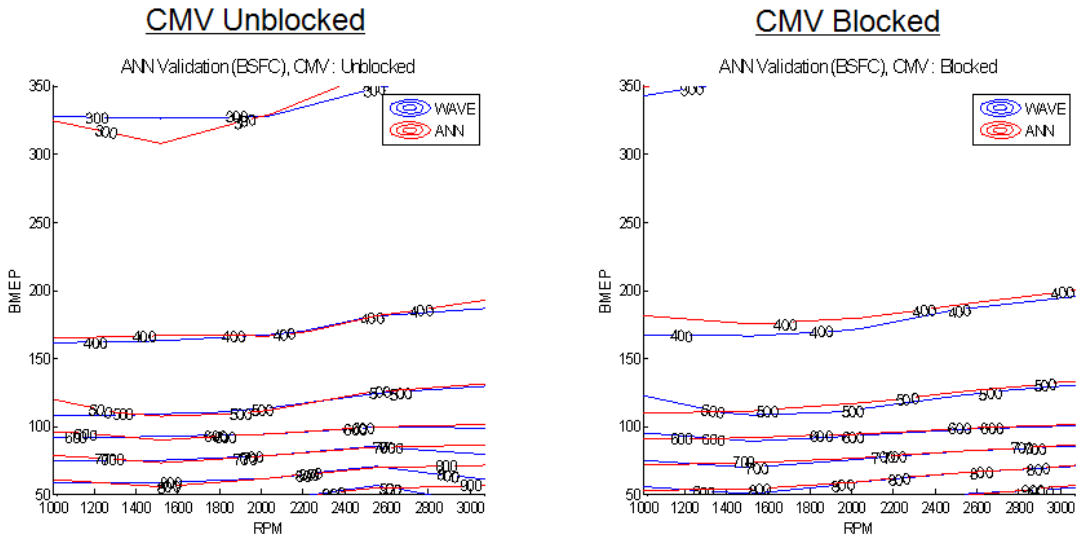

(a) **(b)**

Figure 5-8 Comparison of *bsfc* maps between high-fidelity simulation results and ANNs outputs: (a) CMV blocked case; (b) CMV unblocked case

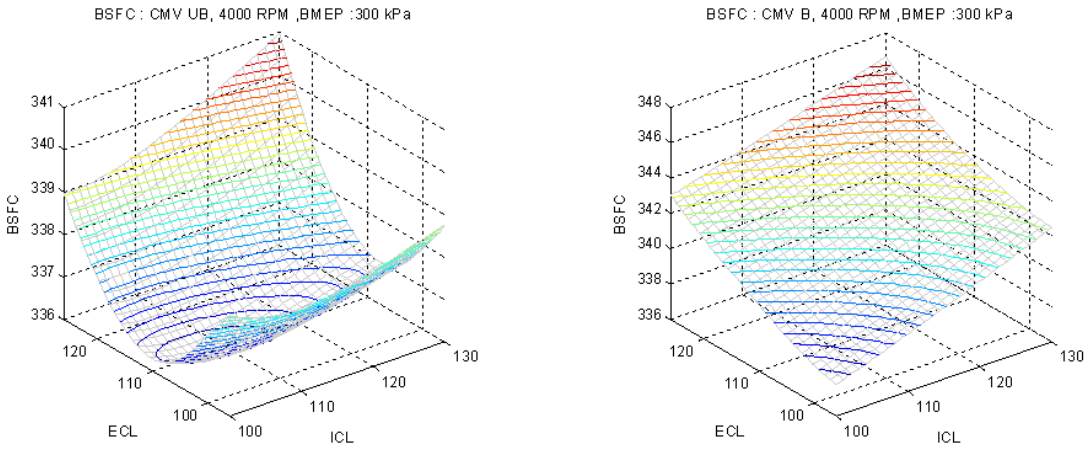

(a) **(b)**

Figure 5-9 *bsfc* response surfaces with respect to the ICL and ECL at the fixed engine speed of 4000 RPM, and the BMEP of 300 kPa: (a) CMV unblocked case; (b) CMV blocked case

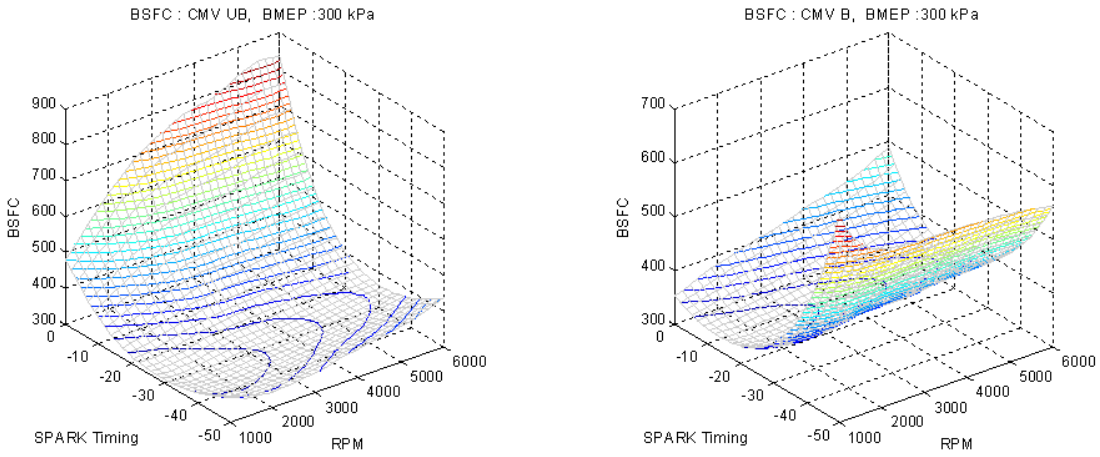

(a) **(b)**

Figure 5-10 *bsfc* response surfaces with respect to the engine speed and the spark timing at the fixed ICL and ECL: (a) CMV unblocked case; (b) CMV blocked case

Figure 5-9 and Figure 5-10 show the resulting *bsfc* surfaces with respect to ICL and ECL, and the resulting *bsfc* surfaces with respect to engine speeds and spark timings respectively. The *bsfc* surfaces show smooth response surfaces without any abnormally complex curvature that is caused by the overfitting of the trained ANN models. The smooth response surfaces enable to determine the global optima by using a gradient based optimization algorithm with a selection of an adequate initial point.

5.4 Mathematical Formulation of Optimal Calibration Problems

Optimal calibration problems with multi objectives are formulated by assigning subjective weights to each objective and summing up all objectives multiplied by their corresponding weight. Since the engine calibration under part load conditions is our

optimization problem, the fuel economy is selected as a prime objective. Then, combustion stability is introduced as an additional objective.

The objective function has six inputs and one output. The six inputs are categorized into two groups. One group expresses engine operating points, which are engine speed (N_{eng}) and engine torque (T_{eng}, expressed as BMEP); and the other group handles actuator control variables, which are intake cam timing (ζ_{IN}), exhaust cam timing (ζ_{EX}), spark timing (σ_{spark}), and CMV position (L_{CMV}). In addition to the objective function, actuator operating ranges are bounded. The CMV operating ranges are restricted below the engine speed of 3000 RPM and the BMEP of 400 kPa, because the COV_{IMEP} becomes high only at low engine speeds and BMEP. In addition to these constraints, the actuator operating rate is also restricted to prevent aggressive actuator operations. For the simplicity of the optimal calibration, the actuator operating rate restriction criteria are assumed as adequate constant values.

The proposed optimization problem is solved by a two-step procedure. The first step is solving the single-objective problem in equation (5-3), whose objective is *bsfc*, at given engine operating point and the CMV position.

$$\text{minimize } f = bsfc(\zeta_{IN}, \zeta_{EX}, \sigma_{spark} \mid N_{eng}, T_{eng}, L_{\text{CMV}}) \tag{5-3}$$

subject to

$$700 \text{ RPM} \le N_{eng} \le 6000 \text{ RPM},$$

$$\text{ATDC } 100 \text{ deg} \le \zeta_{IN} \le \text{ATDC } 130 \text{ deg},$$

$$\text{BTDC } 126 \text{ deg} \le \zeta_{EX} \le \text{BTDC } 90 \text{ deg},$$

$$\text{ATDC } -50 \text{ deg} \le \sigma_{spark} \le \text{ATDC } 0 \text{ deg},$$

$$700 \text{ RPM} \le N_{eng} \mid L_{\text{CMV,b}} \le 3000 \text{ RPM},$$

$0 \text{ kPa} \le T_{eng} | L_{\text{CMV,b}} \le 400 \text{ kPa}$,

$$\left|\frac{\Delta\zeta_{IN}}{\Delta N_{eng}}\right| \le \text{C}_1, \left|\frac{\Delta\zeta_{EX}}{\Delta N_{eng}}\right| \le \text{C}_1,$$

$$\left|\frac{\Delta\zeta_{IN}}{\Delta T_{eng}}\right| \le \text{C}_2, \left|\frac{\Delta\zeta_{EX}}{\Delta T_{eng}}\right| \le \text{C}_2.$$

where C_1 and C_2 are the constants of the limits of the actuator operating rate with respect to the engine speed difference and the BMEP difference respectively, $L_{\text{CMV,b}}$ is a blocked CMV position, and $L_{\text{CMV,ub}}$ is an unblocked CMV position.

By solving the single-objective problem, the optimal actuator set-points of the ICL, ECL, and spark timing are determined at a given engine operating point and the CMV position. The determined optimal actuator set-points for achieving the best *bsfc* at a given CMV position (L_{CMV}) and engine operating point are expressed as

$$\boldsymbol{x}^* = (\zeta_{IN}{}^*, \zeta_{EX}{}^*, \sigma_{spark}{}^*) | (N_{eng}, T_{eng}, L_{\text{CMV}}). \quad (5\text{-}4)$$

The next step is solving the optimization problem with fuel economy and combustion stability objectives in equation (5-5) to determine the CMV position (L_{CMV}) at a given engine operating point.

$$\text{minimize } f = w_1 \times bsfc(L_{CMV} | \boldsymbol{x}^*) + w_2 \times \text{COV}_{\text{IMEP}}(L_{CMV} | \boldsymbol{x}^*) \quad (5\text{-}5)$$

subject to

$700 \text{ RPM} \le N_{eng} \le 6000 \text{ RPM}$,

$\text{ATDC } 100 \text{ deg} \le \zeta_{IN} \le \text{ATDC } 130 \text{ deg}$,

$\text{BTDC } 126 \text{ deg} \le \zeta_{EX} \le \text{BTDC } 90 \text{ deg}$,

ATDC -50 deg ≤ σ_{spark}≤ ATDC 0 deg,

700 RPM ≤ N_{eng} | $L_{\mathrm{CMV,b}}$ ≤ 3000 RPM,

0 kPa ≤ T_{eng} |$L_{\mathrm{CMV,b}}$ ≤ 400 kPa,

$$\left|\frac{\Delta\zeta_{IN}}{\Delta N_{eng}}\right| \le \mathrm{C}_1, \left|\frac{\Delta\zeta_{EX}}{\Delta N_{eng}}\right| \le \mathrm{C}_1,$$

$$\left|\frac{\Delta\zeta_{IN}}{\Delta T_{eng}}\right| \le \mathrm{C}_2, \left|\frac{\Delta\zeta_{EX}}{\Delta T_{eng}}\right| \le \mathrm{C}_2.$$

where w_1 and w_2 are adequate weighting factors, which are subjectively assigned to achieve the desired performance .

5.5 Optimization Algorithm to Find Global Optima

Whenever optimization problems are solved, the question of finding global optimum is a critical issue, but has not been clearly answered by the general optimization theory in a practical way. The local optima, which are the smallest or largest values of the objective function in the local vicinity of these points, are found by using the gradient based optimization algorithm. The typical iteration formula in gradient based optimization algorithms is

$$\boldsymbol{x}_{k+1} = \boldsymbol{x}_k + \alpha_k \boldsymbol{s}_k, \tag{5-6}$$

where $\boldsymbol{x}_k$ is the value of variable $\boldsymbol{x}$ at k+1$^{\mathrm{th}}$ step, α_k is a step length, and $\boldsymbol{s}_k$ is a search direction.

An *n*-dimensional algorithm iterating according to equation (5-6) requires the descent property $\boldsymbol{g}_k^T \boldsymbol{s}_k < 0$ for every *k*, while the gradient $\boldsymbol{g}_k$ is not zero. The value α_k is to ensure an acceptable decrease from f_k to f_{k+1}, that is, $f_k - f_{k+1} > 0$. Basically, α_k can be found by a line search method, and $\boldsymbol{s}_k$ is found by various optimization methods. When an objective function is non-linear with constraints, the sequential quadratic programming (SQP) is considered as the most efficient general purpose non-linear programming (NLP) algorithms today. The SQP mimics the Newton's method with constraints. In each iteration, the Hessian of the Lagrangian function is calculated. Then, the approximation is used to generate a QP sub-problem, whose solution is used to form a search direction for a line search procedure.

The SQP algorithm procedure with line search is summarized as follows:

(1) Initialize

(2) Solve the quadratic programming (QP) to determine a search direction $\boldsymbol{s}_k$.

(3) Minimize a merit function along $\boldsymbol{s}_k$ to determine a step length α_k. The merit function varies in different SQP implementations.

(4) Set $\boldsymbol{x}_{k+1} = \boldsymbol{x}_k + \alpha_k \boldsymbol{s}_k$

(5) Check for termination. Go to 2 if not satisfied.

To find the global optimum for the special case that the complexity of the response surface of the objective function can be approximately estimated, two step optimization procedures are proposed in this study. While knowing the response surface complexity, the global optimum can be found using gradient based optimization algorithms with an adequate initial point. The first step is to find an adequate initial point, and the second

step is to find a global optimum using the gradient based optimization algorithm. After analyzing the response surfaces with respect to actuator input variables, for example, the response surfaces shown in Figure 5-9 and Figure 5-10, an adequate initial point can be determined as the point, which makes the objective function be the maximum (or the minimum), out of adequately sampled initial point candidates.

5.6 Optimal Calibration Results

Optimal engine calibration results of a high DOF engine are achieved by solving optimization problems with multi objectives at every desired engine speed and BMEP. In the proposed optimization problem, subjective weighting factors for each objective should be determined to achieve the desired engine performance. For determining the weightings in equation (5-5), the COV_{IMEP} maps at $\boldsymbol{x}^*$ at both the CMV unblocked as shown in Figure 5-11. The adequate weightings are determined by adjusting the ratio of weightings (w_2/w_1) until the CMV blocked region tightly covers the high COV_{IMEP} regions shown in Figure 5-11. Thus, the determined weightings enable to remove the inferior COV_{IMEP} region, thus, guaranteeing the combustion stability.

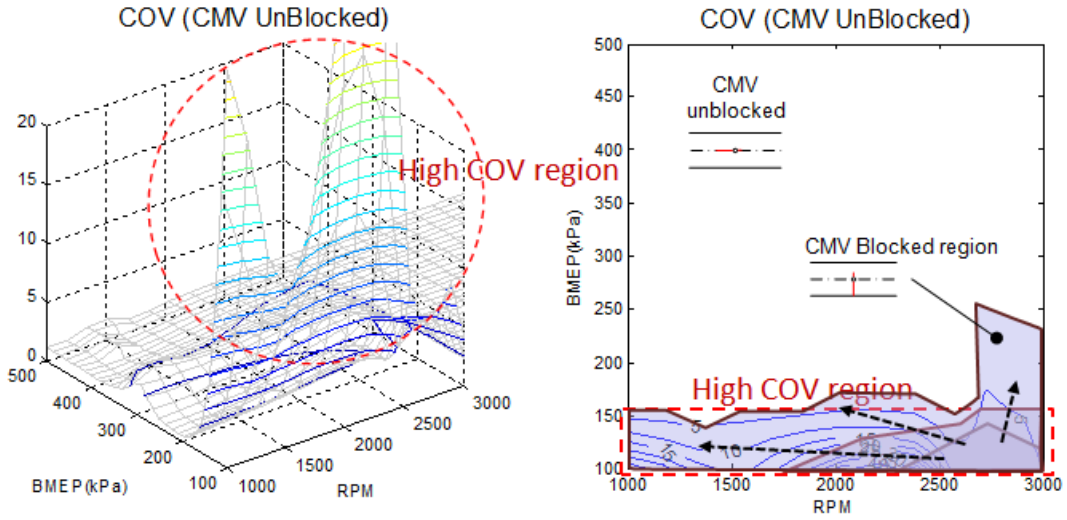

Figure 5-11 COV_{IMEP} map at the optimum actuator set points under the minimum *bsfc* operation at the CMV unblocked case

Figure 5-12 through Figure 5-14 show the determined optimal set-point maps of the each actuator with and without consideration of the combustion stability. The optimal set-point maps determined using the objective functions with multi objectives show the extended CMV operating area as shown in Figure 5-12. When fuel consumption is considered as the only objective, the effect of the CMV on the fuel economy is not significant except in a very small engine operating region. Although the combustion speed and the combustion efficiency are higher at the CMV blocked position, the smaller throttle opening to maintain the target BMEP also increases the pumping loss, thus, results in little benefit in the fuel economy. In contrast, when the objective function includes the combustion stability accompanying the fuel economy, the CMV operating region is extended to remove the less stable combustion region.

The optimal set-point maps of the ICL and the ECL are shown in the Figure 5-13 and Figure 5-14. The resulting valve timings enable to maximize the fuel economy at part

load operating conditions by increasing the valve overlap period until achieving high residual gas fraction while combustion stability is guaranteed. The high residual gas reduces the pumping loss by enabling more throttle valve opening to attain the same level of the intake air into the cylinders. Simultaneously, the high residual fraction reduces the combustion speed, resulting in low combustion efficiency and combustion instability. Thus, the optimal operating set-points of the di-VVT are determined considering the trade-off of between reducing pumping loss and maintaining combustion stability. Depending on CMV positions, optimal spark timing is significantly changed as shown in Figure 5-15 due to the significant combustion speed change.

Figure 5-16 (a) compares the resulting *bsfc* from the optimal calibration result of the di-VVT engine with the fuel consumption objective and the resulting *bsfc* of the fixed valve timing engine. The resulting *bsfc* of the di-VVT engine improves the fuel economy noticeably, compared to the fixed cam timing engine, at low to medium engine speed ranges. When the combustion stability objective is considered accompanying the fuel consumption objective in the engine optimal calibration problem, the maximum *bsfc* degradation is up to 4% region as shown in Figure 5-16 (b), thus, the better fuel economy, while maintaining combustion stability, is achieved without the severe deterioration of fuel economy by introducing the CMV to the di-VVT engine.

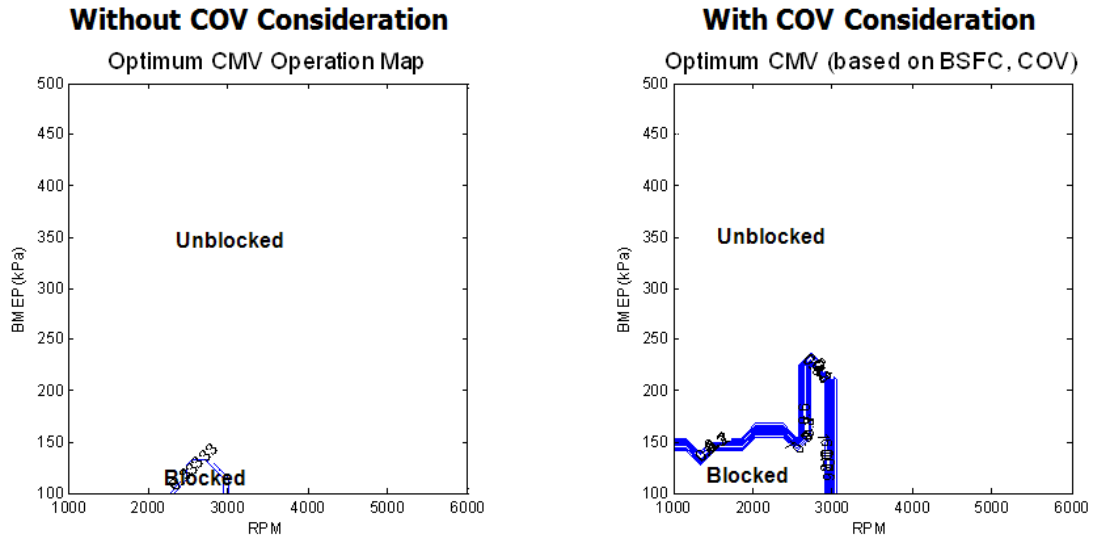

(a) **(b)**

Figure 5-12 Optimized CMV set-point maps: (a) with the fuel economy objective; (b) with the fuel economy and combustion stability objectives

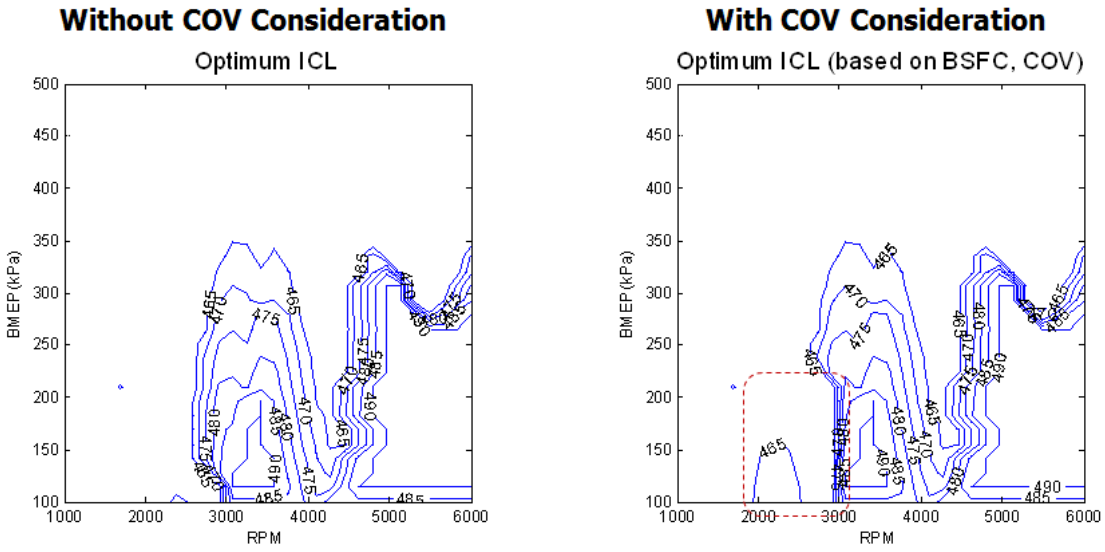

(a) **(b)**

Figure 5-13 Optimized ICL set-point maps: (a) with the fuel economy objective; (b) with the fuel economy and combustion stability objectives

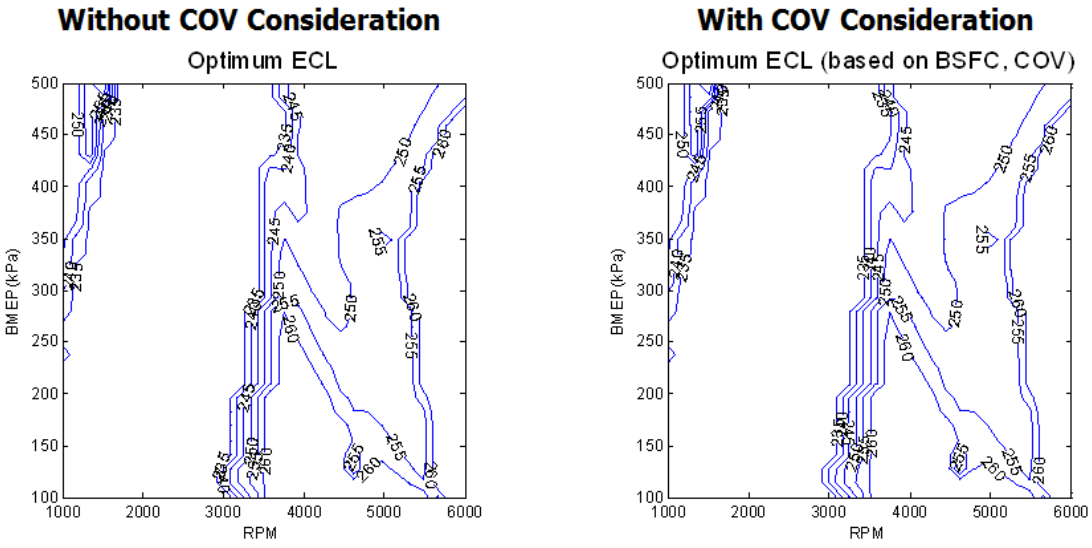

(a) **(b)**

Figure 5-14 Optimized ECL set-point maps: (a) with the fuel economy objective; (b) with the fuel economy and combustion stability objectives

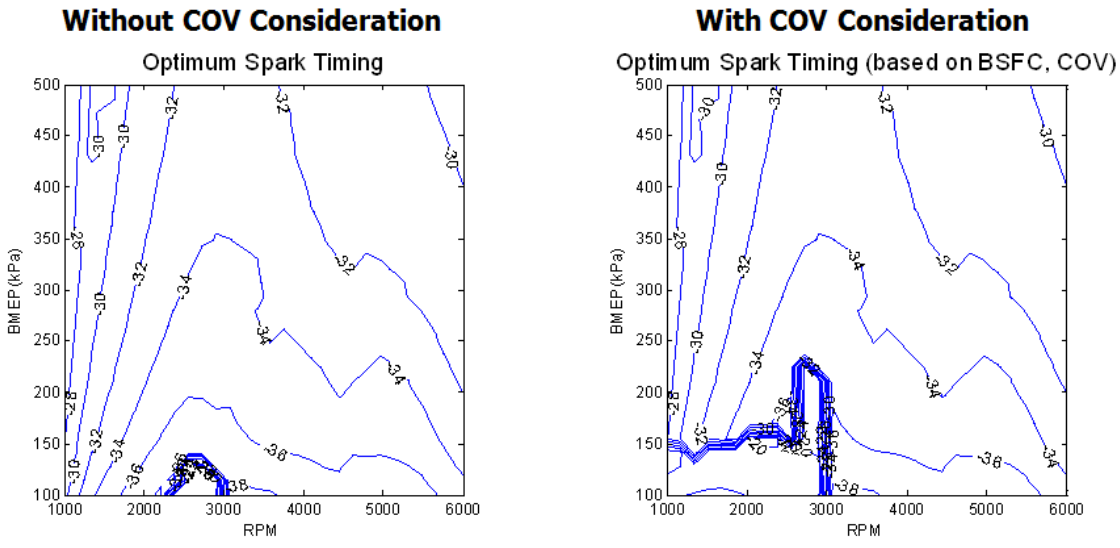

(a) **(b)**

Figure 5-15 Optimized spark timing set-point maps: (a) with the fuel economy objective; (b) with the fuel economy and combustion stability objectives

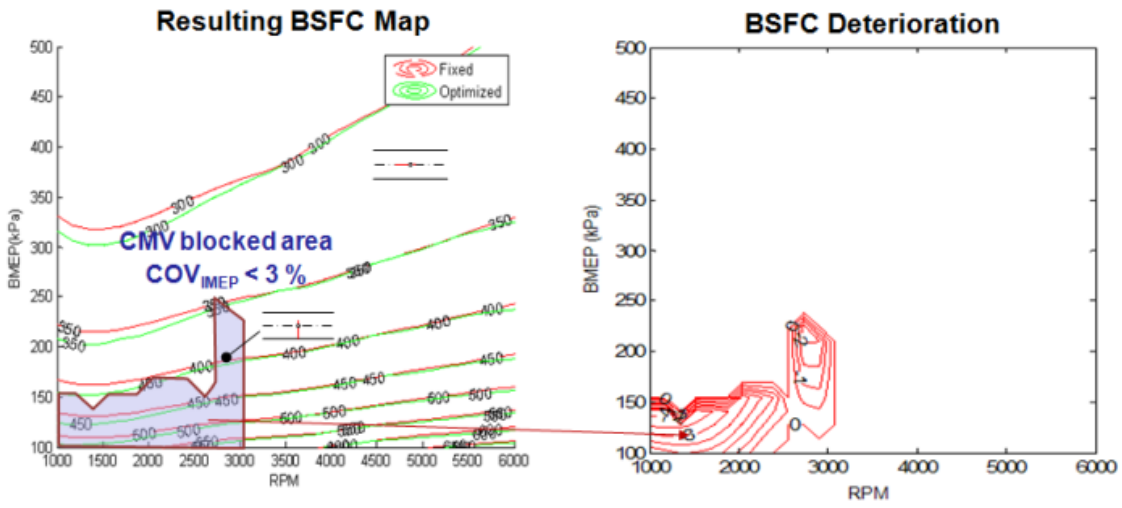

(a) **(b)**

Figure 5-16 (a) Resulting optimized *bsfc* maps with optimized actuator set points and the CMV blocked area to improve COV_{IMEP}; (b) *bsfc* deterioration due to the consideration of the combustion stability as an additional objective

5.7 Summary

The multi-objective optimal calibration of a di-VVT engine with CMVs is investigated to improve fuel economy and combustion stability simultaneously. The optimization framework is designed to calibrate the engine efficiently over the whole engine operating ranges. When addressing optimal calibration problems of high DOF engines, the size of the typical calibration problems increases exponentially to the unmanageable point beyond the experimental capability in the test cell. Thus, the simulation based calibration is used for the reduction of time and cost.

To apply the simulation based calibration to a high-DOF engine, high-fidelity simulation is presented by combining a 1-D gas dynamics simulation model and a quasi-D combustion simulation model. Then, the high-fidelity simulation results are validated

at several important engine operating points. Nevertheless, the relatively long computation time of the high-fidelity simulation is not adequate as a model for the optimal calibration. Thus, ANNs are selected as alternatives to the high-fidelity simulation tools due to the short computation time and sufficient accuracy. To achieve accurate engine inputs-to-output relations in the ANN models, a systematic training procedure is applied to train the ANN models. The data sets for training the ANN models are generated at the sampled cases by the LHS method to reduce the total number of simulations. To improve the computation efficiency, inverse ANN models are used in the formulation of the objective function.

An optimization framework for the optimal calibration of a high DOF engine is proposed to achieve the optimal calibration for minimizing fuel consumption and improving combustion stability. By using the optimization framework, the optimal actuator set-points at every engine operating point are determined through the optimization algorithm devised for finding the global optimum. The devised optimization algorithm is composed of a two-step procedure, which is composed of a step for determining an adequate initial point and a sequential step for finding the optimum using SQP.

In this study, the objectives of the optimal calibration include both fuel consumption and combustion stability objectives. The fuel economy is represented by *bsfc*, which is calculated from the engine output power and fuel consumption, and combustion stability is represented by COV_{IMEP}, which is estimated using regression equations from experimental data. The objective function, which is formulated by combining *bsfc* and

COV_{IMEP} multiplied by adequate subjective weights, is used as the cost function of the optimal calibration problem.

Then, optimal actuator set-point maps are determined by solving the optimization problem with multi objectives over the entire concerning engine operation ranges. As results, the resulting actuator set-point maps improve fuel economy while maintaining combustion stability over the whole engine part load operating ranges, especially at low-to-medium engine speed. The proposed simulation based optimal calibration enables to systematically calibrate high DOF engines while addressing different objectives.

REFERENCES

1. P. Kreuter, P. Heuser, J. Reinicke-Murmann, R. Erz, and U. Peter, "The Meta VVH System – The Advantages of Continuously Mechanical Variable Valve Timing", SAE Technical Paper No. 1999-01-0329, 1999.
2. R. Flierl, and M. Klüting, "The Third Generation of Valvetrains – New Fully Variable Valvetrains for Throttle-Free Load Control", SAE Technical Paper No. 2000-01-1227, 2000.
3. M. Nakamura, S. Hara, Y. Yamada, K. Takeda, N. Okamoto, T. Hibi, S. Takemura, and S. Aoyama, "A Continuous Variable Valve Event and Lift Control Device (VEL) for Automotive Engines", SAE Technical Paper No. 2001-01-0244, 2001.
4. C. Brüstle, and D. Schwarzenthal, "VarioCam Plus – A Highlight of the Porsche 911 Turbo Engine", SAE Technical Paper No. 2001-01-0245, 2001.
5. P. Kreuter, P. Heuser, J. Reinicke-Murmann, R. Erz, U. Peter, and O. Böcker, "Variable Valve Actuation – Switchable and Continuously Variable Valve Lifts", SAE Technical Paper No. 2003-01-0026, 2003.
6. M. Sellnau, and E. Rask, "Two-Step Variable Valve Actuation for Fuel Economy, Emissions, and Performance", SAE Technical Paper No. 2003-01-0029, 2003.
7. W. Hannibal, R. Flierl, L. Stiegler, and R. Meyer, "Overview of Current Continuously Variable Valve Lift Systems for Four-Stroke Spark-Ignition Engines and the Criteria for their Design Ratings", SAE Technical Paper No. 2004-01-1263, 2004.
8. R. Flierl, D. Gollasch, A. Knecht, and W. Hannibal, "Improvements to a Four Cylinder Gasoline Engine Through the Fully Variable Valve Lift and Timing System UniValve®", SAE Technical Paper No. 2006-01-0223, 2006.
9. Z. S. Filipi, and D. N. Assanis, "Quasi-dimensional computer simulation of the turbocharged spark-ignition engine and its use for 2- and 4-valve engine matching studies", SAE Technical Paper No. 910075, 1991.
10. J. B. Heywood, *Internal Combustion Engine Fundamentals*, McGrawHill, 1998.
11. P. Y. Papalambros, and D. J. Wilde, *Principles of Optimal Design*, Cambridge, 2nd edition, 2000.
12. C. Atkinton, and G. Mott, "Dynamic Model-Based Calibration Optimization : An Introduction and Application to Diesel Engines", SAE Technical Paper No. 2005-01-0026.
13. K. Mehrotra, C. K. Mohan, and S. Ranka, *Elements of Artificial Neural Networks*, the MIT Press, Cambridge, Massachusetts, 1997.
14. B. Wu, R. G. Prucka, Z. S. Filipi, D. M. Kramer, and G. L. Ohl, "Cam-Phasing Optimization Using Artificial Neural Networks as Surrogate Models – Maximizing Torque Output", SAE Technical Paper No. 2005-01-3757, 2005.

15. B. Wu, Z. S. Filipi, D. Assanis, D. M. Kramer, G. L. Ohl, M. J. Prucka, and E. DiValetin, "Using Neural Networks for Representing the Air Flow Rate through a 2.4 Liter VVT Engine", SAE Technical Paper No. 2004-01-3054.

16. B. Wu, R. G. Prucka, Z. S. Filipi, D. M. Kramer, and G. L. Ohl, "Cam-phasing Optimization Using Artificial Neural Networks as Surrogate Models – Fuel Consumption and NOx Emissions", SAE Technical Paper No. 2006-01-1512, 2006.

CHAPTER 6

DEVELOPMENT OF A CONTROL ORIENTED ENGINE MODEL USING HIGH-FIDELITY ENGINE SIMULATION AND ARTIFICIAL NEURAL NETWORKS

6.1 Introduction

The automotive industry has been making constant efforts to reduce fuel consumption and to improve the performance of engines incorporating numerous sensors and actuators. Engine designers are adopting new technologies at an accelerated pace to meet often conflicting market, regulatory, and societal demands. Among numerous new technologies, one of the most attractive and widely used is a variable valve actuation (VVA) system. The VVA enables the adjustment of gas exchange parameters for both part load conditions and full load conditions. However, these introduced systems always increase the degree-of-freedom (DOF) of an engine system and result in establishing complex engine calibration and control problems.

Due to the introduced new technologies, the control problems of advanced engines become critical issues in achieving the whole potential engine performance improvement, especially in transient engine operating conditions. Thus, many researchers have worked seriously to find the best control strategy to control complex modern engines.

Nevertheless, the optimum strategy for the transient response of the engine has not yet been clearly found due to the ultimate modeling difficulty caused by high non-linearity and complexity of the engine system and wide-ranging engine operating conditions.

Transient control of conventional engines with low DOF has been achieved based on the feed forward (FF) control using steady-state calibration maps and several correction maps that are introduced to manage transient operation without severe performance degradation. As the system becomes more complex by introducing new devices, the transient responses of each actuator are highly interconnected. Thus, adequate control of actuators is necessary to achieve the target control objectives during transient engine operating conditions. Before devising control methodologies, creating accurate system models is essential to design controllers precisely.

To predict engine transient response with sufficient fidelity within the limited computation power, mean value models (MVM) have been introduced as control oriented models (COM) composed of a manifold filling dynamics model, a rotational dynamics model, and an engine combustion model [3-5]. The validations of this type of the COM have been achieved in several previous studies [6-9]. Thus, the COM based on the MVMs show reasonably accurate input-to-output system behaviors accompanying low computation complexity.

Although many COMs have been developed for the purpose of the transient control of different types of engines, few engine models cover the whole engine operating ranges considering detailed combustion process. Thus, engine parameters closely related to the combustion process have not been adequately treated during engine transient control by using already proposed control oriented engine models, although the combustion related

parameters are critical to the engine performance in modern engines. Thus, a sophisticated COM, which is able to address accurate engine combustion processes, is necessary for the purpose of transient control design.

In this study, the high fidelity COM of a high DOF engine is created to capture both accurate combustion characteristics and engine dynamics under transient operating conditions. The high fidelity COM is created by using high-fidelity engine simulation results. The high-fidelity simulation tools consist of one-dimensional gas dynamics software and a quasi-dimensional combustion code. Since the high-fidelity simulation requires relatively long computation time, artificial neural networks (ANNs) are introduced as fast surrogate engine models. Since the ANN engine model cannot consider the system dynamics, a manifold dynamics model and a rotational dynamics model are augmented to the ANN engine static model to take into account the system dynamics.

To verify the feasibility of high fidelity COMs, a dual-independent variable valve timing (di-VVT) engine accompanying the electronic throttle control (ETC) is selected as a target engine. The di-VVT device can adjust both the amount of inducted air in cylinders and the amount of residual gas in cylinders, thus, enables to improve the fuel economy and engine performance. The proposed COM of the target engine is validated by investigating the predicted engine responses at various transient engine operations.

6.2 Control Oriented Model of a High DOF engine

In this study, the COM of a di-VVT engine with an ETC for engine transient operation is created by augmenting a linear manifold filling dynamics model, a linear actuator dynamics model to a nonlinear steady-state engine model as shown in Figure 6-1. The nonlinear steady-state engine model enables to predict accurate combustion processes, and other linear dynamics models enable to emulate system dynamics. The objective of developing COM is substituting a real engine while developing control algorithm. The COM must have low computational complexity while maintaining reasonable precision to be used for the control design. The COM has been widely used to design controllers and validate modeling fidelity [1-6].

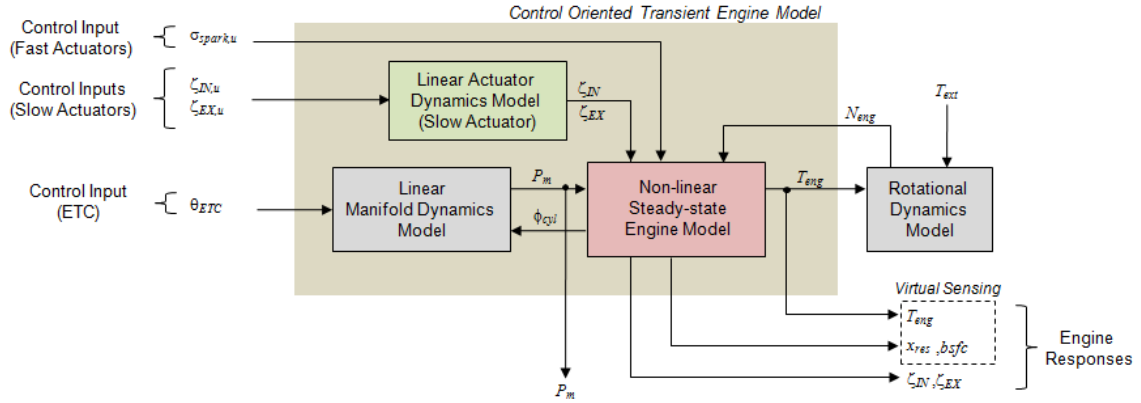

Figure 6-1 Control oriented model for engine transient operation using a non-linear steady-state engine model and linear dynamics models

The proposed COM has four control inputs, and engine responses are predicted from the control inputs. The control inputs of the COM are a throttle control input (θ_{ETC}), an intake valve timing control input ($\zeta_{IN,u}$), an exhaust valve timing control input ($\zeta_{EX,u}$), and a spark timing control input ($\sigma_{spark,u}$). The linear actuator dynamics models determine the

actual actuator positions. The linear manifold dynamics model calculates the intake manifold pressure (P_m). The nonlinear steady-state engine model predicts the mass air flow rate into the cylinders (ϕ_{cyl}), engine torque (T_{eng}), residual gas fraction (x_{res}), and break specific fuel consumption (*bsfc*). The rotational dynamics model determines engine speed at a given external load.

6.2.1 Manifold Filling Dynamics

As a manifold filling dynamics model, a filling and emptying model of the plenum is used accounting for its simplicity and reasonable accuracy [3-6]. Although this model lacks the predictability of pressure wave in a manifold, this model shows relatively high accuracy for predicting the state of a manifold except extreme engine operation conditions such as high engine speed with the wide open throttle (WOT) condition. The equations of the manifold filling dynamics are based on the equations of mass conservation, energy conservation, and the ideal gas law.

$$\dot{m} = \sum_{i=1}^{I} m_{in_i} - \sum_{j=1}^{J} m_{out_j} , \tag{6-1}$$

$$mc_v\dot{T}_m = \dot{Q}_m + \sum_{i=1}^{I} (c_{p_i} T_{in_i} - c_{v_i} T_m)\dot{m}_{in_i} - RT_m \sum_{j=1}^{J} \dot{m}_{out_j} , \tag{6-2}$$

$$P_m = \rho R T_m = \frac{m}{V_m} R T_m , \tag{6-3}$$

where c_p and c_v are the constant pressure and volume specific heat, m is the mass within the manifold at any time, Q is the heat flow into the manifold, R is the specific gas

constant, and P_m, T_m, and V_m are the manifold pressure, temperature, and volume respectively. At normal engine operating conditions, the isothermal assumption is appropriate because the intake manifold temperature is maintained almost constant at a steady-state engine operating condition. Thus, given the isothermal assumption, the manifold filing dynamics equations reduce into the following one first order ordinary differential equation.

$$\dot{P}_m = k_m(\phi_\theta - \phi_{cyl}), \quad k_m = \frac{R \cdot T_m}{V_m}. \tag{6-4}$$

The value of k_m is calculated with the nominal manifold temperature and the manifold volume of the target engine.

6.2.2 Mass Air Flow Rate through the Throttle Body

The mass air flow through the throttle body is modeled by a quasi-steady model of the flow through an orifice. This model assumes that the flow is one-dimensional, steady, and compressible; and the working fluid is ideal gas. The following equation is derived using the thermodynamic relations for isentropic expansion.

$$\dot{m} = A_e \frac{P_{in}}{\sqrt{RT_{in}}} \Psi\left(\frac{P_{in}}{P_{out}}\right), \tag{6-5}$$

where is $\Psi(\cdot)$ defined by

$$\Psi\left(\frac{P_{in}}{P_{out}}\right)=\begin{cases}\kappa^{\frac{1}{2}}\left(\frac{2}{\gamma-1}\right)^{\frac{\kappa+1}{2(\kappa-1)}} & \text{if } \left(\frac{P_{out}}{P_{in}}\right)\le\left(\frac{2}{\kappa-1}\right)^{\frac{\kappa}{\kappa-1}} \\ \left(\frac{P_{out}}{P_{in}}\right)^{\frac{1}{2}}\sqrt{\frac{2\kappa}{\kappa-1}\left[1-\frac{P_{out}}{P_{in}}\right]^{\frac{\kappa-1}{\kappa}}} & \text{if } \left(\frac{P_{out}}{P_{in}}\right)>\left(\frac{2}{\kappa-1}\right)^{\frac{\kappa}{\kappa-1}}\end{cases}, \qquad (6\text{-}6)$$

where A_e is the effective flow area, and the subscripts *in* and *out* indicate the inlet flow and outlet flow respectively. For many working fluids with $\kappa \approx 1.4$, the approximated relationship is proposed as follows.

$$\phi_\theta = g_1(P_m/P_a)\cdot g_2(\theta),\ g_1\left(P_m/P_a\right)=\begin{cases}1 & \text{if } \left(\frac{P_m}{P_a}\right)\le\frac{1}{2} \\ 2\sqrt{\frac{P_m}{P_a}-\left(\frac{P_m}{P_a}\right)^2} & \text{if } \left(\frac{P_m}{P_a}\right)>\frac{1}{2}\end{cases}, \qquad (6\text{-}7)$$

where $g_2(\theta)$ is a third order polynomial in the throttle angle.

6.2.3 Mass Air Flow Rate into the Cylinders

To predict the mass air flow rate into the cylinders (ϕ_{cyl}), empirical relationships, which assume quasi-steady operating conditions, are incorporated to represent the mass air flow rate into the cylinders. Over the wide engine operating conditions, the mass air flow rate into the cylinders is affected by pulsating pressure waves, the intake manifold volume, the geometry of intake runners, and the valve timing. When the VVT system is used to an engine, the analytical prediction of the mass air flow into the cylinders with sufficient accuracy is highly challenging.

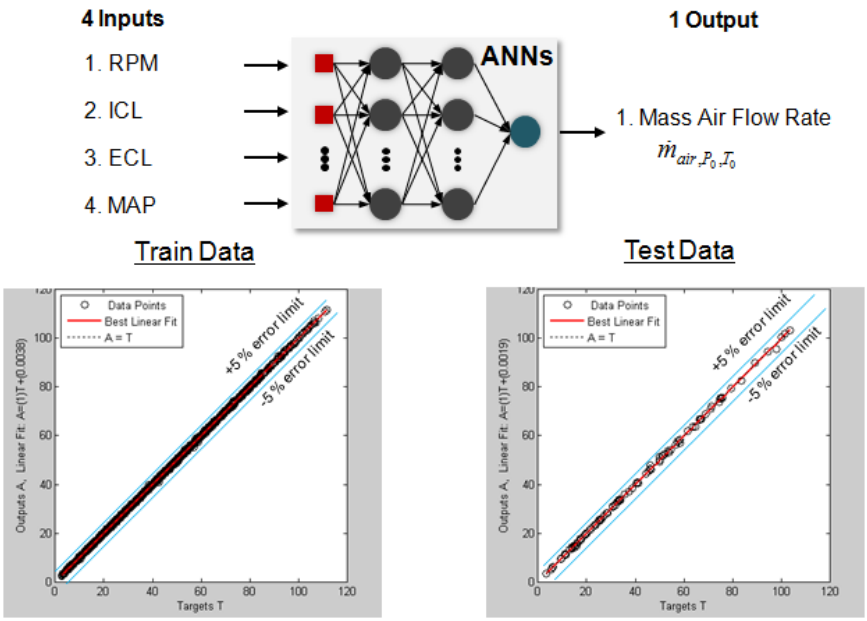

Figure 6-2 Preferred best ANN structure (5-18-18-1) of the mass flow rate at reference ambient pressure and the fitting quality: (a) training data set; (b) test data set

The mass air flow rate into the cylinders of the VVT engines is predicted by an ANN model to capture the complex nonlinear response caused by actuator interactions. The ANN model is trained using high-fidelity simulation results. The mass air flow rate into the cylinders for a conventional fixed cam timing engine is expressed as a function of the intake manifold pressure (P_m) and the engine speed (N_{eng}). In a di-VVT engine, valve timings (ζ_{IN}, ζ_{EX}) are introduced as additional control inputs. The different valve timing changes the amount of the residual gas fraction, thus, affect the mass air flow rate. Thus, the mass air flow rate in steady state operation is expressed as follows.

$$\phi_{cyl} = F(N_{eng}, P_m, \zeta_{IN}, \zeta_{EX}) . \tag{6-8}$$

Figure 6-2 shows the determined ANN mode structure for estimating the mass air flow rate in steady state operation.

6.2.4 Nonlinear Steady State Engine Combustion Model

Combustion process related engine responses are modeled by using ANN models. These responses include engine torque (T_{eng}), residual gas fraction(x_{res}) and *bsfc*. A torque generation model is created using the trained ANNs with high-fidelity simulation results. The high-fidelity simulation assumes uniformly mixed fuel, air, and the residual gas, and a quasi-steady engine operation. The engine torque is generated by complex in-cylinder combustion process. The combustion process is highly interconnected with the combustion chamber geometry, the valve features, the thermodynamic properties of the unburned and burned gas, and the gas exchange processes. Thus, the high-fidelity simulation is used for the generation of training data to capture the complex combustion process.

The variables of the torque generation model in this study are selected as engine speed (N_{eng}), intake manifold pressure (P_m), intake valve timing (ζ_{IN}), exhaust valve timing (ζ_{EX}), and spark timing (σ_{spark}). The individual cylinder torque generation is averaged over one engine event. At a normal engine operation, air-fuel ratio is maintained at stoichiometry to ensure the operation of a catalytic converter with the highest efficiency. The engine torque model is expressed as

$$T_{eng} = F(N_{eng}, P_m, \zeta_{IN}, \zeta_{EX}, \sigma_{spark}). \tag{6-9}$$

Using the same modeling methodology for the engine torque, residual gas fraction(x_{res}) and *bsfc* are modeled using trained ANNs as presented in equations (6-10) and (6-11).

$$x_{res} = F(N_{eng}, P_m, \zeta_{IN}, \zeta_{EX}, \sigma_{spark}) \tag{6-10}$$

$$bsfc = F(N_{eng}, P_m, \zeta_{IN}, \zeta_{EX}, \sigma_{spark}) \tag{6-11}$$

6.2.5 Actuator Dynamics

The dynamics of the di-VVT actuators are modeled as a first order system with a time constant for simplicity. Since VVT actuators are generally operated using hydraulic devices, the basic actuator operation is characterized as an integration action. Although the time constant of actuators depends on engine speed and load, the change of the time constant is considered as insignificant with respect to the engine operating conditions for the simplicity of simulation.

$$\frac{\zeta_{actual}}{\zeta_{commanded}} = \frac{1}{\tau_{act} s + 1}, \tag{6-12}$$

where ζ_{actual} is actual actuator response, $\zeta_{commanded}$ is actuator command. τ_{act} is a time constant of actuator dynamics. The time constant τ_{act} changes at different engine operating conditions. Nevertheless, the time constant is assumed constant for simplicity of analysis.

6.2.6 Rotational Dynamics

For the purpose of transient engine control, the rotational dynamics model of an engine is simply determined by considering effective inertia, external load, and engine output torque. The effective inertia includes engine rotating inertia and effective vehicle inertia. The external loads include engine friction, vehicle drag, and vehicle friction. The engine output torque is calculated at the current engine operation condition.

$$\frac{dN_{eng}}{dt} = \frac{60}{2\pi} \frac{(T_{eng} - T_{ext})}{\mathrm{I}_{\mathrm{eff}}}, \tag{6-13}$$

where N_{eng} is the engine speed in rpm, T_{eng} is the engine output torque, T_{ext} is the external loads on the crankshaft, and I_{eff} is the effective inertia including the engine and vehicle.

6.3 Nonlinear Steady State Engine Model

The combustion model under steady-state operation is created using high-fidelity simulations and artificial neural network models to achieve fast computation time and accurate prediction of combustion characteristics.

6.3.1 High-Fidelity Simulation Tools

High-fidelity simulation tools consist of the 1-D gas dynamics model and the quasi-D combustion model. The 1-D gas dynamics model which is one part of the high-fidelity simulation tools is created with the commercial software Ricardo WAVE including all air

flow paths from the air box to the exhaust tail pipe. Figure 6-3 shows the gas dynamics simulation model of the target engine. The piping and manifolds of the intake and exhaust systems are modeled by using duct and junction components.

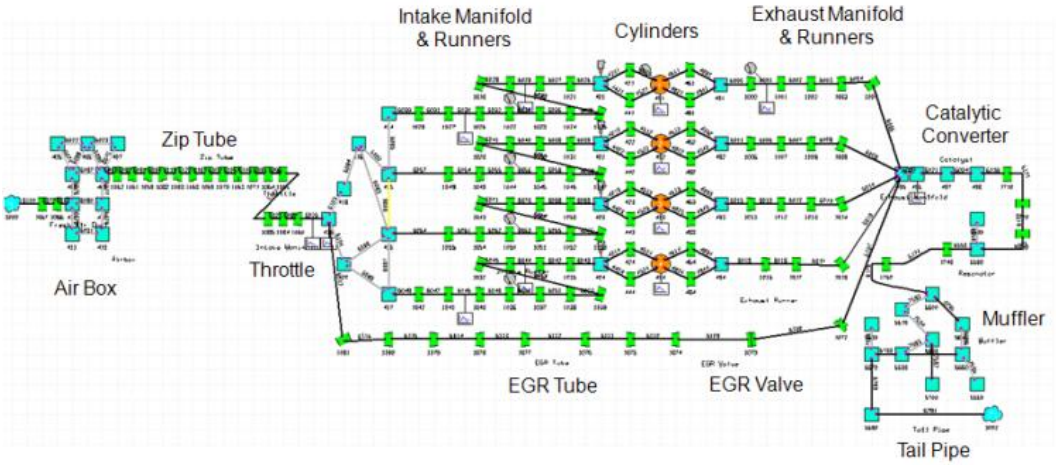

Figure 6-3 One-dimensional gas dynamics simulation model built with the Ricardo WAVE [13,14]

Accompanying the 1-D gas dynamics model, the quasi-D combustion model is used to predict combustion process over the whole possible engine operating conditions with high accuracy. The quasi-D combustion model is based on mass and energy conservation and phenomenological models for turbulence, combustion and heat transfer in a cylinder. The combustion sub-model is the turbulent flame entrainment [15-21]. The combustion model is complemented by a single-zone turbulence model, which calculates crank-angle resolved global turbulence throughout the whole cycle. Flame propagation is assumed to move spherically from an ignition point. The governing differential equations are as follows.

The rate of mass entrainment is

$$\frac{dm_e}{dt} = \rho_u A_f (u' + S_L), \tag{6-14}$$

where m_e is the mass entrained, t is time, ρ_u is density of unburned charge, A_f is the flame front area, u' is turbulent intensity, and S_L is laminar flame speed. Since the magnitude of u' is usually much larger than the laminar flame speed, the rate of mass entrainment strongly depends on the flame front area and turbulence. Therefore, the exact calculation of the flame front area is critical to improve simulation fidelity.

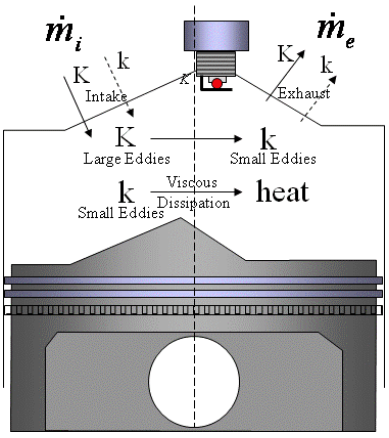

Figure 6-4 Turbulent energy cascade model to estimate turbulent flow

The rate of burning is estimated by the characteristic velocity and length scale. The length scales of turbulence structure are divided into macroscale L (or integral scale), Taylor microscale λ, and Kolmogorov microscale η. The macroscale is the measure of the size of a large energy containing flow structure. The Taylor microscale is useful in characterizing a turbulent flow. It is defined by relating the fluctuating strain rate of turbulent flow field to turbulence intensity. The Kolmogorov scale η defines the smallest structures of flow where small-scale kinetic energy is dissipated via molecular viscosity.

The rate of burning is

$$\frac{dm_b}{dt} = (m_e - m_b)/\tau\,, \tag{6-15}$$

and

$$\tau = \frac{\lambda}{S_L}\,, \tag{6-16}$$

where m_b is the mass of burned products, and λ is the Taylor microscale.

The turbulent model consists of a zero-dimensional energy cascade. Figure 6-4 illustrates the energy cascade model. Mean flow kinetic energy *K* is supplied to the cylinder through the valves. Then, the mean kinetic energy *K* is converted to turbulent kinetic energy *k* through a turbulent dissipation process. The turbulent kinetic energy is converted to heat through viscous dissipation. The mean and turbulent kinetic energy flows into and out of the cylinder through intake valves and exhaust valves. The equations for a zero-dimensional energy cascade are as follows.

$$\frac{dK}{dt} = \frac{1}{2}\dot{m}_i v_i^2 - P - K\frac{\dot{m}_e}{m}\,, \tag{6-17}$$

$$\frac{dk}{dt} = P - m\varepsilon - k\frac{\dot{m}_e}{m}\,, \tag{6-18}$$

where $\dot{m}_i$ and $\dot{m}_e$ are mass flow rates into and out of the cylinder respectively. v_i is the gas flow velocity into the cylinder. ε is the dissipation rate of turbulent kinetic energy per unit mass by assuming turbulence is isotropic. *P* is the production rate of turbulent kinetic energy and calculated from the equation for turbulence production over flat plates. *K* is the mean kinetic energy and *k* is the turbulent kinetic energy.

6.3.2 Nonlinear Steady State Engine Model Using Artificial Neural Network Model

The ANN models are used to predict nonlinear steady state engine responses. Since the total number of engine operating points is large, the engine model for calculating the objective function should have fast calculation speed accompanying high accuracy to reduce time and cost during the engine calibration process. Figure 6-5 illustrates the procedure to create a non-linear steady state engine model.

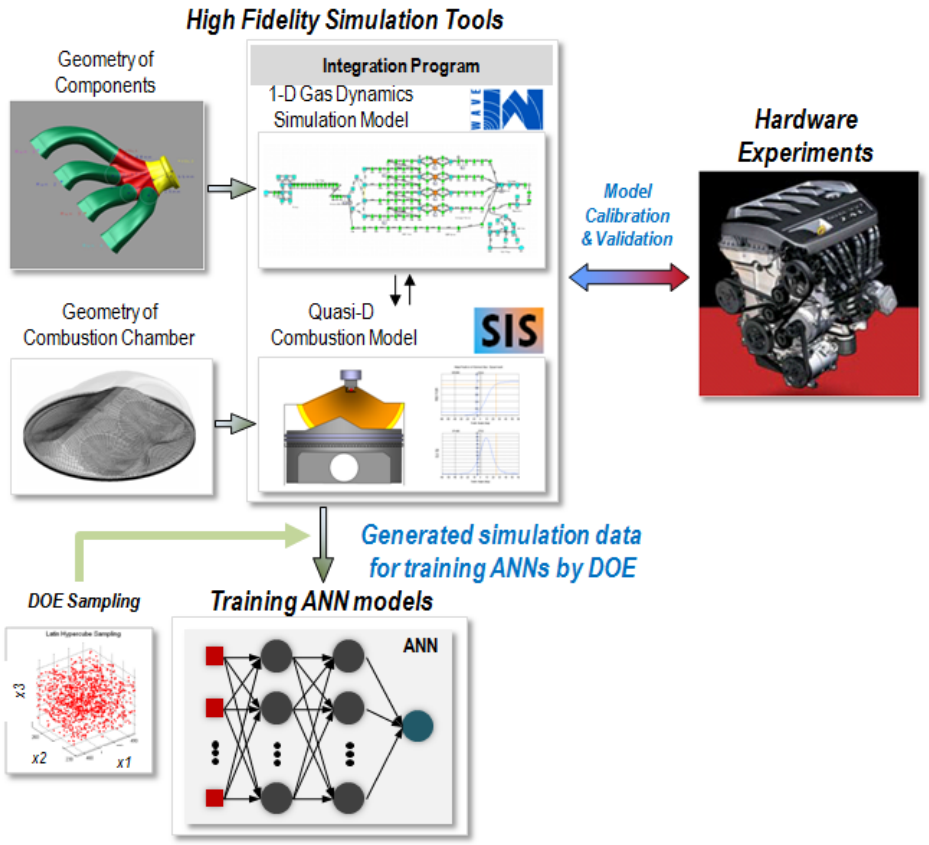

Figure 6-5 Illustration of the procedure to build a non-linear steady state engine model by training ANNs

A fast non-linear steady state engine model is created by the following steps:

(1) High-fidelity simulation tools are created by combining a 1-D gas dynamics simulation model and a quasi-D combustion model, to guarantee the simulation accuracy.
(2) The high-simulation tools are validated at several important engine operating points by using experiment data.
(3) The experimental design is determined using the Latin Hypercube Sampling (LHS) method to reduce the total number of experiments. The experiments should represent all possible combinations of actuator inputs and engine operating points.
(4) Simulation results are generated by the experimental design.
(5) ANN models, which estimate engine responses and states, are trained to substitute the high-fidelity simulation tools, which require long computation time, by using the high-fidelity simulation results.
(6) The engine responses and states are estimated using the ANN models.

6.4 Simulation Results of the COM of the di-VVT Engine

The created COM of a high DOF engine for transient operation is investigated at several engine operating conditions. To assess the transient response of the COM, two types of engine transient response tests are selected. These transient tests are: (1) the test

of engine transient responses with step throttle inputs at fixed engine speeds, and (2) the test of engine transient responses with step valve timing inputs at fixed engine speeds.

Figure 6-6 shows the simulation results of engine transient responses with step throttle inputs. When a step throttle input is assigned to an engine, the mass air flow rate through the throttle body increases instantaneously. Then, intake manifold pressure starts to gradually increase until the mass flow rate into the cylinders becomes equal to the mass flow rate through the throttle body.

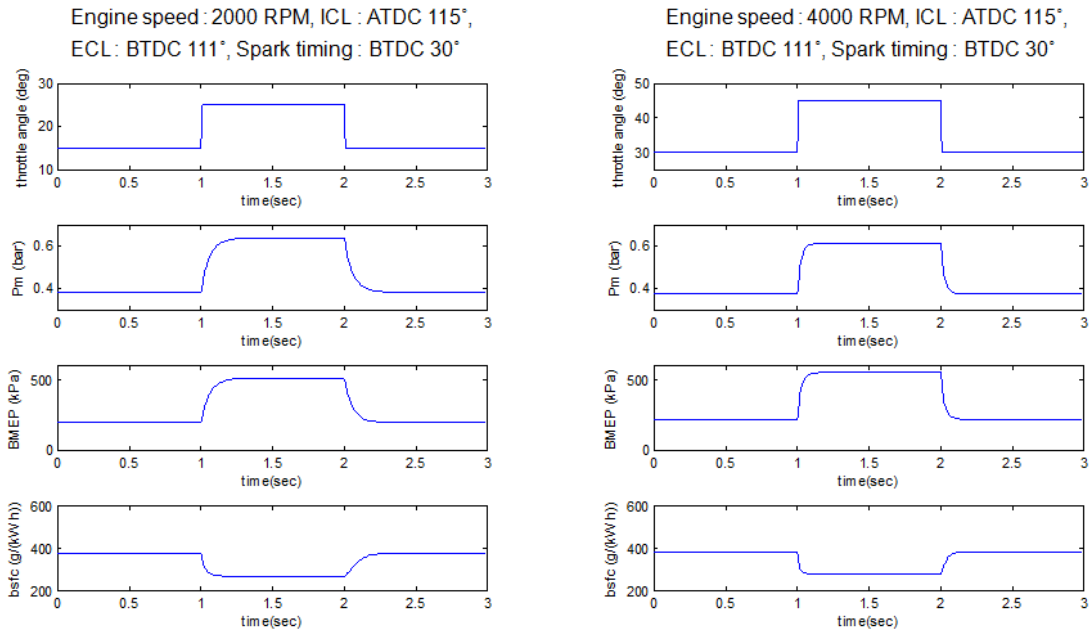

(a) **(b)**

Figure 6-6 Transient responses of the COM by step throttle inputs: (a) fixed engine speed of 2000 rpm, fixed ICL of ATDC 115 deg, fixed ECL of BTDC 111 deg, and fixed spark timing of BTDC 30 deg; (b) fixed engine speed of 4000 rpm, fixed ICL of ATDC 115 deg, fixed ECL of BTDC 111 deg, and fixed spark timing of BTDC 30 deg

In equation (6-4), $\dot{P}_m = k_m(\phi_\theta - \phi_{cyl})$, the mass flow rate into the cylinder ϕ_{cyl} in equation (6-8) can be expressed as

$$\phi_{cyl} = \frac{\eta_v \rho_a V_d N_{eng}}{2} \tag{6-19}$$

by a quasi-steady approximation and a constant temperature assumption. Where η_v is volumetric efficiency, ρ_a is the air density, and V_d is the displaced cylinder volume per cycle.

From the ideal gas law $P_m V_m = m_{a,m} R T_m$, equation (6-4) can be written as

$$\frac{dP_m}{dt} + \frac{\eta_v V_d N}{2V_m} P_m = k_m \phi_\theta, \tag{6-20}$$

where V_m is the volume of the intake manifold and $m_{a,m}$ is the air mass in the intake manifold. Although both η_v and ϕ_{cyl} weakly depend on P_m, equation (6-20) would be a first-order equation for P_m with time constant $\tau_{MAP} = 2V_m / \eta_v V_d N_{eng}$. Thus, equation (6-20) becomes

$$\frac{dP_m}{dt} + \frac{1}{\tau_{MAP}} P_m = \phi_\theta \frac{RT_m}{V_m}, \tag{6-21}$$

Therefore, the intake manifold pressure response is similar to the response of the first order system by throttle inputs. As engine speed increases, the time constant τ_{MAP} becomes smaller because the engine speed N_{eng} is shown in the denominator in the time constant equation. In Figure 6-6 (a) and (b), the time constant of the intake manifold

pressure response becomes small at higher engine speed of 4000 rpm, thus, tracking the desired P_m more rapidly.

Next, transient engine responses with step valve position inputs are investigated. Figure 6-7 and Figure 6-8 show the simulation results of the COM with step valve position inputs at a fixed engine speed, a fixed throttle angle, and fixed spark timing. Because the mass air flow rate into cylinders, ϕ_{cyl}, is a function of valve timings as expressed in equation (6-8), the ϕ_{cyl} is changed with respect to the change of valve timings. Thus, the change of valve timings induces the change of intake manifold pressure, BMEP, and *bsfc* at steady state.

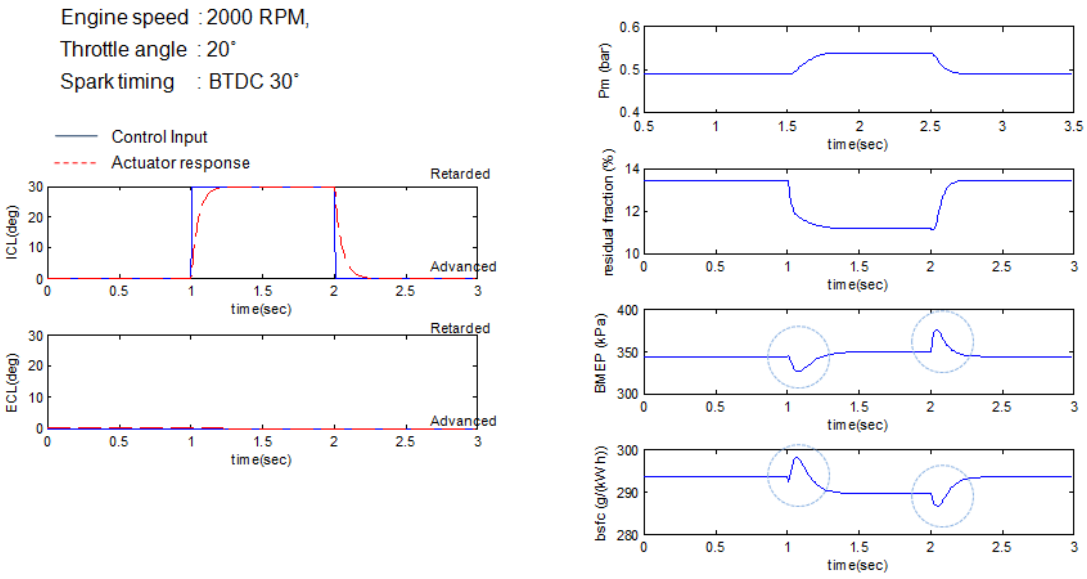

Figure 6-7 Transient responses of the COM by step ICL inputs at the engine speed of 2000 rpm, the throttle angle of 20 deg, the ECL at most advanced position, and the spark timing of BTDC 30 deg

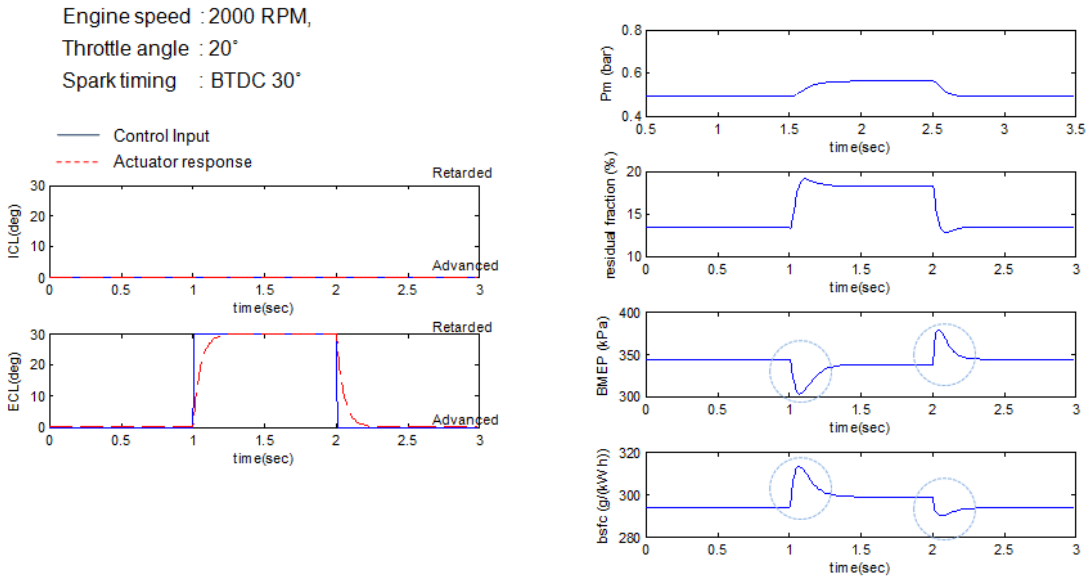

Figure 6-8 Transient responses of the COM by step ECL inputs at the engine speed of 2000 rpm, the throttle angle of 20 deg, the ICL at most advanced position, and the spark timing of BTDC 30 deg

The mass air flow rate into the cylinders is not the same as the amount of the mass flow rate into the cylinder during transience. The intake manifold pressure is changed until the mass air flow rate into the cylinders becomes equal to the mass air flow rate through the throttle valve. The difference of the mass air flow rate with respect to the target mass air flow rate causes BMEP peaks and *bsfc* peaks during transience.

6.5 Summary

As engine system introduces many new technologies to improve engine performance, engine system control for achieving the best hardware performance requires intensive work for control design, especially on the fast transient engine operating conditions. Transient control of conventional low DOF engine has been realized using the FF control

referring to steady-state calibration maps and correction maps. However, the increased system complexity of a high DOF engine demands advanced control design to achieve the target control objectives. While applying any advanced control methodology, creating accurate engine models is the first step for control design. However, the ultimate non-linearity of the engine system causes a high difficulty in creating a sufficiently reliable COM.

In this study, the high fidelity COM is developed as a solution for resolving the difficulty in predicting precise engine responses by combining engine sub-models. The COM includes a manifold filling dynamics model, an actuator dynamics model, a rotational dynamics model, and a steady state non-linear engine combustion model. Among those sub-models, a nonlinear engine combustion model is the essential part for capturing the complex combustion process. While creating a nonlinear engine combustion model, simulation based approaches is more appropriate for the high DOF engine system with the flexibility of predicting complex engine system responses.

The engine combustion models are created by using a high-fidelity engine simulation tools and ANNs. Then, the engine steady state combustion models are augmented to take into account for the system dynamics. The developed high fidelity COM can capture not only the engine input-to-output relations over the whole possible engine operating points but also the system dynamics. The created COM is assessed by the transient responses of the engine at several different engine operating conditions. In addition, the developed high fidelity COM provides a good prediction of engine responses with arbitrary engine control inputs over the whole possible engine operation points.

REFERENCES

1. A. G. Stefanopoulou, J. S. Freudenberg, and J. W. Grizzle, "Variable Camshaft Timing Engine Control", *IEEE Transaction on Control Systems Technology*, Vol 8, No. 1, pp 23-34. January 2000.
2. S. C. Hsieh, J. S. Freudenberg, and A. G. Stefanopoulou, "Multivariable Controller Structure in a Variable Cam Timing Engine with Electronic Throttle and Torque Feedback", *Proc 1999, Conf. on Control Applications*, pp. 465-470. 1999.
3. L. Guzzella, and C. H. Onder, *Introduction to Modeling and Control of Internal Combustion Engine System*, Springer, 2004.
4. A. G. Stefanopoulou, J. A. Cook, J. S.Freudenberg, and J. W. Grizzle, "Control-Oriented Model of a Dual Equal Variable Cam Timing Spark Ignition Engine", , *ASME Journal of Dynamic Systems, Measurement, and Control*, vol. 120, pp. 257-266, 1998.
5. A. G. Stefanopoulou, *Modeling and Control of Advanced Technology Engines*, Ph.D. Dissertation, University of Michigan, Feb. 1996.
6. Y. He, and C. Lin, "Development and Validation of a Mean Value Engine Model for Integrated Engine and Control System Simulation", SAE Technical Paper No. 2007-01-1304, 2007.
7. J. A. Cook, and B. K. Powell, "Modelling of an Internal Combustion Engine for Control Analysis," *IEEE Control Systems Magazine*, Vol. 8, No. 4, 1988, pp 20-26.
8. E. Hendricks, and S. C. Sorenson, "Mean value modeling of spark ignition engines", SAE Technical Paper No. 900616, 1990.
9. M. Livshiz, M. Kao, and A. Will, "Validation and Calibration Process of Powertrain Model for Engine Torque Control Development", SAE Technical Paper No. 2004-01-0902, 2004.
10. J. B. Heywood, *Internal Combustion Engine Fundamentals*, McGrawHill, 1998.
11. C. F. Taylor, The Internal-combustion engine in Theory and Practice Volume I : Thermodynamics, Fluid Flow, Performance, The M.I.T. Press. 1985.
12. H. Heisler, *Advanced Engine technology*, Society of Automotive Engineers, Inc., 1995.
13. WAVE V8 Basic Reference Manual, Ricardo Software, Ricardo, Inc., 2008.
14. WAVE V8 Engine Reference Manual, Ricardo Software, Ricardo, Inc., 2008.
15. Z. S. Filipi, and D. N. Assanis, "Quasi-dimensional computer simulation of the turbocharged spark-ignition engine and its use for 2- and 4-valve engine matching studies", SAE Technical Paper No. 910075, 1991.
16. Z. S. Filipi, "Investigation of Variable Valve Area Strategies for a Turbocharged SI-Engine." *Proceedings of the IMechE* 1994-6, *5th International Conference on Turbocharging and Turbochargers*, London, 1994, pp. 93–102.

17. Z. S. Filipi, and D. N. Assanis, "The Effect of Stroke-to-Bore Ratio on Combustion, Heat Transfer and Performance of a Homogeneous-Charge Spark-Ignited Engine of Given Displacement", *International Journal of Engine Research*, Volume 1, No. 2, JER0500, London, 2000, pp. 191-208.

18. T. Morel, M. Flemming, and L. A. LaPointe, "Characterization of manifold dynamics in the Chrysler 2.2l S.I. engine by measurements and simulation", SAE Technical Paper No. 900679, 1990.

19. R. J. Tabaczynski, C. R. Ferguson, and K. Radhakrishnan, "A turbulent entrainment model for spark-ignition engine combustion", SAE Technical Paper No. 770647, 1977.

20. R. J. Tabaczynski, F. H. Trinker, and B. A. Shannon, "Further refinement and validation of a turbulent flame propagation model for spark-ignition engines", *Combustion and Flame*, Vol. 39, No. 2, 1980, pp. 111-121.

21. S. G. Poulos, and J. B. Heywood, "The effect of chamber geometry on spark-ignition engine combustion", SAE Technical Paper No. 830334, 1983.

CHAPTER 7

NONLINEAR MODEL PREDICTIVE CONTROL OF DUAL-INDEPENDENT VARIABLE VALVE TIMING ENGINES WITH ELECTRONIC THROTTLE CONTROL

7.1 Introduction

Many new technologies have been introduced and applied to modern internal combustion engines to improve fuel economy and performance. Simultaneously, the control problems of a high degree-of-freedom (DOF) engine become critical issues for achieving the whole potential engine hardware performance, especially under the transient engine operating conditions. Many studies have been investigated to find the best control strategy to control complex modern engines. Nevertheless, clear and explicit transient control strategies of engines have been still intensively researched due to the non-linearity and wide-ranging operating conditions of engines. Because of the difficulty in developing transient control strategies, feed forward (FF) control has been used as a main control methodology for both steady-state and transient operating condition. FF control is generally achieved by using steady-state calibration maps and several correction maps.

For the convenience of the control design in a high DOF engine system, torque-based control was firstly proposed by the Robert Bosch Co. [1], and subsequently reviewed in several papers [2-4]. In the torque-based control, driver demands are interpreted as torque demands, and a desired engine operating point is determined based on engine speed and interpreted torque demand. In general, actuator set-point maps are calibrated based on engine speed and torque in steady state operating conditions, and are used for the reference of engine control. However, since the engine operating conditions are highly transient under various driving conditions, an adequate control of actuators is necessary to achieve the target control objectives during transient engine operating conditions.

During fast transient engine operating conditions, unfavorable engine responses are caused by the slow actuator response time. As a simple solution, limiting the actuator rate was proposed by Stefanopoulou et al. [5]. A more comprehensive way to control VVT devices to resolve the unfavorable engine operating conditions was proposed using model based controllers [6]. However, these proposed control methods did not provide the optimal control under transient operation.

One method to improve engine performance under transient condition is to account for transient engine operation while calibrating engines [7,8]. However, for high DOF engines, addressing all possible combinations of engine transient operating patterns is exceptionally difficult in a transient engine calibration process. Moreover, the resulting calibration maps require large amount of memory to store the information for all possible engine transient operation cases.

To reduce the difficulty of the off-line transient engine calibration, stochastic approach was recently introduced to find optimal transient engine operating conditions. The optimal engine operating conditions are adaptively determined considering driving style after gathering the sufficient information of the driving style in real time [9-11]. However, this transient calibration based on stochastic processes cannot find the optimal engine transient operating conditions instantly whenever driving cycles are changed. Moreover, while searching feasible engine operating domains to gather sufficient information for probability matrices, engine operations can become unstable when engines run close to the marginally stable operating conditions.

Various control methods have been applied to the transient control of high DOF engines. When a small number of actuators are used to control engines, classical proportional-integral-derivative (PID) control is widely used to improve the engine transient performance [12]. However, the classical PID methods do not guarantee satisfactory performance in multi-inputs-multi-outputs (MIMO) system. To deal with MIMO system, linear quadratic gaussian (LQG) control was introduced [13]. However, the nonlinear engine system must be linearized at every concerned equilibrium point. While applying state feedback control without the linearization procedure, a nonlinear turbo engine model was directly used to manage transience [14]. However, the optimal gain to achieve desired performance must be tuned iteratively because of the strong nonlinearity in the engine model. As another approach to handle system nonlinearity directly, lyapunov function based nonlinear control was applied for transience control of engines [15,16]. However, system performance specifications cannot be determined

without the subjective decision of control gains. The subjective decision procedure requires intensive calibration processes to design adequate controllers.

To overcome the difficulties of the transient control of modern engines, model predictive control (MPC) [17-19] has been introduced as one of the most promising control methodologies. The basic idea of the MPC is solving an optimal control problem with a finite horizon at every time step in real time. Since the MPC requires high computation power, the MPC is initially applied to a chemical process control whose dynamics is relatively slow [17]. Nowadays, the tremendous expansion of computing power provides the possibility of using the MPC for the fast dynamic systems such as internal combustion engines. The MPC was recently applied to the control of diesel engines [20,21], the torque tracking and air-to-fuel ratio (AFR) regulation problems [22], the control of homogeneous charge compression ignition (HCCI) engines, and the control of variable cam timing (VCT) engines [23]. However, most of the previous studies used simplified combustion model while the control of engine transient operation with the MPC. Hence, previous research rarely considered in-cylinder states, such as residual gas fraction and emission, for the control of high DOF engines. By considering the detailed engine combustion process and the in-cylinder engine states, more sophisticated engine transient control can be realized to achieve the control objectives. Moreover, the previous MPC researches did not explicitly determine the control horizon and the prediction horizon to achieve the desired transient responses and to guarantee the system stability.

In this study, the nonlinear model predictive control (NMPC) methodology is selected as a key control methodology to manage engine transient responses (1) to achieve fast torque responses, (2) to rejecting unfavorable emissions, and (3) to track the

optimal actuator responses tightly. While designing the NMPC, the control horizon and the prediction horizon are determined as short as possible by introducing the dead-beat control concept. The short control horizon and prediction horizon enable to reduce the computation time. Using the determined control and prediction horizon, the transient responses of the engine by the NMPC are assessed under fast transient engine operating conditions.

While designing the NMPC controller, an accurate engine predictive model is required to improve control accuracy. The engine model for the NMPC must be capable of predicting engine transient responses with sufficient fidelity with the limits of computation power. Thus, a mean value model (MVM) is introduced as a control oriented model (COM). The MVM is composed of a manifold filling dynamics model, a rotational dynamics model, and an engine combustion model [24-26]. The validity of the MVM has been provided in several previous studies [27,28]. The MVM enables to capture the input-output behavior of the system with reasonable accuracy and low computation complexity. The COM of a high DOF engine is created to capture both accurate combustion characteristics and engine dynamics under transient operating conditions. Then, the created COM is used as a predictive model of a high DOF engine for the NMPC algorithm under fast transient engine operating conditions

This chapter is organized as follows. First, the transient control problem of a high DOF engine is introduced. Then, the COM as a predictive engine model is created. The NMPC is formulated to find the optimal control inputs of all actuators simultaneously. The control horizon and prediction horizon are determined to achieve dead-beat control

of engine responses and smooth operations. Finally, resulting transient responses of the target engines using the NMPC are analyzed at different operating conditions.

7.2 Transient Control Problem

The acceleration pedal is the unique driver control input to achieve a desired engine torque. In the modern high DOF engine control, current vehicle speed and an assigned acceleration pedal position are interpreted as an engine torque demand for the convenience of the control design of a high DOF engine system [1]. Using the desired engine torque at a current engine speed, actuator control commands are determined using the pre-calibrated actuator set-point maps. For the control purpose, actuators are categorized as a fast actuator and a slow actuator depending on actuator response characteristics. When the actuator responses are not fast enough, the actual actuator response delay must be accounted for under transient conditions.

Figure 7-1 illustrates transient control problems originating from the actuator response delays under transient operating conditions. When the actuator response is fast enough to follow the desired reference actuator set-points, the desired engine performance is achieved under fast transient operation. In contrast, delayed actuator responses deteriorate the system performance. The deterioration is caused by the discrepancy of the actuator responses from the reference actuator set-points. Thus, when transient control problems are addressed, real time compensation of the discrepancy between the actual actuator responses and the reference actuator set-points must be achieved to improve the system transient performance.

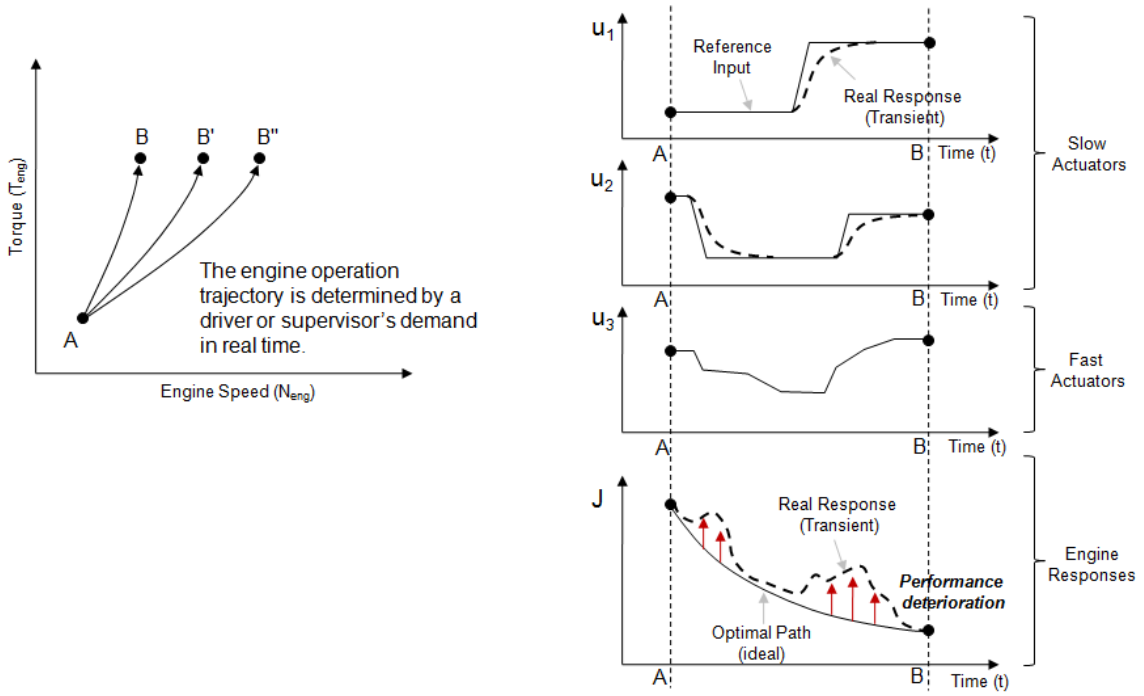

Figure 7-1 Transient control problems arise from finite actuator response time under engine transient operating conditions

Unfortunately, few clear methods for treating engine transience have been introduced because of the difficulties in creating accurate and fast engine models. According to the difficulties, the FF control algorithms have been widely used in the automotive industry. When the FF based control is used in the transient control of engines, intensive calibration considering the wide ranges of engine transient operating conditions is indispensable to achieve the desired transient performance and to guarantee smooth engine operation. In addition, increasing DOF of the engine system significantly extends the total efforts of the calibration process. To resolve the difficulties under transience, the NMPC is selected as one of the most promising control methodologies for the transient control of a high DOF engine.

7.3 Control Oriented Model (COM) of a High DOF Engine

The target engine for the transient control design is a dual independent variable valve timing (di-VVT) engine with an electronic throttle control (ETC). In this study, the COM of a di-VVT engine with an ETC for engine transient operation is created using the MVM by considering a linear manifold filling dynamics model, a linear actuator dynamics model, and a nonlinear steady-state engine model as shown in Figure 7-2. The MVM has been widely used to design controllers and validate modeling fidelity [5,13,24-26].

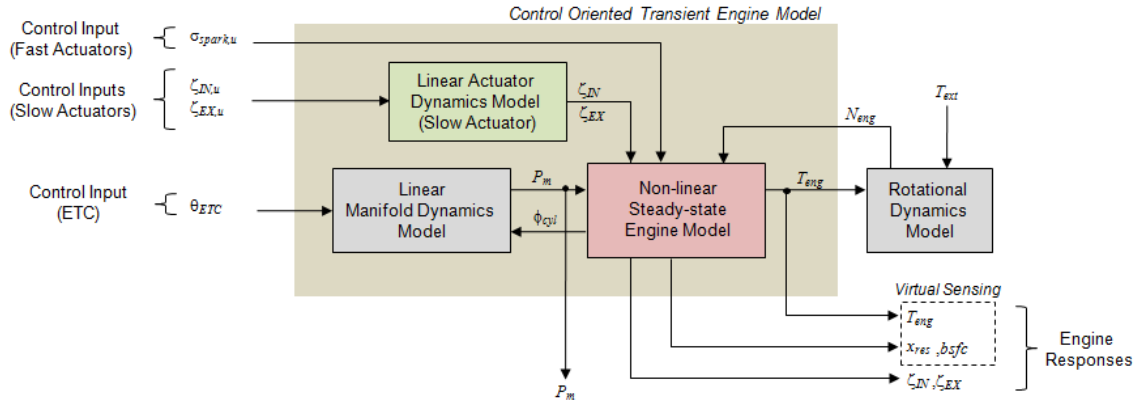

Figure 7-2 Control oriented model for engine transient operation using a non-linear steady-state engine model and linear dynamics models

The control inputs of the COM are an ETC control input (θ_{ETC}), an intake valve timing control input ($\zeta_{IN,u}$), an exhaust valve timing control input ($\zeta_{EX,u}$), and a spark timing control input ($\sigma_{spark,u}$). Linear actuator dynamics models predict the actual actuator positions. A linear manifold dynamics model calculates the intake manifold pressure (P_m) using the mass flow rate through the throttle body (ϕ_{thrt}) and the mass flow rate into the cylinders (ϕ_{cyl}). Using actuators control inputs and P_m, the non-linear steady-state engine

model predicts ϕ_{cyl}, engine torque (T_{eng}), residual gas fraction (x_{res}), and break specific fuel consumption (*bsfc*).

7.4 Nonlinear Model Predictive Control (NMPC)

Model Predictive Control (MPC), also referred as moving horizon control or receding horizon control, is one of the most general methods that are capable of considering transient control problems in a time domain. The main advantages of MPC are : (1) the formulation of control problems intuitively and flexibly; (2) the use of the advantage of optimal and feedback (FB) control for a general nonlinear system; (3) the achievement of the advantage of FF control; (4) the use of a non-linear model for prediction; (5) the consideration of feedback by re-initialization for each optimization run; (6) the capability of handling states constraints. However, the MPC requires high computation efforts to solve an optimization problem at every sampling time, and full state measurements. Nevertheless, since the MPC is the only control methodology that combines the advantage of optimal and feedback control for general nonlinear systems with constraints, the MPC is still attractive in dealing with control of highly nonlinear systems. Research on improving computation efficiency is not considered in this study.

The MPC is categorized into a linear MPC and a nonlinear MPC (NMPC). The linear MPC uses a linear plant model to predict the system dynamics, although the dynamics of the closed-loop system is nonlinear. The linear MPC has been successfully used in the chemical industry in quite a mature manner. However, since many systems, including engine systems, are inherently nonlinear, linear MPC often barely capture the plant

dynamics with sufficient accuracy. Thus, the consideration of system nonlinearity is required to describe system dynamics.

7.4.1 Basic Principle of Nonlinear Model Predictive Control

The basic ideas of the NMPC are:

(1) Explicit use of a nonlinear plant model to predict the plant nonlinear response at future time instants (horizon).

(2) Calculation of the control sequence to minimize an appropriate objective function.

(3) Use of the receding strategy to incorporate feedback control characteristics. In other words, the prediction horizon is displaced toward the future.

The methodology of the MPC family is characterized as solving a finite horizon open-loop optimal control problem in real time subject to system dynamics and constraints involving states and controls. Figure 7-3 illustrates the basic principle of the MPC. The future outputs for a determined horizon T_P, called the prediction horizon, are predicted at each time instant t_i using the plant model. The control inputs for a determined horizon T_C (in general, $T_C \leq T_P$), called the control horizon, are determined by optimizing an established open-loop performance objective function. If the objective function is linear and quadratic without constraints, an explicit solution can be obtained. Otherwise, an iterative optimization methodology must be used. Measurements of system states are achieved at every sampling time δ.

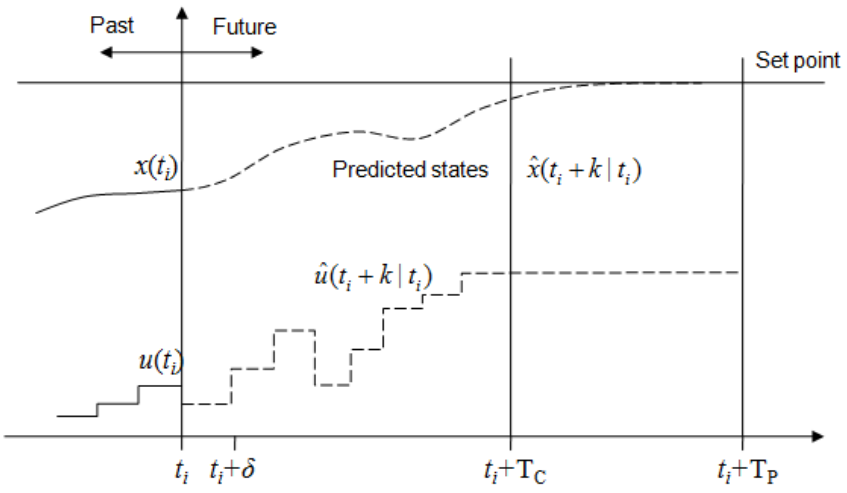

Figure 7-3 Principle of Model Predictive Control

When the plant model is perfect and no disturbance exists, the established control inputs at time t_i can be applied for all time $t \geq t_i$. However, in general, because of inaccurate plant models and external disturbances, the real system behaves differently from the predicted response. Thus, some feedback mechanisms are necessary to compensate modeling inaccuracies and disturbances. To incorporate feedback characteristics, the first control input of the established open-loop control inputs sequences at time t_i is applied to the plant until the next measurements become available at the next sampling time $t_i + \delta$. When the next measurements become available, the prediction horizon and control horizon are shifted to the new time instant at $t_i+\delta$. Then, new control inputs for the control horizon are determined by optimizing an established open-loop performance objective function.

7.4.2 Mathematical Formulation of NMPC

The stabilization problem of a nonlinear system is given in the following differential equations

$$\dot{\boldsymbol{x}}(t) = f(\boldsymbol{x}(t), \boldsymbol{u}(t)), \quad \boldsymbol{x}(0) = \boldsymbol{x}_0 \tag{7-1}$$

subject to the input and state constraints of the form

$$\boldsymbol{u}(t) \in U, \forall t \geq 0, \quad \boldsymbol{x}(t) \in X, \forall t \geq 0, \tag{7-2}$$

where $\boldsymbol{x}(t) \in \mathbb{R}^n$ is the vector of system states and $\boldsymbol{u}(t) \in \mathbb{R}^m$ is the vector of system control inputs. For simplicity, the equilibrium point of the system in equation (7-1) is at the origin (f (0,0) = 0). In addition, all states $\boldsymbol{x}$ of the system in equation (7-1) can be measured or estimated. Usually, the finite horizon open-loop optimal control problem is mathematically formulated as follows.

$$\min_{\hat{\boldsymbol{u}}(\cdot)} E(\hat{\boldsymbol{x}}(t_i + T_P)) + \int_{t_i}^{t_i+T_P} F(\hat{\boldsymbol{x}}(\tau), \hat{\boldsymbol{u}}(\tau)) d\tau \tag{7-3}$$

subject to

$$\dot{\hat{\boldsymbol{x}}}(\tau) = f(\hat{\boldsymbol{x}}(\tau), \hat{\boldsymbol{u}}(\tau)), \ \hat{\boldsymbol{x}}(t_i) = \boldsymbol{x}(t_i), \tag{7-4a}$$

$$\hat{\boldsymbol{u}}(\tau) \in \mathrm{U}, \ \forall \tau \in \left[t_i, t_i + \mathrm{T_C}\right], \tag{7-4b}$$

$$\hat{\boldsymbol{u}}(\tau) = \hat{\boldsymbol{u}}(\tau + \mathrm{T_C}), \ \forall \tau \in \left[t_i + \mathrm{T_C}, t_i + \mathrm{T_P}\right], \tag{7-4c}$$

$$\hat{\boldsymbol{x}}(\tau) \in \mathrm{X}, \ \forall \tau \in \left[t_i, t_i + \mathrm{T_P}\right], \tag{7-4d}$$

$$\hat{\boldsymbol{x}}(t_i + \mathrm{T_P}) \in \Omega, \tag{7-4e}$$

where $\hat{x}$ and $\hat{\boldsymbol{u}}$ denote predicted engine states and future control inputs respectively, t_i denotes the sampling instants, T_P and T_C are the prediction and the control horizon with $T_C \leq T_P$, and U and X are given by the form

$$U = \{\boldsymbol{u} \in R^m \mid \boldsymbol{u}_{min} \leq \boldsymbol{u} \leq \boldsymbol{u}_{max}\}, \tag{7-5a}$$

$$X = \{\boldsymbol{x} \in R^n \mid \boldsymbol{x}_{min} \leq \boldsymbol{x} \leq \boldsymbol{x}_{max}\}. \tag{7-5b}$$

The function F is the stage cost that specifies the desired control performance with the consideration of the desired system performance. The simplest and most often used form is the standard quadratic form as follows.

$$F(\hat{\boldsymbol{x}}, \hat{\boldsymbol{u}}) = (\hat{\boldsymbol{x}} - \boldsymbol{x}_S)^T Q\ (\hat{\boldsymbol{x}} - \boldsymbol{x}_S) + (\hat{\boldsymbol{u}} - \boldsymbol{u}_S)^T R(\hat{\boldsymbol{u}} - \boldsymbol{u}_S), \tag{7-6}$$

where $\boldsymbol{x}_s$ and $\boldsymbol{u}_s$ denote given set-points, and Q and R denote positive definite, symmetric weighting matrices. The weighting matrices Q and R are determined by the required system performance. Ω, so called the terminal region, is used as the terminal equality constraint to guarantee NMPC stability.

The most intuitive way to guarantee the stability of the NMPC is to use an infinite horizon cost ($T_P \rightarrow \infty$). When the system is linear and has no constraints, the optimal control problem becomes the same as the LQ problem. Since the system is nonlinear and computation time needs to be short, the NMPC uses a finite horizon length. Because the finite horizon NMPC does not guarantee the stability of the closed loop system, the terminal region constraint in equation (7-4e) is considered. In addition, the terminal penalty term $E(\hat{\boldsymbol{x}}(t_i + T_P))$ is included in the cost function in equation (7-3). This approach, which includes the terminal penalty term, is called the quasi-infinite horizon

NMPC approach. In the quasi-infinite horizon NMPC approach, the terminal penalty term E and the terminal region Ω are chosen as

$$E(\boldsymbol{x}) = \boldsymbol{x}^T P\boldsymbol{x}, \quad \Omega = \{\boldsymbol{x} \in \mathrm{R}^n \mid \boldsymbol{x}^T P\boldsymbol{x} \le \alpha\} \tag{7-7}$$

with the state feedback $\boldsymbol{u} = K\boldsymbol{x}$ using a quadratic stage cost $F(\boldsymbol{x}, \boldsymbol{u}) = \boldsymbol{x}^{\mathrm{T}} Q\,\boldsymbol{x} + \boldsymbol{u}^{\mathrm{T}} R\boldsymbol{u}$ with $Q \ge 0$ and $R > 0$. The basic idea of the quasi-infinite horizon NMPC is to approximate the infinite horizon optimal control problem by introducing the terminal cost $E(x)$ to the finite horizon optimal control problem. The quasi-infinite horizon NMPC procedure is summarized as follows.

Step 1 : Solve the linear control problem based on the Jacobian linearization (A,B) of equation (6-1) to obtain a locally stabilizing state feedback $\boldsymbol{u} = K\boldsymbol{x}$.

Step 2 : Choose a constant $\kappa \in [0, \infty]$ satisfying $\kappa < -\lambda_{\max}(A_K)$ and solve the Lyapunov equation

$$(A_K + \kappa I)^T P + P(A_K + \kappa I) = -(Q + K^T R K) \tag{7-8}$$

to get a positive definite and symmetric matrix P. where $A_K = A + BK$.

Step 3 : Find the largest possible α_1 defining a region

$$\Omega_1 = \{\boldsymbol{x} \in \mathrm{R}^n \mid \boldsymbol{x}^T P\boldsymbol{x} \le \alpha_1\}, \tag{7-9}$$

such that $K\boldsymbol{x} \in \mathrm{U}$, for all $\boldsymbol{x} \in \Omega_1 \subseteq \mathrm{X}$.

Step 4 : Find the largest possible $\alpha \in (0, \alpha_1]$ specifying a region

$$\Omega = \{\boldsymbol{x} \in \mathrm{R}^n \mid \boldsymbol{x}^T P\boldsymbol{x} \le \alpha\}, \tag{7-10}$$

such that the optimal value of the following optimization problem is non-positive:

$$\max_{\boldsymbol{x}} \{\boldsymbol{x}^T P\varphi(\boldsymbol{x}) - \kappa\, \boldsymbol{x}^T P\boldsymbol{x} \mid \boldsymbol{x}^T P\boldsymbol{x} \le \alpha\}, \tag{7-11}$$

where $\varphi(\boldsymbol{x})$ = f($\boldsymbol{x}$, $K\boldsymbol{x}$) – $A_K\boldsymbol{x}$. This procedure determines E and Ω that stabilize the linearized closed loop system at the origin.

When the above procedure is considered for a high DOF engine with wide operating ranges, the determination of E and Ω at every possible engine operating point is extremely laborious. The number of cases for the Jacobian linearization (A,B) at every possible engine operating point increases exponentially with respect to the increase of system DOF. Thus, a different approach is used for the stability of the closed loop system in this study.

Suppose that an infinite horizon NMPC procedure can be achieved, then, the cost function is expressed as

$$J = \int_{t_i}^{\infty} F(\hat{\boldsymbol{x}}(\tau), \hat{\boldsymbol{u}}(\tau))d\tau = \int_{t_i}^{t_i+T_p} F(\hat{\boldsymbol{x}}(\tau), \hat{\boldsymbol{u}}(\tau))d\tau + \int_{t_i+T_p}^{\infty} F(\hat{\boldsymbol{x}}(\tau), \hat{\boldsymbol{u}}(\tau))d\tau\,. \tag{7-12}$$

By comparing equations (7-3) and (7-12), the second integral term

$\int_{t_i+T_p}^{\infty} F(\hat{\boldsymbol{x}}(\tau), \hat{\boldsymbol{u}}(\tau))d\tau$ can be considered as $E(\hat{\boldsymbol{x}}(t_i + T_P))$. If the second integral term is small enough to be negligible, the cost function can be expressed as

$$J = \int_{t_i}^{\infty} F(\hat{\boldsymbol{x}}(\tau), \hat{\boldsymbol{u}}(\tau))d\tau \cong \int_{t_i}^{t_i+T_p} F(\hat{\boldsymbol{x}}(\tau), \hat{\boldsymbol{u}}(\tau))d\tau\,, \tag{7-13}$$

Thus, the prediction horizon T_p needs to be adequately determined to validate equation (7-13).

The transient response of a high DOF engine is governed by the slowest system dynamics, which is the manifold dynamics for the di-VVT engine. Thus, estimated the time constant of manifold dynamics can determine the prediction horizon that enables to force $E(\hat{\boldsymbol{x}}(t_i + T_P))$ to be negligible.

In this study, the resulting mathematical formulation of the NMPC is reduced as follows.

$$\min_{\hat{\boldsymbol{u}}(\cdot)} \int_{t_i}^{t_i+T_P} F(\hat{\boldsymbol{x}}(\tau), \hat{\boldsymbol{u}}(\tau)) d\tau \tag{7-14}$$

subject to

$$\dot{\hat{\boldsymbol{x}}}(\tau) = f(\hat{\boldsymbol{x}}(\tau), \hat{\boldsymbol{u}}(\tau)),\ \hat{\boldsymbol{x}}(t_i) = \boldsymbol{x}(t_i), \tag{7-15a}$$

$$\hat{\boldsymbol{u}}(\tau) \in \mathrm{U},\ \forall \tau \in \left[t_i, t_i + \mathrm{T_C}\right], \tag{7-15b}$$

$$\hat{\boldsymbol{u}}(\tau) = \hat{\boldsymbol{u}}(\tau + \mathrm{T_C}),\ \forall \tau \in \left[t_i + \mathrm{T_C}, t_i + \mathrm{T_P}\right], \tag{7-15c}$$

$$\hat{\boldsymbol{x}}(\tau) \in \mathrm{X},\ \forall \tau \in \left[t_i, t_i + \mathrm{T_P}\right], \tag{7-15d}$$

7.4.3 Determination of Control Horizon and Prediction Horizon

The short control horizon and prediction horizon are necessary to reduce the computation time. The short control horizon decreases the number of control parameters that are used as the variables of the online optimization process. In addition, the short prediction horizon also helps to reduce the computation time during the online optimization.

The engine control signal is assumed to be generated at every engine cycle. The control problem can be treated as a discrete control system with a sampling period of

$$\tau_{seg} = \frac{2\pi n}{\omega_e n_{cyl}}, \tag{7-16}$$

where n indicates a two-stroke (n=1) or a four-stroke engine (n=2), n_{cyl} is the number of cylinders of the engine, and τ_{seg} is the sampling time in seconds, usually referred to as the segment time.

The cycle time, which is the time for one complete cycle, is defined by the expression

$$\tau_{cycl} = n_{cyl} \cdot \tau_{seg}. \tag{7-17}$$

Because control inputs are determined at every cycle time, the sampling time δ of the NMPC is chosen as the cycle time τ_{cycl}.

The manifold dynamics of a di-VVT engine is modeled as a first-order system, and the time constant of the manifold dynamics τ_{MAP} is estimated as

$$\tau_{MAP} = 2V_m / \eta_v V_d N_{eng}, \tag{7-18}$$

where η_v is volumetric efficiency, N_{eng} is the engine angular speed [rad/sec], V_m is the manifold volume, and V_d is the displaced cylinder volume per cycle.

Since the engine control signal is generated at every cycle time, the control system can be considered as a discrete control system. Figure 7-4 illustrates the system responses depending on the different discrete control methodologies. When the FF control inputs are accurate enough to achieve the desired set point, the system response converges

gradually to the desired set point as shown in Figure 7-4 (a). The setting time t_s with 5% criterion is generally expressed as

$$t_s = 3 \cdot \tau_{sys} = 3 \cdot \tau_{cycl} . \tag{7-19}$$

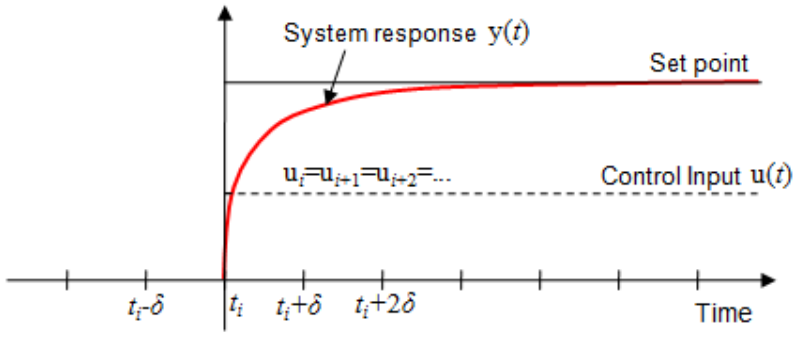

(a)

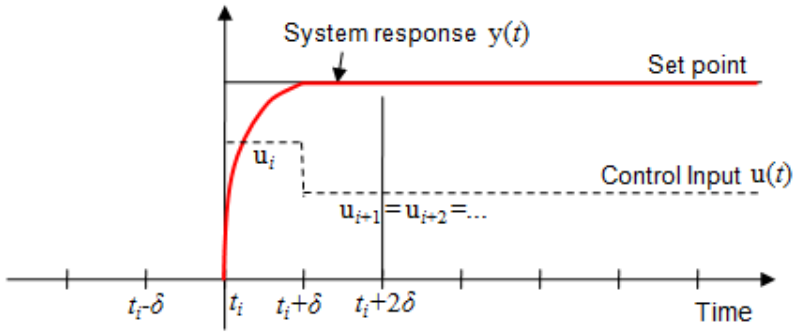

(b)

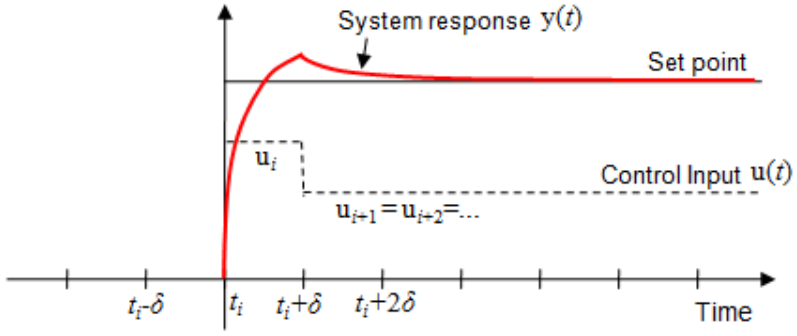

(c)

Figure 7-4 Comparison of the first order system responses: (a) feed forward control; (b) dead-beat control at an ideal case; (c) dead-beat control with presence of errors, such as modeling discrepancy and noise factors

When FB control is used for a first order discrete system, the system response converges to the set point within one time step as shown in Figure 7-4 (b). Thus, a dead-beat like optimal control is achieved. However, when the control inputs to the system for the optimal control have slight errors caused by modeling discrepancy or various noises, the system cannot achieve the desired responses within two steps as shown in Figure 7-4 (c). The system responses shown in Figure 7-4 (c) are more plausible in general system controls, because the modeling error, input noise, and processing noise always exist. In this study, the shortest control horizon length is initially determined as two times of cycle time ($2 \cdot \tau_{cycl}$), which is the shortest control sequence for the dead-beat like optimal control.

Accompanying the control horizon, the prediction horizon should be determined as short as possible to reduce the computation effort. A long prediction horizon improves the closed loop system stability. However, the prediction horizon length should be shortened while guaranteeing the system stability and maintaining sufficiently smooth system responses. When the order of the time constant of the manifold dynamics τ_{MAP} and the cycle time τ_{cycl} is assumed same, the finite setting time is initially determined as $3 \cdot \tau_{cycl}$ for the first order stable system shown in equation (7-19).

7.5 Control Design using a FF Controller and a NMPC Controller

The objectives of the control design of the target engine are: (1) to achieve fast torque responses, (2) to rejecting unfavorable emissions, and (3) to track the optimal actuator responses tightly. To achieve these control objectives, the slowest system dynamics must be adequately managed. In a conventional spark ignition engine, manifold

dynamics is the slowest system dynamics. Manifold dynamics is mainly affected by the mass flow rate through the throttle valve and into the cylinders.

The desired mass flow rate is achieved using the NMPC accompanying the FF control. At steady state operation, the engine is controlled by the FF control using the steady state optimal calibration maps. Under transient operation, the NMPC is used to compensate the performance degradation from engine transient responses besides the feed forward control. The NMPC can simultaneously manage all control variables to achieve the desired performance.

7.5.1 Overview of the Control Structure

Figure 7-5 illustrates a schematic diagram of the engine control strategies during engine operations. In view of the computational load, applying the NMPC for determining control inputs at every cycle is not the best control strategy. Thus, engine control strategies are divided into two cases. When the engine transience is negligible, only the FF controller is used to generate control inputs. In contrast, when the engine transient response becomes significant, the NMPC starts to be used to generate control inputs. In the NMPC algorithms, the weighting matrices Q and R in equation (7-6) are differently determined depending on the desired performance in an acceleration case and a deceleration case.

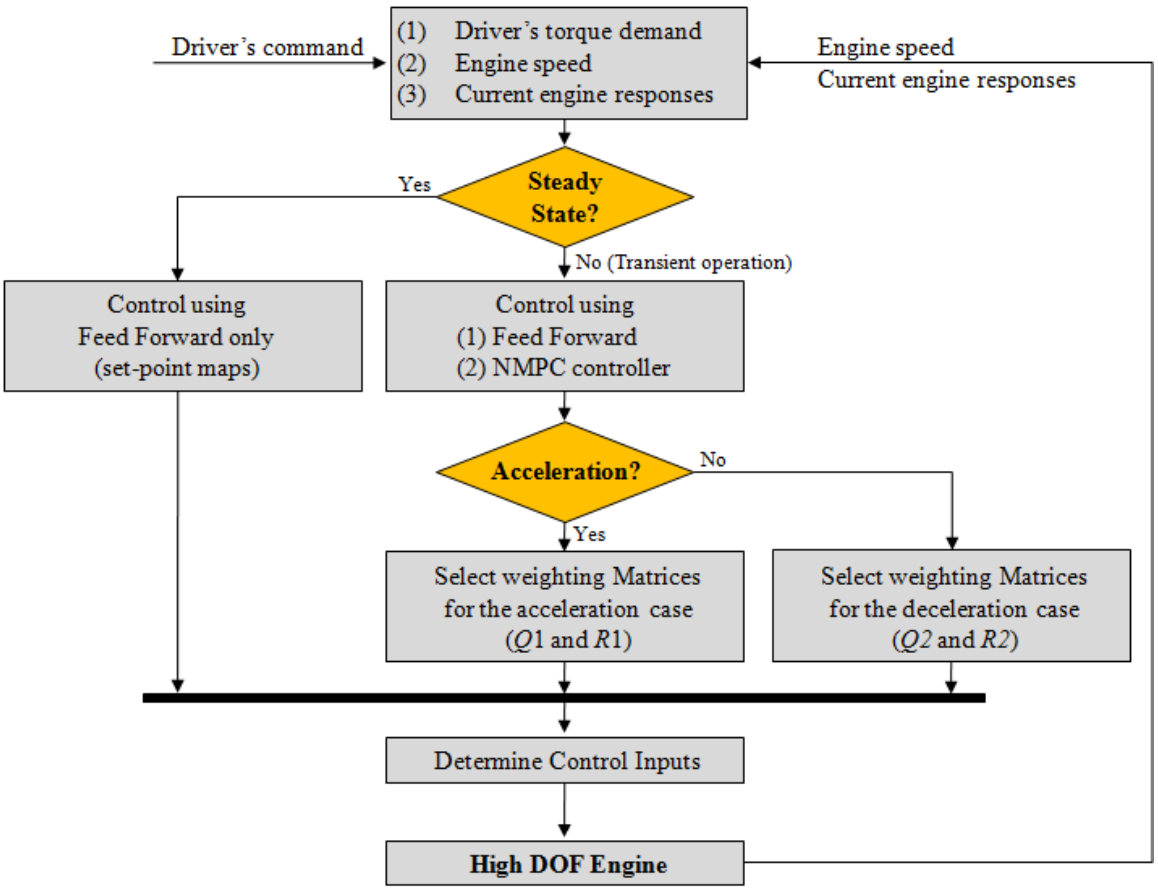

Figure 7-5 Controller schematic diagram for the control of high DOF engines under transient operating conditions using a feed forward controller and a NMPC controller

7.5.2 NMPC Controller Design for the di-VVT Engine with the ETC

Figure 7-6 illustrates a schematic diagram of an NMPC structure. Driver's demand is interpreted as a desired engine torque. The reference control inputs of each actuator are determined by the optimally calibrated actuator set-point maps at desired engine torque and current engine speed. These reference control inputs are generally used as FF control inputs.

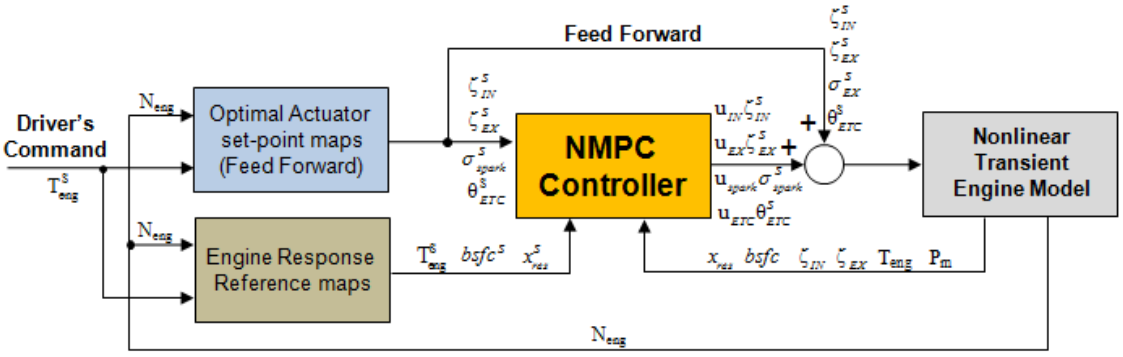

Figure 7-6 Schematic diagram of a NMPC structure

The NMPC controller is modeled using MATLAB® Simulink®. The simulink model calls a sub-routine, which is coded using an S-function, to solve a finite horizon open-loop optimal control problem for finding compensation control signals. The sub-routine includes the nonlinear transient engine model, which enables to predict the target system transient responses. The determined compensation control signals accompanying the FF control signals enable to improve engine transient responses. The controller inputs of the NMPC are categorized into:

(1) Reference actuator set-points, which are the reference intake valve timing (ζ_{IN}^{S}), reference exhaust valve timing (ζ_{EX}^{S}), reference spark timing (σ_{spark}^{S}), and reference ETC position (θ_{ETC}^{S}).

(2) Reference engine responses, which are the reference residual gas fraction (x_{res}^{S}), and reference engine torque (T_{eng}^{S}).

(3) Current engine responses, which are the current residual gas fraction (x_{res}), current intake valve timing (ζ_{IN}), current exhaust valve timing (ζ_{EX}), current engine torque (T_{eng}), and current intake manifold pressure (P_m). Current engine

responses are directly measured using sensors, or estimated using virtual sensing methodology.

Under transient engine operations, the NMPC controller determines control inputs for improving engine transient responses. The control objectives are achieved by tight tracking of the desired engine torque T^{S}_{eng} and residual gas fraction x^{S}_{res} respectively. The reference actuator set-points are determined by the steady-state engine calibration results. Current engine states and responses, which are x_{res}, ζ_{IN}, ζ_{EX}, T_{eng}, and P_m, are updated as the inputs to the NMPC controller. The updated current engine states and responses are used to reinitialize the optimization problem of the NMPC at every current time t_i.

The inputs and responses used in the optimization problem of the NMPC are expressed by using set-point centered normalized coordinates as follows.

$$\boldsymbol{x} = \left[x_1, x_2\right]^{\mathrm{T}}, \text{ and } \boldsymbol{u} = \left[u_{IN}, u_{EX}, u_{spark}, u_{ETC}\right]^{T}, \tag{7-20}$$

where $x_1 = \dfrac{x_{res} - x^{S}_{res}}{x^{S}_{res}}$, $x_2 = \dfrac{T_{eng} - T^{S}_{eng}}{T^{S}_{eng}}$, and

$$u_{IN} = \frac{\zeta_{IN} - \zeta^{S}_{IN}}{\zeta^{S}_{IN}},\ u_{EX} = \frac{\zeta_{EX} - \zeta^{S}_{EX}}{\zeta^{S}_{EX}}, u_{spark} = \frac{\sigma_{spark} - \sigma^{S}_{spark}}{\sigma^{S}_{spark}}, u_{ETC} = \frac{\theta_{ETC} - \theta^{S}_{ETC}}{\theta^{S}_{ETC}}.$$

The super script denotes the set-point of variables. By choosing an adequate prediction horizon and using equation (7-20), equation (7-14) can be expressed as

$$F(\boldsymbol{x}(\tau), \boldsymbol{u}(\tau)) = \boldsymbol{x}(\tau)^{\mathrm{T}} Q\, \boldsymbol{x}(\tau) + \boldsymbol{u}(\tau)^{\mathrm{T}} R \boldsymbol{u}(\tau), \tag{7-21}$$

where Q and R are positive definite symmetric matrices. Furthermore, control inputs limitations from actuator saturation are considered as constraints of the optimization problem. The constraints are expressed as $\boldsymbol{u} \in [\boldsymbol{u}_{\text{lb}}, \boldsymbol{u}_{\text{ub}}]$, where $\boldsymbol{u}_{\text{lb}} = [460, 245, -50, 0]$, and $\boldsymbol{u}_{\text{ub}} = [490, 275, 0, 80]$. The control input vector $\boldsymbol{u}$ is assumed to be assigned to the engine at every cycle. The engine state and response vector $\boldsymbol{x}$ is predicted using the transient engine model from current time t_i to the prediction time t_i+T_p.

7.6 Simulation Results

7.6.1 Influence of the Length of the Control Horizon

To verify the effect of the length of the control horizon, two different control horizon length cases are investigated under the same torque demand sequence and the same engine speed condition. Figure 7-7 shows the simulation results comparison between the FF control and the NMPC at different control horizon lengths. Compared to the FF control, the NMPC controller improves the transient torque response regardless of the control horizon length as shown in Figure 7-7. When the control horizon is $T_c = 1 \cdot \tau_{cycl}$, torque response is only slightly improved compared to the FF control results. In contrast, when the control horizon is $T_c = 2 \cdot \tau_{cycl}$, desired torque response is achieved within two cycle time as proposed in Figure 7-4 (c).

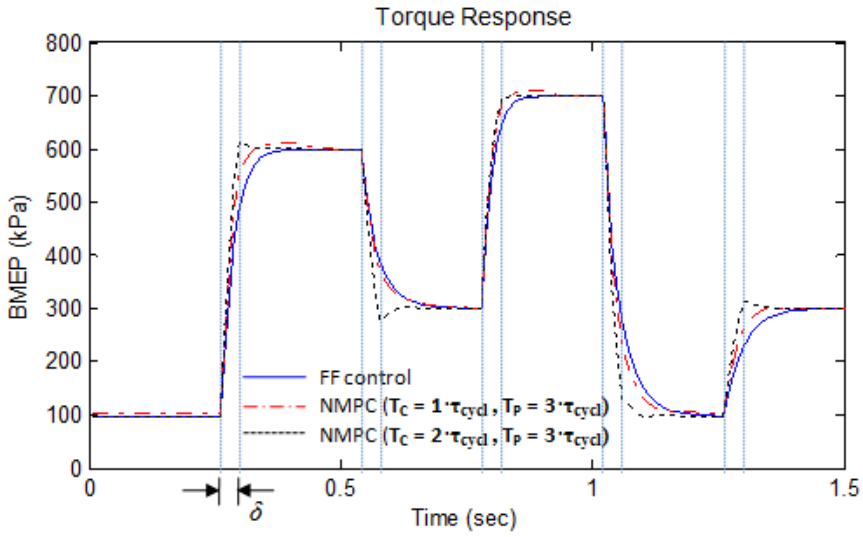

Figure 7-7 Comparison of simulation results by using the FF controller and the NMPC controller at the engine speed of 3000 rpm: (1) $T_c = 2 \cdot \tau_{cycl}$, $T_p = 3 \cdot \tau_{cycl}$; (2) $T_c = 1 \cdot \tau_{cycl}$, $T_p = 3 \cdot \tau_{cycl}$

7.6.2 Influence of the Length of the Prediction Horizon

The length of the prediction horizon is related to the closed loop system stability. Although a longer prediction horizon improves the system stability, a longer prediction horizon also requires longer computation time. To reduce the computation time, the prediction horizon is determined as short as possible while the closed loop system stability is guaranteed and system responses are smooth enough.

The influence of the length of the prediction horizon is investigated by changing the prediction horizon. Figure 7-8 shows the simulation results of the NMPC with respect to the different prediction horizon. When the prediction horizon is $T_p = 2 \cdot \tau_{cycl}$, small fluctuation is shown during transience, although the amount is negligible. To achieve

smooth responses and short computation time, the prediction horizon of the NMPC for controlling the target engine is determined as $T_p = 3 \cdot \tau_{cycl}$.

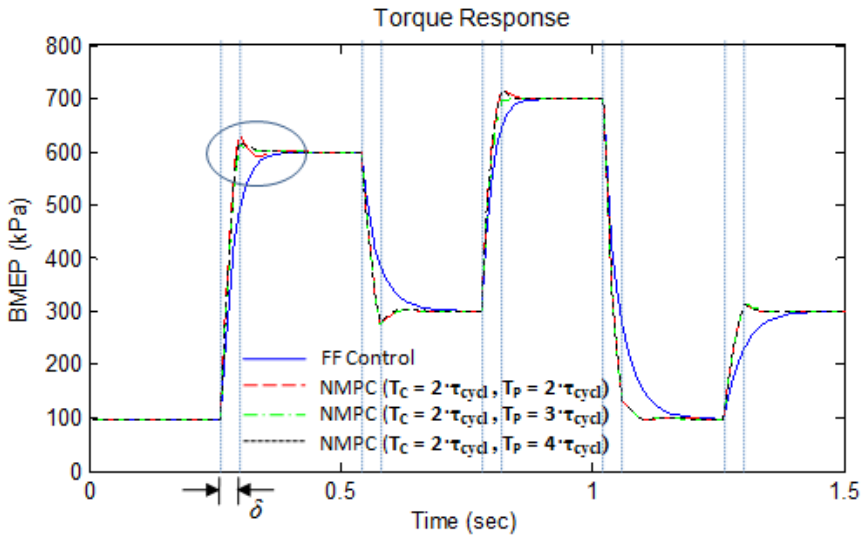

Figure 7-8 Comparison of simulation results by using the FF controller and the NMPC controller at engine the speed of 3000 rpm: (1) $T_c = 2 \cdot \tau_{cycl}$, $T_p = 2 \cdot \tau_{cycl}$; (2) $T_c = 2 \cdot \tau_{cycl}$, $T_p = 3 \cdot \tau_{cycl}$; (3) $T_c = 2 \cdot \tau_{cycl}$, $T_p = 4 \cdot \tau_{cycl}$

7.6.3 Simulation Results under Fast Transience

Transient responses control by the NMPC is investigated under fast transient torque demand at constant engine speed using the control horizon $T_c = 2 \cdot \tau_{cycl}$ and the prediction horizon $T_p = 3 \cdot \tau_{cycl}$. Without adequate transient control, slow torque responses, especially at low engine speed, are not compensated, and NO_x emission peaks may appear under the fast transience. The NO_x emission peaks are caused by the less residual gas fraction than the amount of the optimal residual gas fraction.

The NMPC determines the optimal control inputs of all actuators simultaneously to achieve the desired actuator responses and the desired system dynamics as shown in

Figure 7-9 (a) and Figure 7-10 (a). The actuator positions are controlled within the operating limits. Regardless of the engine speed, the engine torque is precisely controlled to the target torque within two cycle time as shown in Figure 7-9 (b) and Figure 7-10 (b). The resulting system responses track the target responses within one cycle time. The residual gas fraction tracks the target value without any severe excursion, and peaks of the emission index of NO_x are reduced significantly by the NMPC.

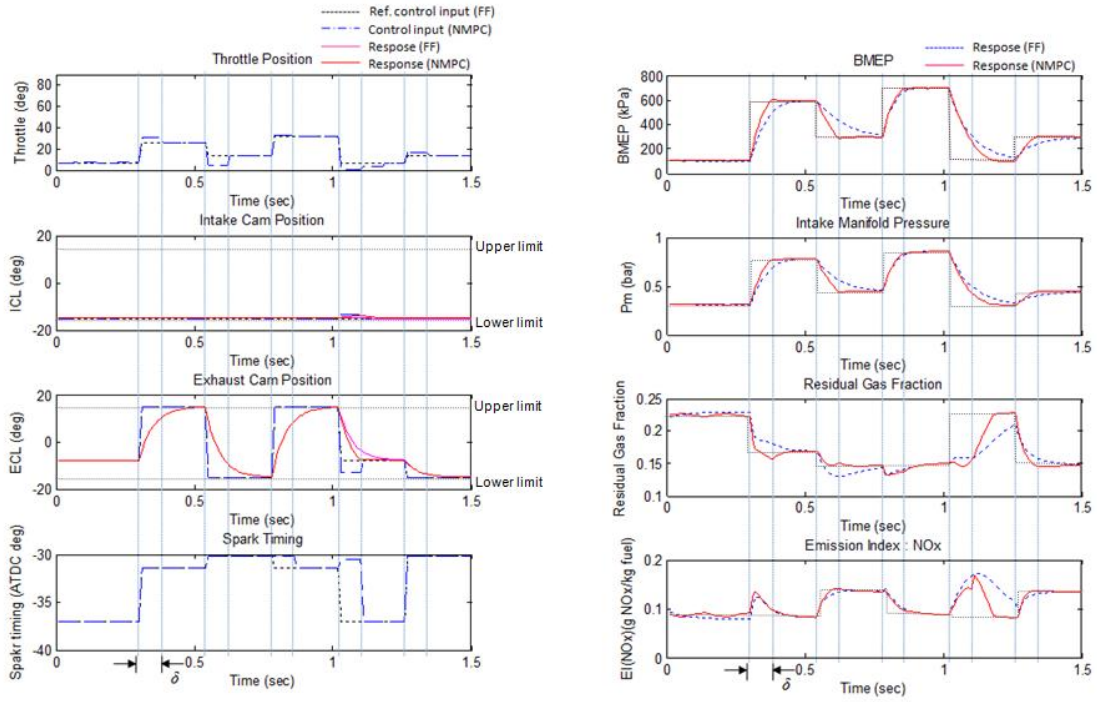

(a) **(b)**

Figure 7-9 Comparison of simulation results between FF control and NMPC control at the constant engine speed of 1500 rpm with $T_c = 2 \cdot \tau_{cycl}$, and $T_p = 3 \cdot \tau_{cycl}$: (a) control inputs and actuator responses; (b) system responses

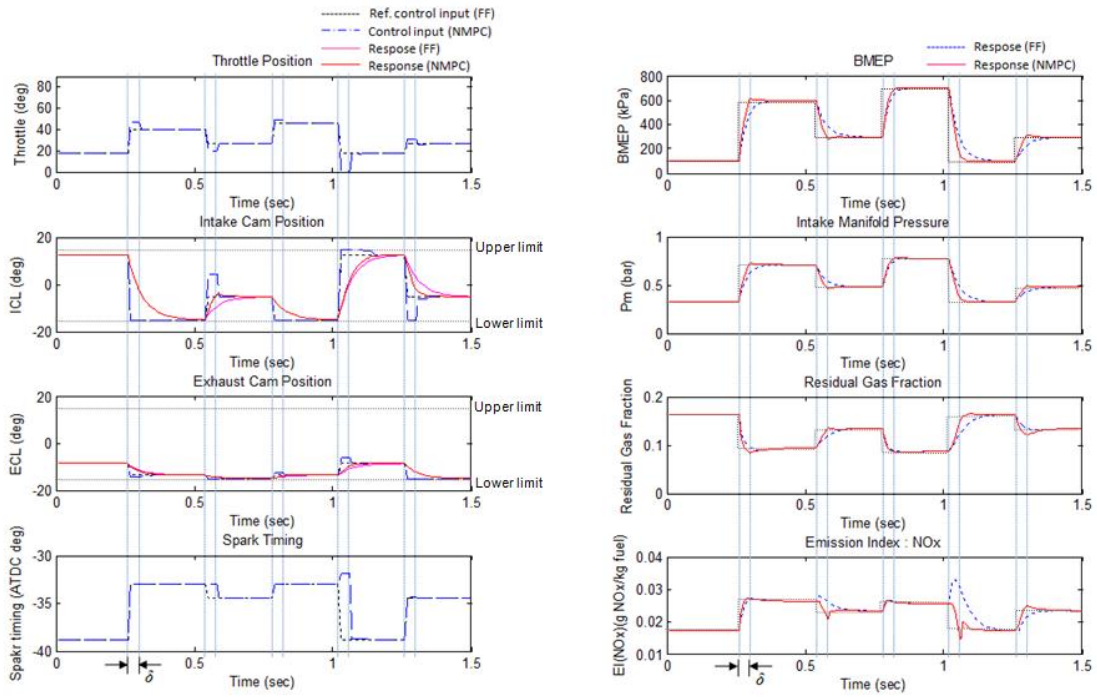

(a) **(b)**

Figure 7-10 Comparison of simulation results between FF control and NMPC control at the constant engine speed of 3000 rpm with $T_c = 2 \cdot \tau_{cycl}$, and $T_p = 3 \cdot \tau_{cycl}$: (a) control inputs and actuator responses; (b) system responses

Next, the transient control using the NMPC is investigated under fast transience accounting for vehicle dynamics with the control horizon of $T_c = 2 \cdot \tau_{cycl}$ and the prediction horizon of $T_p = 3 \cdot \tau_{cycl}$. The FF control inputs are determined based on the desired torque demand and current engine speed. While determining the optimal control inputs by using the NMPC, the engine speed is assumed to be constant because the engine speed change is much slower than other system dynamics. The resulting engine responses with the consideration of vehicle dynamics follow the desired responses within two engine cycles as shown in Figure 7-11. Thus, the quasi-steady engine speed assumption with the consideration of vehicle dynamics is valid for the NMPC.

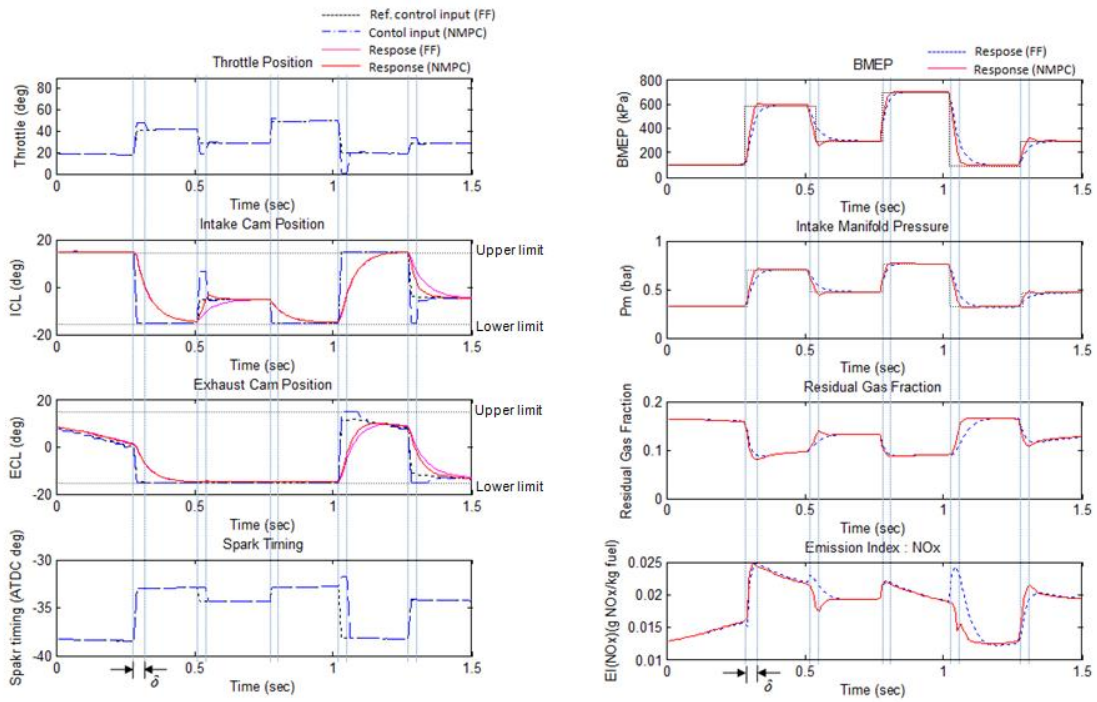

(a) **(b)**

Figure 7-11 Comparison of simulation results between FF control and NMPC control considering vehicle dynamics around 3300 rpm with $T_c = 2 \cdot \tau_{cycl}$, and $T_p = 3 \cdot \tau_{cycl}$: (a) control inputs and actuator responses; (b) system responses

7.7 Summary

As a powerful transient control tool for a highly non-linear system, the NMPC is introduced into the engine transient control problem. Before designing the NMPC based controller, the COM is created by combining a non-linear steady state engine combustion model, and linear system dynamics models. The target engine of this study incorporates di-VVT actuators and an ETC. Because the target engine is too complex to simulate using high-fidelity simulation tools, the non-linear engine model is created using the trained ANN model due to its short calculation time and the capability of capturing

highly nonlinear input-to-output relations. Then, the linear system dynamics models are augmented to consider the system dynamics. The system dynamics models include a manifold dynamics model, actuator dynamics models, and a rotational dynamics model. The created COM is assessed by the transient responses of the engine at several different engine operating conditions.

The NMPC shows the advantages of the FF control and the FB control, even though the NMPC requires high computational load. The characteristics of the FF control in the NMPC allow faster transient response of the system than any other type of FB control. This faster response is achieved through the finite horizon optimization procedure using predicted responses of the system. The finite horizon optimization problem is formulated by considering the desired control objectives. Subsequently, the cost function is created by introducing adequate positive definite weighting matrices, which are exclusively selected depending on the accelerating condition and decelerating condition.

The control horizon and prediction horizon are determined to achieve the dead-beat like optimal control as well as stable and smooth engine responses. The determined control horizon is $T_c = 2 \cdot \tau_{cycl}$ and the prediction horizon $T_p = 3 \cdot \tau_{cycl}$. Simulation results for both the constant engine speed case and the considering vehicle dynamics case show that the NMPC controller significantly improves engine responses under fast transient operations. The NMPC optimally simultaneously adjusts the actuator control inputs to achieve the control objectives. The developed NMPC procedure can be universally applied to various different control problems.

REFERENCES

1. T. Bertram, R. Bitzer, R. Mayer, and A. Volkart, "CARTRONICS – An Open Architecture for Networking the Control Systems of an Automobile", SAE Technical Paper No. 980200, 1998.
2. D. W. Guenther, and J. Gerhardt, "MOTRONIC – Torque Guided Engine Management Systems to Meet Future Challenges in Emissions and Fuel Consumption Reduction", SAE Technical Paper No. 2000-01-1420, 2000.
3. B. Mencher, H. Jessen, L. Kaiser, and J. Gerhardt, "Preparing for CARTRONIC – Interface and New Strategies for Torque Coordintion and Conversion in a Spark Ignition Engine – Management System", SAE Technical Paper No. 2001-01-0268, 2001.
4. N. Heintz, M. Mews, G. Stier, A. J. Beaumont, and A. D. Noble, "An Approach to Torque-Based Engine Management Systems", SAE Technical Paper No. 2001-01-0269, 2001.
5. A. G. Stefanopoulou, J. S. Freudenberg, and J. W. Grizzle, "Variable Camshaft Timing Engine Control", *IEEE Transaction on Control Systems Technology*, Vol 8, No. 1, pp 23-34. January 2000.
6. J. F. Sinnamon, "Co-Simulation Analysis of Transient Response and Control for Engines with Variable Valvetrains", SAE Technical Paper No. 2007-01-1283, 2007.
7. C. Atkinson, and G. Mott, "Dynamic Model-Based Calibration Optimization : An Introduction and Application to Diesel Engines", SAE Technical Paper No. 2005-01-0026, 2005.
8. M. Hafner, "Step Towards an Optimization of The Dynamic Emission Behavior of IC Engines : Measurement Strategies –Modeling –Model Based Optimization", SAE Technical Paper No. 2001-01-1793/4214, 2001.
9. A. A. Malikopoulos, P. Y. Papalambros, and D. N. Assanis, "A State-space Representation Model And Learning Algorithm For Real-Time Decision-Mating Under Uncertainty", *ASME 2007 International Mechanical Engineering Congress and Exposition*, IMECE 2007-41258, 2007.
10. A. A. Malikopoulos, P. Y. Papalambros, and D. N. Assanis, "A Learning Algorithm for Optimal Internal Combustion Engine Calibration in Real Time", *ASME 2007 International Design Engineering Technical Conferences & Computers and Information in Engineering Conference*, DETC 2007-34718, 2007.
11. A. A. Malikopoulos, D. N. Assanis, and P. Y. Papalambros, "Real-Time, Self-Learning Optimization of Diesel Engine Calibration", *Proceedings of ICEF07, 2007 Fall Technical Conference of the ASME Internal Combustion Engine Division*, ICEF 2007-1603, 2007.
12. D. Blomqvist, S. Byttner, U. Holmberg, and T. S. Rognvaldsson, "Different Strategies for Transient Control of the Air-Fuel Ratio in a SI Engine", SAE Technical Paper No. 2000-01-2835, 2000.

13. S. C. Hsieh, J. S. Freudenberg, and A. G. Stefanopoulou, "Multivariable Controller Structure in a Variable Cam Timing Engine with Electronic Throttle and Torque Feedback", *Proc 1999, Conf. on Control Applications*, pp. 465-470, 1999.

14. A. Ekdahl, "Transient Control of Variable Geometry Turbine on Heavy Duty Diesel Engines", *Proceedings of the 2005 IEEE Conference on Control Applications*, pp. 1228-1233, 2005.

15. M. Jankovic, and I. Kolmanovsky, "Constructive Lyapunov Control Design for Turbocharged Diesel Engines", *IEEE Transactions on Control Systems Technology*, Volume 8, Issue 2, Page(s):288 - 299 , 2000.

16. J. Chauvin, G. Corde, and N. Petit, "Transient control of a Diesel engine airpath", *Proceedings of the 2007 American Control Conference*, pp. 4394-4400, 2007.

17. E. F. Camacho, and C. Bordons, *Model Predictive Control in the Process Industry : Advances in Industrial Control*, Springer, 1995.

18. R. Soeterboek, *Predictive Control : A Unified Approach*, Prentice Hall, 1992.

19. B. Kouvaritakis, and M. Cannon, *Nonlinear Predictive Control : Theory and Practice*, The Institution of Electrical Engineer, 2001.

20. P. Orter, and L. Re, "Predictive Control of a Diesel Engine Air Path", *IEEE Transactions on Control Systems Technology*, Volume 15, No. 3, Page(s):449 – 456, 2007.

21. M. Herceg, T. Raff, R. Findeisen, and F. Allgöwer, "Nonlinear Model Predictive Control of a Turbocharged Diesel Engine", *2006 IEEE International Conference on Control Applications*, Oct. 2006, pp. 2766 – 2771.

22. A. Dutka, H. Javaherian, and M. J. Grimble, "Model-Based Nonlinear Multivariable Engine Control", *American Control Conference*, pp. 3671-3677, 2007.

23. J. Bengtsson, P. Strandh, R. Johansson, P. Tunestål, and B. Johansson, "Model Predictive Control of Homogeneous Charge Compression Ignition (HCCI) Engine Dynamics", *2006 IEEE International Conference on Control Applications*, pp. 1675 – 1680, 2006.

24. L. Guzzella, and C. H. Onder, *Introduction to Modeling and Control of Internal Combustion Engine System*, Springer, 2004.

25. A. G. Stefanopoulou, J. A. Cook, J. S.Freudenberg, and J. W. Grizzle, "Control-Oriented Model of a Dual Equal Variable Cam Timing Spark Ignition Engine", , *ASME Journal of Dynamic Systems, Measurement, and Control*, vol. 120, pp. 257-266, 1998.

26. A. G. Stefanopoulou, *Modeling and Control of Advanced Technology Engines*, Ph.D. Dissertation, University of Michigan, Feb. 1996.

27. Y. He, and C. Lin, "Development and Validation of a Mean Value Engine Model for Integrated Engine and Control System Simulation", SAE Technical Paper No. 2007-01-1304, 2007.

28. M. Livshiz, M. Kao, and A. Will, “Validation and Calibration Process of Powertrain Model for Engine Torque Control Development”, SAE Technical Paper No. 2004-01-0902, 2004.

CHAPTER 8

CONCLUSIONS AND FUTURE WORK

8.1 Dissertation Summary

This dissertation proposed the entire procedure to achieve the optimal calibration and the best transient control of a high DOF engine. The first step of the procedures is creating accurate engine simulation tools (called as high-fidelity simulation tools) to capture engine responses with sufficient accuracy. The high fidelity simulation consists of a one-dimensional (1-D) gas dynamics simulation model and a quasi-dimensional (quasi-D) combustion model. The accuracy of simulation is improved by tuning the key parameters and calculating the flame front area map accurately. The developed high-fidelity simulation can capture engine responses with a high accuracy.

Then, as prerequisites of the optimal calibration and transient control problems, virtual sensing methodologies are developed by using (1) artificial neural networks (ANNs), and (2) statistical regression analysis. First, a virtual sensing methodology of the mass air flow rate is proposed for a dual independent variable valve timing (di-VVT) engine with charge motion valves (CMVs). The CMV is a special inlet air flow control device to improve combustion stability. To realize the virtual sensing methodology,

artificial neural network (ANN) is proposed as a preferred solution because of its capability of capturing highly nonlinear input-to-output relations. A specific virtual sensor structure is presented to account for ambient pressure compensation. To generate data sets for training ANNs, high fidelity simulations are used as substitutes of experiments. Then, the optimal ANN structures are determined by using the systematic training procedure. The virtual sensing results at different engine operating conditions show significant effects of the CMVs on the mass air flow rate, and also provide trends of the mass air flow rate depending on various actuators set-points.

As another important virtual sensing topic, an indirect prediction methodology of combustion stability based on the statistical analysis of substitutive measurements is proposed. First, from the analysis of combustion related parameter, adequate combustion stability related parameters are determined. Then, trends of the COV_{IMEP} are investigated by assessing experimental data. To find adequate relations between the COV_{IMEP} and other measurable parameters, statistical regression analysis procedures are used. A regression model is determined from the trend analysis. Finally, the COV_{IMEP} is characterized by a function of 10-90% burn duration and manifold absolute pressure (MAP) around the minimum spark advance for best torque (MBT). The resulting regression equations enable to estimate the combustion stability in real time for the optimal calibration and transient control of engines.

Next, simulation based multi-objective optimal calibration of high DOF engines is investigated using the developed virtual sensing methodologies. As an internal combustion engine system adopts more new technologies, engine optimal calibration problems become a critical issue to achieve the whole engine hardware potential. As one

objective of the engine calibration at part load operating condition, fuel economy has been widely used. In addition to the fuel economy objective, combustion stability should be considered as additional objective in order to guarantee vehicle drivability and driving feel. Because of the difficulty in direct measuring combustion stability, the combustion stability has been rarely considered in the most engine calibration problems. In this dissertation, combustion stability objective as well as fuel economy objective is considered while calibrating high DOF engines at part load conditions. The engine calibration is achieved using simulation based procedure. First, high-fidelity engine simulation tools are created to capture engine responses over the whole engine operating points. The calculated engine response results are used to train artificial neural network (ANN) models, which are used as fast surrogate engine models. Then, an optimization framework is devised for efficient high-degree-of-freedom engine calibrations. Objective functions, which consider both fuel economy and combustion stability at part load conditions, are created by combining several ANN models. The optimal engine operating set-points are determined by solving multi-objective constrained optimization problem over the concerned engine part load operating conditions. As results of the optimal engine calibration, the fuel economy is improved over the engine part load operating points, especially in low-to-medium engine speed, accompanying the improvement of combustion stability.

In addition to the steady-state optimal engine calibration, to achieve the best hardware performance under fast transient engine operations, a nonlinear transient control methodology is proposed by using nonlinear model predictive control (NMPC). For the precise control of high DOF engines under transience, an accurate control

oriented model (COM) of high DOF engines is essential. Thus, a high fidelity COM is developed to capture the ultimate non-linearity caused by the complex combustion process. The steady-state engine combustion models are created by using high-fidelity engine simulation and artificial neural networks (ANNs). Then, the steady-state combustion models are augmented to account for system dynamics. The developed high fidelity COM can capture not only the engine input-to-output relations over the whole possible engine operating points but also the system dynamics. In addition, the developed high fidelity COM provides a good prediction of engine responses with arbitrary engine control inputs over the whole possible engine operation points.

Then, nonlinear model predictive control (NMPC) is designed to deal with the dynamic response of a high-DOF engine. It combines the advantages of both feed forward control and feedback control considering constraints. While designing the NMPC, the length of control horizon and prediction horizon are determined to achieve the dead-beat control and to eliminate or diminish transient excursions. The NMPC significantly improves engine responses under high transient operations by adjusting each actuator control inputs simultaneously to achieve the control objectives.

8.2 Summary of Contributions

The contributions of this dissertation are

(1) High-fidelity models, which are composed by a 1-D gas dynamics model and a quasi-D combustion model, are extended to consider the additional DOF of an engine system, especially in the consideration of the charge motion valve

(CMV). Moreover, the simulation accuracy of quasi-D combustion model is largely improved by increasing the accuracy of the flame front area calculation through formulating the combustion chamber geometry with a finite element method (FEM) modeling technique.

(2) Virtual sensing methodology for the estimation of the mass air flow rate is extended to account for the flexible intake system. The designed virtual sensor for the mass air flow rate enables to predict sufficiently accurate air mass flow rate into the cylinder without the direct measurement of intake port pressure behind the CMV. The estimated air mass flow can be used for the feedback control of air-to-fuel ratio under engine transient operation.

(3) Methodology to indirectly predict the combustion stability in real time is developed by using statistical regression analysis of substitutive measurements. Adequate parameters are selected to capture the characteristics of combustion stability. Then, the best regression equations of the combustion stability with 10-90% burn duration and manifold absolute pressure (MAP) are determined by the proposed statistical regression analysis procedure.

(4) Engine optimal calibration methodology with multi objectives is proposed with the fuel economy objective and the combustion stability objective at part load conditions. The proposed simulation based optimal calibration framework improves the efficiency of the engine calibration procedure by introducing the

inverse ANN models. Adaptation of weights associated with respective objectives allows characterization of the trade-off between fuel economy and combustion stability at near idle conditions.

(5) Control oriented model (COM) of high DOF engines is developed to accurately predict engine dynamic responses. To create the COM, the steady-state engine combustion model is created using the trained ANNs, and linear system dynamics models are added to the combustion model. Since the created COM can capture the combustion process with sufficient accuracy, the parameters directly related to the combustion process can be treated as the performance variables for transient control design.

(6) Non-linear Model Predictive Control based transient control methodology of high DOF engine is proposed to achieve dead-beat like optimal control within one cycle time. The proposed methodology combines a FF controller and a NMPC controller. The FF controller determines control inputs based on the steady state calibration maps, and the NMPC controller eliminate excursions from the steady-state optimum under transient conditions by adjusting trajectories of actuator commands. This control methodology can be extended to the control problems of any high DOF engine.

8.3 Future Work

In this dissertation, the entire procedure for calibrating a high DOF engine and transient control of a high DOF engine are developed. In reality, the implementation of the NMPC controller to mass produced engines is limited because of the demanding high computation power. To resolve the computation power limitation, two different approaches must be considered in the future, which are (1) creating fast enough transient engine model that can be used in real time optimization, and (2) developing fast enough optimization algorithm that can find desired optimum within given short computation time.